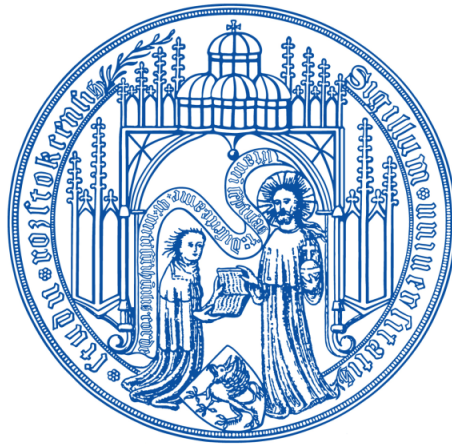# Applications of Physics
# of Stochastic Processes
to Vehicular Traffic Problems

Dissertation
zur
Erlangung des akademischen Grades
doctor rerum naturalium (Dr. rer. nat.)
der Mathematisch-Naturwissenschaftlichen Fakultät
der Universität Rostock

Julia Hinkel, geb. Tolmacheva

geboren am 06.08.1979 in Charkiv, Ukraine

Rostock, den 27.11.2007

Approved, Thesis Committee:

First Reader (Supervisor)

Priv.-Doz. Dr. Reinhard Mahnke
Institute of Physics,
University of Rostock,
D–18051 Rostock, Germany.
E–mail: reinhard.mahnke@uni-rostock.de

Second Reader (Referee)

Prof. Dr. Steffen Trimper
Department of Physics,
Martin Luther University of Halle–Wittenberg,
Von–Seckendorff–Platz 1, D–06099, Halle (Saale), Germany.
E–mail: trimper@physik.uni-halle.de

Abstract

A many–particle system imitating the motion of the vehicular ensemble on a one lane road without crossroads is under study. Taking into account the properties of real traffic, both deterministic and stochastic approaches are applied in order to describe the system dynamics. Despite of the car interaction being local in nature, it gives rise to cooperative phenomena that manifests the formation, dissolution and joining of large car clusters. Such processes correspond to the different states of traffic flow which can be treated in terms of phase transitions.

In this connection, the theory of the three traffic states proposed by Kerner is taken as a hypothesis for present investigations. Starting from the microscopic level based on the optimal velocity ansatz, the detailed analysis of the possible traffic states is developed. In view of the fact that such an approach can describe either free flow or congestions, the problem of understanding and description of the intermediate states has been addressed within the framework of this thesis. The new approach is based on study of dynamical states controlled by kinetic coefficients taking into account their anomalous properties and their dependence on position in phase space. The interaction between the noise and the dynamical trap can cause certain anomalies in the system dynamics.

One of the main manifestations of the traffic congestion is the traffic breakdown phenomenon regarded as a random process developing via the cluster formation mechanism. In this manner, the probabilistic description based on the concept of first passage time is developed and the breakdown probability is calculated in terms of the solution of the corresponding Fokker–Planck equation given as a initial–boundary–value–problem. In order to interpret the obtained analytical result, its comparison with the empirical data is performed.

ii

Contents

1 Introduction

Nowadays the concepts and techniques of theoretical physics are applied to study complex systems [28, 76, 99] coming from chemical, biological and social sciences. Not a long time ago, investigations in this field have been determined as inter-disciplinary research. Traffic flow [29] and granular matter [69], ant colony behaviour [85] and transactions in financial markets [1] provide examples of complex systems. These systems are interesting not only as objects of natural sciences but also from the physical points of view for fundamental understanding and detailed analysis of such exotic phenomena.

Our work is devoted to the description of *traffic flow*. Recently, this topic is actively discussed in different fields of our society and has found a great interest in physical community. As a result of the growth of vehicle traffic in many cities of the world, the traffic volume runs up to such high values, that car congestions become usual and almost the only possible state of the car motion (see Fig. 1.1). For this reason, the still open and often discussed questions are the optimal control of the congested traffic and the methods of the jam prevention.

The empirical analysis shows that traffic has complex and nonlinear structure. Physicists all over the world try to explain such a complicated behaviour and to describe it using theoretical approaches [25, 33, 80]. The main goal of such investigations is to invent a theoretical model which can describe the general features of the typical vehicular traffic. The theoretical analysis and computer simulation of these models help in better understanding of the complex phenomena observed in real traffic.

There are two different approaches for traffic modeling. One of them is called the *fluid–dynamical* description [14, 29] where the individual properties of a vehicle are not taking into account explicitly. Another way of looking at it is to investigate the dynamics of each car on the *microscopic* level. Within the context of such a model, the both deterministic and stochastic approaches are possible. The deterministic models based on classical Newtonian description are provided by the so–called *car following theory* [78, 87]. The model assumes that the acceleration of the car is specified by the leading neighboring vehicle. In this sense, the velocity changing in time is controlled by some function, which depends, in general, on the velocity difference and the headway distance. This function is called the *optimal velocity* function and its different approximations have been considered [3, 27, 30, 31, 50, 51, 74]. In contrast, the *cellular automata* model, which belongs to the class of *particle hopping* models, describes the traffic from the stochastic point of view [14, 100]. In this case, it has been proposed to divide the

Fig. 1.1: The example of the complex structure of traffic congestion. This photo shows the Smolenskaya square on Sadovoe ring in Moscow: `http://www.englishrussia.com/?p=429`.

length of street into cells and the time into intervals [72]. The update of the car position is performed in parallel and takes place according to some predetermined rules. The stochasticity endows the model as a parameter which describes the velocity fluctuations due to delayed acceleration. To sum up this short overview, it should be mentioned, that the microscopic models are not accident free and it is still not found such a model which would be able to imitate the real traffic.

One of the most interesting property of traffic is the *jam formation*. There are different reasons of its appearance. For example, lane reductions or dense traffic can surely cause car congestion. Nevertheless, the jams have been observed in the situation when there was no reason for their formation [96]. This spontaneous congestion is called *phantom jams*. In this manner, the process of the cluster formation can be considered as a stochastic one and, as its characteristic, the cluster size can be analyzed in time. Obviously, the cluster size is a discrete value and, by drawing analogy to cellular automata model [29], the *probabilistic* approach should be applied for the investigation of this problem. In this sense, the *master equation* [34] and, as its continuous analog, the *Fokker–Planck equation* [24, 66, 81] should be used. This problem description brings up the question about the *traffic breakdown* [52, 53, 58].

1.1 Aim of the Work

In the last few decades the investigations in the field of physics of traffic flow have been addressed to the correct physical interpretation of the properties of the vehicular traffic. For this purpose, a lot of theoretical models based on principles of statistical physics have been proposed for the fundamental understanding of the complex nature of traffic. Within the framework of such a research, both microscopic and macroscopic approaches have been involved.

It has been assumed that a car (or vehicle) can be represented as a particle. In this manner, the ensemble of particles has been taken for a car set and the particle interaction has been considered. However, it is quite difficult to understand the dynamics of the system completely without the thorough analysis of the behaviour of its individual elements. In this regard, the microscopic description allows an detailed understanding of the dynamic properties. The microscopic approach is based on concepts of the Newtonian mechanics where the governing equation is given by Newton's second law. As it has been already mentioned in the Introduction, the extensively used microscopical description of traffic is the car following model which imitates the particle motion on a one lane road. This approach is based on so–called response–stimulus relation. The updating of the velocity and coordinate occurs depending on a stimulus function composed on many factors.

Generally, it is assumed that for car following model two main factors for the adequate motion of the car should be included:

- to move at speed of leading car;

- to avoid collisions.

However, the car motion is controlled by the driver. It means that the human factor should be also taken into account. The driver acts according to his personal physical and mental properties. In this sense, the system of traffic flow can be regarded as the system with motivations. The fundamental property of the system with motivations is its cooperative behaviour. The cooperative behaviour in traffic has been also observed empirically. In spite of the fact that some attempts have been already made in order to explain the cooperative motion for traffic systems, a generally accepted theory describing such a phenomenon is still missing. For example, in the framework of such discussion, it has been proposed to take into the model description the time delay term which allows a car to reach the velocity of the leader with a time lag. It should be mentioned that this approach is beyond the scope of Newtonian description.

The cooperative motion plays the important role for the description of the traffic phases. As a result of prolonged discussions, the hypothesis about the three traffic states has been proposed by Kerner [41–47], contrary to popular opinion about the existence of only two phases in traffic. He discerns:

- free flow;

- synchronized flow;

- wide moving jams.

The main objective of this work is to provide the detailed analysis of the possible states of traffic flow dynamics. The analytical investigations in this field present a challenging problem. Therefore the numerical integration of the many–particle system has been applied for both deterministic and stochastic descriptions.

In framework of the present thesis, the microscopic description of vehicular ensemble governed by optimal velocity ansatz [3, 4, 66] for motion on a circle one lane road has been examined in detail. The following analysis has been performed:

- the model has been thoroughly tested on car collisions in order to determine the safe domain of system control parameters. The analysis has been done by a numerical integration of the many–particle system given by multidimensional system of nonlinear differential equations;

- the temporal dependence for the car positions, velocities and headways have been obtained under the influence of control parameters. The cooperative motions characterized by the formation of large numbers of car clusters has been observed;

- the phase portrait in terms of headway distances and velocities has been analysed for different time moments in order to determine the possible states of traffic;

- the stochastic force in terms of multiplicative white noise has been included in car dynamics and the system of stochastic differential equations has been integrated in order to get the probability distribution functions of headways and velocities under the influence of control parameters;

- the energy balance equation has been considered and the total energy of the car system together with the energy flux function have been constructed.

In view of the fact that these is a hypothesis about three phases of traffic flow, the problem of understanding and description of the intermediate states has been addressed within the framework of this thesis. The new approach is based on study of dynamical states controlled by kinetic coefficients taking into account their anomalous properties and their dependence on position in phase space. For this purpose, the motion of two cars has been analysed. The leading car has been assumed to move at constant speed. The following car is specified by the system of stochastic differential equations in phase space of the headway and velocity difference with additive white noise. The following analysis has been performed:

- the dynamical trap concept has been introduced for the follow the leader model;

- by way of numerical integration, it has been shown that dynamical traps induce the formation of the macroscopic states which do not characterize by stationary points of the deterministic force but by complex and cooperative motion of particles. These dynamical states can be interpreted as a new type of phase transition.

One of the main effects of the car congestion is the traffic breakdown. This phenomenon has a probabilistic nature. In order to calculate the traffic breakdown, its stochastic description is defined as a car cluster formation process. For this reason the model of traffic flow on a freeway section has been considered and the spontaneous formation of a jam regarded as a large car cluster arising on the road has been studied. For this purpose, the following analysis has been performed:

- on mathematical language of stochastic differential equation the term of traffic breakdown has been formulated;

- the corresponding Fokker–Planck equation in terms of probability density distribution has been solved analytically;

- the cumulative probability for traffic breakdowns has been obtained and compared with empirical traffic data.

1.2 Structure of the PhD Thesis

The general review of the theory of stochastic differential equations is given in Chapter 2. This subject is very extensive and, mainly, the different ways of the description of stochastic processes are discussed here. In view of the difficulties of finding the analytical solution, the central question is to develop the numerical methods of the stochastic equations.

Chapter 3 presents the microscopic description of the car following model based on the optimal velocity function. The detailed analysis of the nonlinear dynamics described by deterministic and stochastic approaches has been performed. The results have been obtained numerically. The noiseless system has been integrated by usage of the Runge–Kutta method of 4–th order. The stochastic case with diagonal multiplicative noise has been solved by explicit strong schemes of the 1.5 order. Due to the fact, that traffic flow system is a not conservative one, the energy balance equation has been derived.

The anomalies in the kinetic coefficient are discussed in Chapter 4. By way of example, the rather simple model of the motion of two cars is studied and its

dynamics is analyzed numerically. The lead car has a constant speed. The following car is specified by the system of stochastic differential equations including additive white noise. The equation for acceleration includes the term which describes the delay in the driver reaction with perception depending on the velocity difference. The perception determines the dynamical trap region near the headway axis where the velocity difference becomes sufficiently low. The anomalies of the system behaviour have been investigated.

The physical interpretation and explanation of the traffic breakdown are given in Chapter 5. The calculations are based on Fokker-Planck equation including balance equation where the main quantity is the probability density distribution which has to satisfy the reflecting boundary condition at zero cluster size and absorbing one at escape cluster size. The drift – diffusion process was considered in detail as special case of Fokker-Planck equation with linear potential. The obtained result has been compared with empirical data.

2 Stochastic Description of Physical Processes

2.1 Introduction to Stochastic Differential Equations

In framework of this Chapter, a brief introduction to the theory of stochastic differential equations will be given [24, 34, 38, 81]. As an example, rather simple and almost historical processes such as Brownian motion will be analyzed [6, 97]. Starting from the microscopical description of stochastic differential equations, the main properties of the Wiener process given in terms of the Ito description will be discussed together with the numerical methods of its representation [15, 94]. In order to generalize the features of the stochastic processes described on microscopic level, the mesoscopic approach in terms of the corresponding Fokker-Planck or master equations will be considered [23, 24, 81]. The different special cases will be presented and analyzed by using certain analytical technique as well as numerical approximations [48, 79, 94].

The Brownian motion which observed originally by Robert Brown in 1827 has initiated the development of a new branch in physics [73]. By modelling of the nature phenomena, it has been concluded, that the well–investigated deterministic approach based on the Newton theory could not give the correct description of such processes. It has been found that the systems under study do not have the deterministic behaviour. The detailed experimental investigations of the Brownian motion have shown that the observed motion is irregular and unpredictable. First explanations of the Brownian motion have been given by Einstein and Smoluchowski [16, 18, 24] and were provided in terms of probability density distribution. Langevin has used another approach based on Newton's law [16, 24]. He assumed that there are two forces having the influence on the particle dynamics: deterministic force given by friction and stochastic force which fluctuates rapidly. In next Section, the main properties of the stochastic force will be discussed using as an example the one–dimensional case.

2.1.1 Wiener Process

The one–dimensional stochastic differential equation in terms of the Langevin notation has the form [24]

$$\frac{dx}{dt} = \xi(t) \, . \tag{2.1}$$

with the rapidly fluctuating random term $\xi(t)$. The stochastic force $\xi(t)$ presented by Gaussian white noise, can be explained more strongly from the mathematical point of view. Mathematically speaking, there is the problem that the Langevin equation is impossible to integrate [24]. The integral of the random term is not differentiable. As result, another approach has to be used. Such a technique is the *stochastic integration* [15]. The stochastic integral is defined as a limit of the partial sums which include the increment of the *Wiener process*. The stochastic differential equation in terms of the Wiener increment is the mathematical analogue of the Langevin equation (2.1). The Wiener process is the simplest continuous in time one–dimensional stochastic process [24] and its dynamics obeys the equation

$$dx(t) = dW(t) \tag{2.2}$$

together with the initial condition

$$x(t = 0) = 0 \, . \tag{2.3}$$

The process (2.2) – (2.3) is characterized by the following properties:

- The Wiener process $W(t)$ is normally distributed with mean value

$$\langle W(t) \rangle = 0 \qquad \text{and variance} \qquad \langle (W(t))^2 \rangle - \langle W(t) \rangle^2 = t \, . \tag{2.4}$$

- All increments

$$\Delta W(t) = W(t + \Delta t) - W(t) \tag{2.5}$$

  are independent, therefore

$$\langle \Delta W(t) \rangle = 0 \qquad \text{and} \qquad \langle (\Delta W(t))^2 \rangle = \Delta t \, . \tag{2.6}$$

These analytical properties help us to calculate the increment $\Delta W(t)$ (stochastic space step $\Delta x = \Delta W$) numerically from standard normally distributed random numbers $Z \sim N(0, 1)$ via
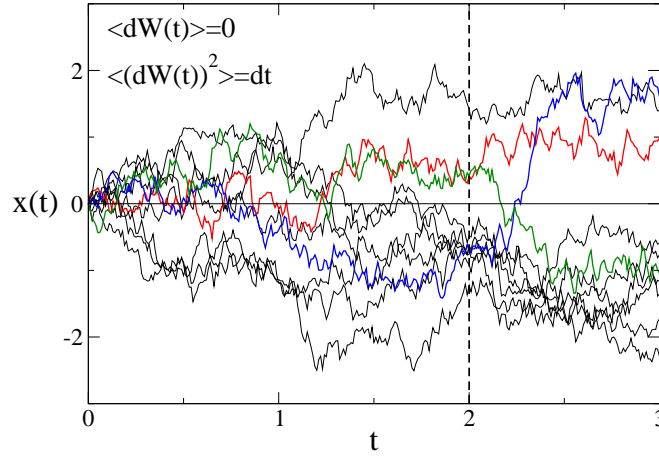
$$\Delta W(t) = Z \sqrt{\Delta t} \, . \tag{2.7}$$

We have studied three different algorithms to get normally distributed random numbers Z. All of them produce the transformation to generate from uniform distributed random numbers $U_i \in (0, 1)$ numbers $Z \sim N(0, 1)$. The transformation by *Polar method* has three steps [94]:

Fig. 2.1: Ten stochastic trajectories resulting from Wiener process (2.2) – (2.3) and obtained by using *P*olar method.

1. Generate two uniform distributed random numbers U_1 and U_2;

2. Define $V_i = 2U_i - 1$;

3. Check the condition that $W = V_1^2 + V_2^2 < 1$;

4. If 'yes' create $Z = V_1 \sqrt{-2 \log(W)/W}$;

5. If 'no' generate new random numbers (go to 1) and check this condition again;

For the same realization the *Box-Müller method* [94] proposes the necessary transformation after the generation $U_1, U_2 \in (0,1)$ only by one step

$$Z = \sqrt{-2 \ln U_1} \, \cos\left(2\pi\,U_2\right). \tag{2.8}$$

It seems, that the difference between both described methods is insignificant and connected only with the simulation time. Fig. 2.1 shows ten different realizations of the time evolution given by Wiener process (2.2) – (2.3). The third used strategy to calculate variable Z is based on theoretical explanations [20, 86]. It is well-known that the uniform distribution at the interval $[0, 1]$

$$p_{uniform}(x) = \left\{ \begin{array}{ccc} 0 & : & x < 0 \\ 1 & : & 0 < x < 1 \\ 0 & : & x > 1 \end{array} \right\} \tag{2.9}$$

has the mean value $\mu = 1/2$, because of

$$\mu = \int_{-\infty}^{+\infty} x \, p_{uniform}(x) \, dx = \int_0^1 x \, dx = \frac{1}{2} \tag{2.10}$$

and the variance σ^2 which equals to

$$\sigma^2 = \int_{-\infty}^{+\infty} (x - \mu)^2 \, p_{uniform}(x) \, dx = \int_0^1 \left(x - \frac{1}{2} \right)^2 dx = \frac{1}{12} \,. \qquad (2.11)$$

Therefore, the new variable

$$Z = \sum_{i=1}^{12} \left(U_i - \frac{1}{2} \right) \qquad (2.12)$$

has to be approximately the normal distributed one with parameters

$$\langle Z \rangle \;=\; 0 \quad \text{and} \quad \langle Z^2 \rangle - \langle Z \rangle^2 = 1 \,. \qquad (2.13)$$

It is necessary to generate twelve uniform distributed random numbers for calculation Z for one time step $[t, t + \Delta t]$ following this procedure. Box-Müller and Polar methods need for it only two random numbers.

2.1.2 Vector Description of Stochastic Differential Equations

In general, the stochastic differential equations in n–dimensional case can be defined by

$$dr = A(r) \, dt + B(r) \, dW(t) \qquad (2.14)$$

with any initial condition

$$r(t = t_0) = r_0 \,, \qquad (2.15)$$

where $r = r(t) \in \mathbb{R}^n$ is the phase vector, $A(r)$ is a drift vector (deterministic part) with the same dimension as phase vector $r(t)$, $B(r) \in \mathbb{R}^{n \times n}$ is the positive-defined matrix and $dW(t)$ is n–dimensional increment of the Wiener process [24]. The matrix $B(r)$ is called diffusion matrix and together with the $dW(t)$ form the stochastic part of the equation (2.14).

The theoretical model which describes the motion of a free Brownian particle is known as Ornstein–Uhlenbeck process [97]. The model definition can be schematically presented as the following system of differential equations according to coordinate x and velocity v

$$\frac{dx}{dt} \;=\; v \,, \qquad (2.16)$$

$$m \frac{dv}{dt} \;=\; F(x, v, t) \,. \qquad (2.17)$$

The right part of the equation (2.17) contains the resulting force $F(x, v, t)$ of all forces acting on a particle. In this case, following the Langevin approach, the force $F(x, v, t) = F_{det}(x, v, t) + F_{stoch}(x, v, t)$ is the sum of the two contributions, i. e, the deterministic term $F_{det}(v) = -m \, \gamma \, v$ is given as dissipation force with

friction constant γ and, due to the randomness, the stochastic force $F_{stoch}(t) = m \sqrt{2 B}\, dW_v(t)$ with noise intensity parameter B. Finally, the two–dimensional process is described by the system of stochastic differential equations including additive white noise

$$dx \;=\; v\, dt\,, \tag{2.18}$$

$$dv \;=\; -\gamma\, v\, dt + \sqrt{2 B}\, dW_v(t) \tag{2.19}$$

with initial conditions $x(t = t_0) = x_0$ and $v(t = t_0) = v_0$. The system (2.18) – (2.19) can be written in general form in notations of (2.14) as

$$r(t) = \begin{pmatrix} x(t) \\ v(t) \end{pmatrix}, \quad A(r) = \begin{pmatrix} v(t) \\ -\gamma\, v(t) \end{pmatrix}, \tag{2.20}$$

$$B(r) = \begin{pmatrix} 0 & 0 \\ 0 & \sqrt{2 B} \end{pmatrix}, \quad dW(t) = \begin{pmatrix} dW_x(t) \\ dW_v(t) \end{pmatrix}. \tag{2.21}$$

2.2 Probabilistic Description of Physical Processes

Up to now we have spoken about the process on microscopic level, i. e. we have looked for the different realizations of the stochastic variable. Nevertheless, it is not enough to have the authentic view of the concrete dynamics. In order to obtain the detailed information about the general properties of the given stochastic process, the probabilistic description has to be introduced. In this case, the ensemble of trajectories is under consideration and the probability density distribution plays the role of the common characteristic.

2.2.1 Fokker–Planck Equation

The equation which gives the time evolution of the probability density for the system governed by the multidimensional stochastic differential equation (2.14) is the Fokker–Planck equation [23, 24, 81] and reads as

$$\frac{\partial p(r,t)}{\partial t} = -\sum_i^n \frac{\partial}{\partial r_i} A_i(r)\, p(r,t) + \frac{1}{2} \sum_i^n \sum_j^n \frac{\partial^2}{\partial r_i \partial r_j} B_{ij}(r)\, p(r,t)\,. \tag{2.22}$$

The initial condition (2.15) is included by the conditional probability

$$p(r,t|r_0,t_0) = \delta(r - r_0) \tag{2.23}$$

and the normalization condition has to be fulfiled

$$\int_{\mathbb{R}^n} p(r,t)\, dr = 1\,. \tag{2.24}$$

The equation (2.22) can be written in the form of continuity equation [24, 81]

$$\frac{\partial p(r,t)}{\partial t} = -\sum_i^n \frac{\partial J_i(r,t)}{\partial r_i} \tag{2.25}$$

in terms of flux $J_i(r,t)$

$$J_i(r,t) = A_i(r)\,p(r,t) - \frac{1}{2}\sum_j^n \frac{\partial}{\partial r_j} B_{ij}(r)\,p(r,t)\,. \tag{2.26}$$

Hence, the stationary solution $p^{st}(r)$ can be found from the identity

$$\sum_i^n \frac{\partial J_i(r,t)}{\partial r_i} = 0\,. \tag{2.27}$$

For example, the one–dimensional pure diffusion process

$$dx = \sqrt{2\,D}\,dW\,, \tag{2.28}$$
$$x(t=t_0) = x_0 \tag{2.29}$$

with constant diffusion $D > 0$ is considered [24, 34]. In this case, the Fokker–Planck equation takes the simplest form

$$\frac{\partial p(x,t)}{\partial t} = D\,\frac{\partial^2 p(x,t)}{\partial x^2} \tag{2.30}$$

with the initial distribution

$$p(x,t|x_0,t_0) = \delta(x - x_0) \tag{2.31}$$

and the normalization condition

$$\int_{-\infty}^{+\infty} p(x,t)\,dx = 1\,. \tag{2.32}$$

The above–mentioned equation (2.30) is known as *diffusion equation* and has been derived and explained by A. Einstein in 1905 [18]. The Gauss or normal distribution is the solution of the problem (2.30) – (2.31)

$$p(x,t) = \frac{1}{\sqrt{4\,\pi\,D\,t}}\exp\left(-\frac{(x-x_0)^2}{4\,D\,t}\right)\,. \tag{2.33}$$

The diffusion equation (2.30) is a striking example when the analytical solution can be found. In order to check our future numerical results we have made the simulation test and have compared it with the theoretical expression (2.33).

It should be mentioned that, in general, the Fokker–Planck equation (2.22) is referred to the class of partial differential equations of the parabolic type [89, 92]. In principle, there are computation schemes for the direct integration of equations of this class [88]. Here, we would like to present the numerical algorithm for the integration of the diffusion equation (2.30) by way of the statistical analysis [35]. The next procedure presents the method to get the probability density $p(x, t)$ for fixed (observation) time t_{obs} in the interval $x \in [x, x + \Delta x]$ numerically. The idea consists in the following:

1. Generate the ensemble of N stochastic trajectories from stochastic differential equations which correspond to the given Fokker-Planck equation;

2. Calculate the number of trajectories $n_{[x, x + \Delta x]}$ which belong to the interval $[x, x + \Delta x]$;

3. Calculate the probability density $p_{[x, x + \Delta x]}$ that at the time moment t_{obs} the system is in the interval $[x, x + \Delta x]$

$$p_{[x, x+\Delta x]} = \frac{n_{[x, x+\Delta x]}}{N \cdot \Delta x} . \tag{2.34}$$

Following the explained procedure and *Box-Müller method*, the numerical calculation of the probability density distribution have been performed for the ensemble of 2 million trajectories specified by the stochastic differential equation (2.28). The observation time have been chosen as $t_{obs} = 1$ s. The result is shown in Fig. 2.2. Fig. 2.3 presents the influence of the observation time t_{obs} on the probability density distribution $p(x, t)$. Expectedly, there is the tendency that probability density decreases with the growth of time and the solution tends to zero for a large enough time $t_{obs} \to \infty$.

For completeness of the numerical analysis, the statistical error χ^2

$$\chi^2 = \frac{1}{N_x} \sum_{i=1}^{N_x} \left(p_{theory}(x_i) - p_{simulate}(x_i) \right)^2 \tag{2.35}$$

together with the global error ε

$$\varepsilon = \max_{i=1, \cdots N_x} |p_{theory}(x_i) - p_{simulate}(x_i)| \tag{2.36}$$

have been calculated for different numbers N of the generated trajectories [11]. The parameter N_x means the size of the numerical discretisation for coordinate x and can be obtained by

$$N_x = \text{int} \left[\frac{x_{max} - x_{min}}{\Delta x} \right] , \tag{2.37}$$
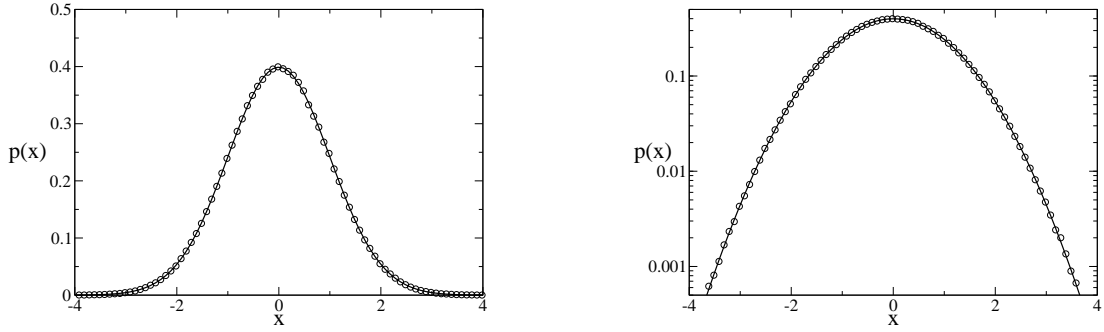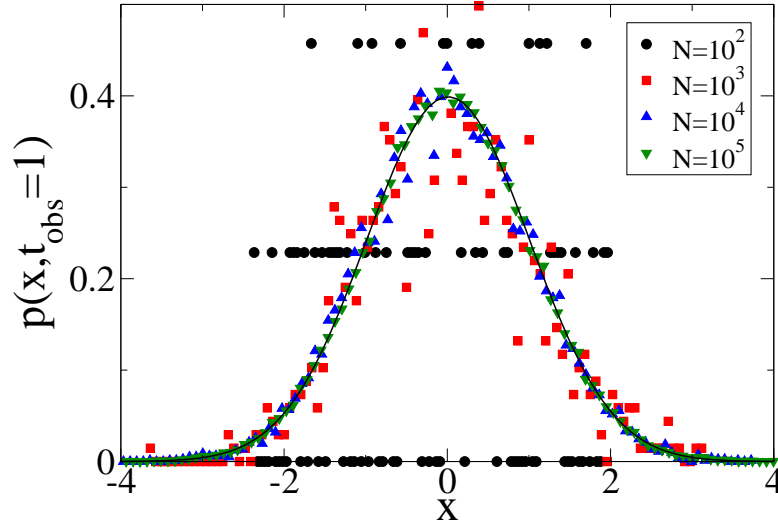
Fig. 2.2: Numerical results (circles) obtained by the procedure (2.34) for the solution $p(x, t)$ of the one–dimensional diffusion equation (2.30) with diffusion constant $D = 1$ m^2/s for an ensemble of 2 millions trajectories generated by Box–Müller method with the initial condition $x(t = 0) = x_0 = 0$ m and for the observation time $t = t_{obs} = 1$ s. The simulation has been done for $\Delta t = 10^{-2}$ s and $\Delta x = 10^{-1}$ m. The theoretical normal distribution given by the equation (2.33) is shown by the smooth curve. The right plot presents the same results but in logarithmic scale.
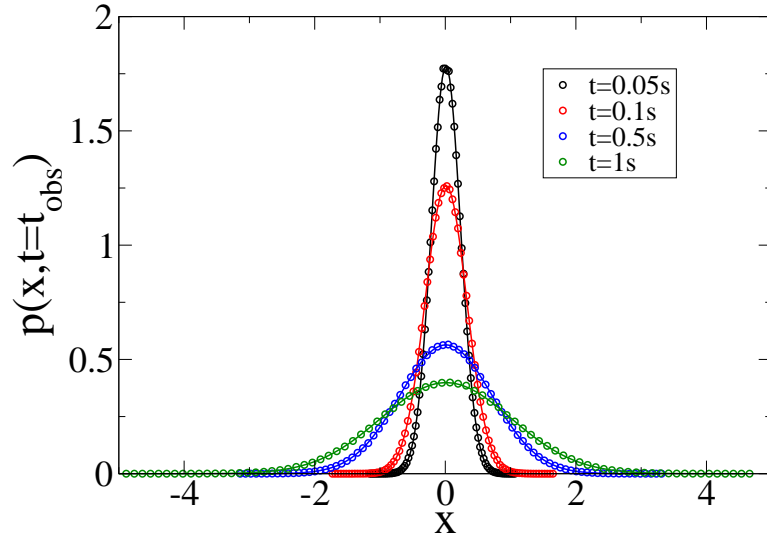
**Fig. 2.3:** Numerical results obtained by the procedure (2.34) for the solution $p(x, t)$ of the diffusion equation (2.30) with diffusion constant $D = 1$ m^2/s for an ensemble of 1 millions trajectories with the initial condition $x_0 = 0$ m for $t = 0$ s for the different observation times t_{obs}, i. e. from the bottom to the top $t_{obs} = 1$ s, $t_{obs} = 0.5$ s, $t_{obs} = 0.1$ s, $t_{obs} = 0.05$ s, respectively.

Tab. 2.1: The statistical χ and global ε errors calculated by formulae (2.35) and (2.36) respectively for different ensemble sizes N. The computing time T is measured in seconds.

N	χ^2	ε	$T,\ s$
10^1	0.6004	1.7469	0.004
10^2	$3.0246 \cdot 10^{-2}$	0.5204	0.012
10^3	$1.5530 \cdot 10^{-3}$	0.1353	0.080
10^4	$1.4036 \cdot 10^{-4}$	$4.7264 \cdot 10^{-2}$	0.340
10^5	$5.7380 \cdot 10^{-5}$	$2.0790 \cdot 10^{-2}$	2.896
10^6	$3.9776 \cdot 10^{-5}$	$1.5627 \cdot 10^{-2}$	28.262

Fig. 2.4: Numerical results (symbols) obtained by the procedure (2.34) for the solution $p(x,t)$ of the one–dimensional diffusion equation (2.30) with diffusion constant $D = 1$ m^2/s for the different ensemble size N trajectories generated by Box–Müller method with the initial condition $x(t = 0) = x_0 = 0$ m and for the observation time $t = t_{obs} = 1$ s. The simulation has been done for $\Delta t = 10^{-2}$ s and $\Delta x = 10^{-1}$ m. The theoretical normal distribution given by the equation (2.33) is shown by the smooth curve.
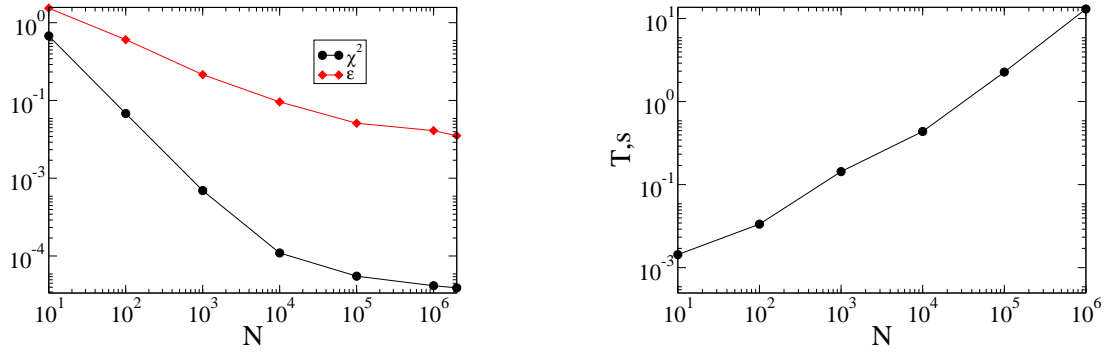
Fig. 2.5: The numerical error analysis is shown. The left plot is the statistical χ^2 and global ε errors as functions of ensemble size N (see Tab. 2.1 and Fig. 2.4). The right figure is the N–dependence of the computing time T measured in seconds.

where x_{max} and x_{min} are the maximum and minimum value of simulated points x_i. The problem of the optimal ensemble size N is discussed and results are explained by Tab. 2.1 and in Figs. 2.4 and 2.5.

The obvious example of the multidimensional Fokker–Planck equation is the Brownian motion described by the stochastic differential equations (2.18) – (2.19) [6, 24]. In this case of Ornstein–Uhlenbeck, the dynamics is given by

$$\frac{\partial p(x,v,t)}{\partial t} = -\frac{\partial}{\partial x}\left(v\,p(x,v,t)\right) + \gamma\,\frac{\partial}{\partial v}\left(v\,p(x,v,t)\right) + B\,\frac{\partial^2}{\partial v^2}p(x,v,t) \qquad (2.38)$$

taking into account the initial condition

$$p(x,v,t=0) = \delta(x-x_0)\,\delta(v-v_0)\,. \qquad (2.39)$$

The equation (2.38) can be considered as the one-dimensional Fokker–Planck equation for the velocity distribution $p_v(v,t)$ after the transformation

$$p_v(v,t) \;=\; \int_{-\infty}^{+\infty} p(x,v,t)\,dx \qquad (2.40)$$

and the probability density function $p_v(v,t)$ is the solution of the problem

$$\frac{\partial p_v(v,t)}{\partial t} = \gamma\,\frac{\partial}{\partial v}\left(v\,p_v(v,t)\right) + B\,\frac{\partial^2}{\partial v^2}p_v(v,t) \qquad (2.41)$$

with $p_v(v,t=0) = \delta(v-v_0)$. Due to the relation (2.27), the stationary probability density $p^{st}(v)$ satisfies the equality

$$\frac{d}{dv}\left[\gamma\,v\,p^{st}(v) + B\,\frac{d}{dv}p^{st}(v)\right] = 0\,. \qquad (2.42)$$

Taking into account that $p^{st}(v \to \infty) = 0$, the following identity holds

$$\gamma \, p^{st}(v) + B \, \frac{d}{dv} p^{st}(v) = 0 \, . \tag{2.43}$$

The transformation $u(v) = \ln(p^{st}(v))$ simplifies the integration and the equation for $u(v)$ reads as

$$\frac{du}{dv} = -\frac{\gamma}{B} \, v \tag{2.44}$$

and allows to get the solution for $u(v)$

$$u(v) = -\mathcal{N} \frac{\gamma}{2 \, B} \, v^2 \tag{2.45}$$

with an accuracy of the integration constant $\mathcal{N}$. Taking into account the inverse transformation $p^{st} = \exp(u(v))$ together with the initial condition $p_v(v, t = 0) = \delta(v - v_0)$ and the normalization (2.24), the stationary solution for the velocity distribution function $p^{st}(v)$ has the form

$$p^{st}(v) = \sqrt{\frac{\gamma}{2 \, \pi \, B}} \cdot \exp\left(-\frac{\gamma}{2 \, B} \, v^2\right) \, . \tag{2.46}$$

Fig. 2.6 illustrates the function (2.46) together with an example of the motion of a Brownian particle obtained numerically by using the algorithm called *explicit 1.5 order strong scheme* [48].

On the other hand, these are no interactions between Brownian particles. Hence, the previous result (2.46) has to coincide with the Maxwell distribution

$$p^{st}(v) = \sqrt{\frac{m}{2 \, \pi \, k_B \, T}} \cdot \exp\left(-\frac{m \, v^2}{2 \, k_B \, T}\right) \tag{2.47}$$

with the temperature T, Boltzmann constant k_B and the particle mass m. Then, the following correspondence holds

$$B = \frac{\gamma \, k_B \, T}{m} \, . \tag{2.48}$$

The relation (2.48) is known as *fluctuation–dissipation theorem*. Its first explanation has been given by Einstein in 1905 [18] and based on the fact that the viscous friction γ of a Brownian particle has to be connected to the diffusion constant B, i. e. the deterministic force F_{det} (friction force) should be related to the stochastic force F_{stoch} (see Sec. 2.1.2).

2.2.2 Master Equation

The differential form of the Chapman–Kolmogorov equation [24, 66] for Markov processes is called the master equation [38] and reads as

$$\frac{\partial p(x, t)}{\partial t} = \int \left[w(x, x') p(x', t) - w(x', x) p(x, t) \right] dx' \, , \tag{2.49}$$
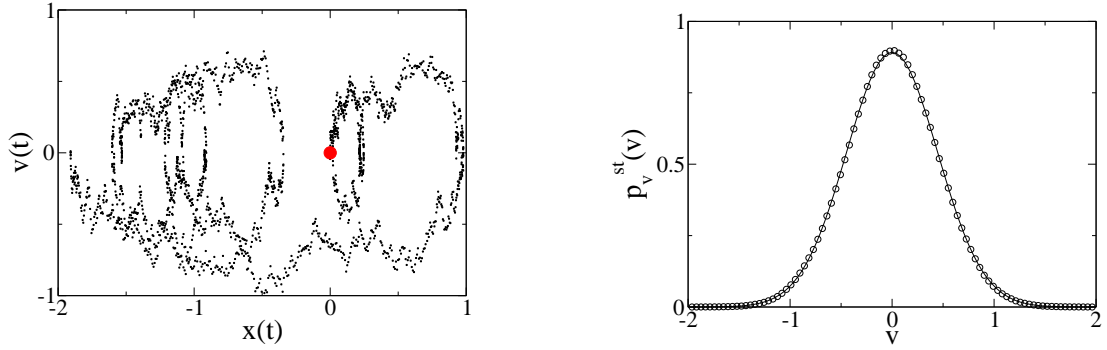
Fig. 2.6: The left diagram shows the realization of the Brownian motion described by the set of equations (2.18)–(2.19) on the phase space of the coordinate x and velocity v for the first 10 s of the motion. The initial position $x(t = 0) = x_0 = 0$ m and $v(t = 0) = v_0 = 0$ m/s is marked by the circle. The right plot presents the stationary velocity distribution calculated numerically (circles) and is compaired with the analytical solution (2.46). The following parameters have been used: $\gamma = 0.5$ s^{-1}, $B = 0.1$ m^2/s^3.

where $w(x, x')$ are transition probabilities per time unit and have to be defined according to the problem under consideration. The analytical solution $p(x, t)$ should be found by means of the direct integration of the integro–differential equation (2.49) with respect to time t. Unfortunately, there are only some special cases when it is possible. It is significant that the master equation (2.49) can be approximated by Fokker–Planck equation (2.22) [24,38]. Hence, in the case when it is impossible to get the exact solution of (2.49), its expansion to the Fokker–Planck equation (2.22) has to be done. The explained transformation is known as Kramers–Moyal equation or expansion [24] and given by

$$\frac{\partial p(x,t)}{\partial t} = \sum_{i=1}^{+\infty} \frac{(-1)^i}{i!} \frac{\partial^i}{\partial x^i} \left(\alpha_i(x,t)\, p(x,t) \right), \qquad (2.50)$$

where function $\alpha_i(x, t)$ is the i–th moment of the transition probability $w(x, x')$

$$\alpha_i(x,t) = \int_{-\infty}^{+\infty} (x - x')\, w(x, x')\, dx' . \qquad (2.51)$$

The truncation of the expression (2.50) for $i = 1, 2$ produces the Fokker–Planck equation.

If the stochastic variable x takes the discrete states n, then the dintegro–differential equation 2.49) reduces to

$$\frac{\partial p(n,t)}{\partial t} = \sum_{n' \neq n} \left[w(n, n')\, p(n', t) - w(n', n)\, p(n, t) \right] . \qquad (2.52)$$
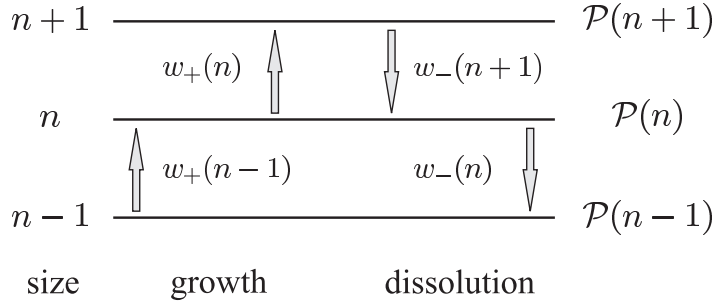
Fig. 2.7: Possible variation of the stochastic variable n for the one–step process described by the master equation (2.53).

The well–known and extensively used example of such a problem is a *birth–death process*. In this case, the discrete stochastic variable $n \geq 0$ is interpreted as the current size of a population ($n = 0, 1, 2, \ldots N$) and can change only by ± 1 per event. The increasing ($n \rightarrow n+1$) or decreasing ($n \rightarrow n-1$) of the population size happend due to the beforehand defined transition rules $w_+(n)$ and $w_-(n)$ respectively. The birth-death or generation–recombination process belongs to the *one–step process* and its dynamics is described by the *one–step master equation*

$$\frac{\partial p(n,t)}{\partial t} = w_+(n-1)p(n-1,t) + w_-(n+1)p(n+1,t) - [w_+(n) + w_-(n)]\, p(n,t)\,,$$
(2.53)

where $w_+(n)$ and $w_-(n)$ can be interpreted as the *growth* and the *dissolution* transition rates respectively to increase or decrease the stochastic variable n by one per time unit. The schematic illustration of a such a procedure is shown on Fig. 2.7.

By analogy with the diffusion equation (2.30) the numerical solution of probability density $p(n,t)$ can be found. As before, an ensemble of N stochastic trajectories $n(t)$ has to be generated. The simulation algorithm of the one–step process is under consideration. The method with stochastic time step Δt has been used according to the following procedure:

1. Calculate transition probabilities $w_+(n_{old})$ and $w_-(n_{old})$;

2. Calculate conditional probability y_1 that a jump takes place and n decrease

$$y_1 = \frac{w_-(n_{old})}{w_+(n_{old}) + w_-(n_{old})}$$
(2.54)

3. Generate uniform distributed random numbers ξ_1 from the interval $[0, 1]$;

4. Calculate stochastic step size Δt

$$\Delta t = -\frac{\ln \xi_1}{w_+(n_{old}) + w_-(n_{old})}\,;$$
(2.55)
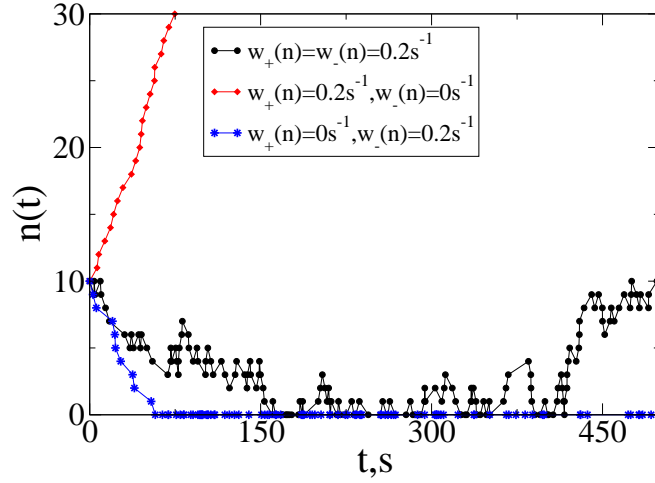
Fig. 2.8: Three stochastic trajectories for the one–step process governed by the master equation (2.53) with constant transition rates $w_-(n) = w_1$ and $w_+(n) = w_2$ obtained by the numeric method for the random time step have been generated. Three different cases are shown, i.e. the circles illustrate the time evolution for $w_1 = w_2 = 0.2$ s^{-1}, the diamond points describe the pure growth process with $w_1 = 0$ s^{-1} and $w_2 = 0.2$ s^{-1} and the stars reflect the dissolution process with $w_1 = 0.2$ s^{-1} and $w_2 = 0$ s^{-1}.

5. Increase the time by $t_{new} = t_{old} + \Delta t$;

6. Generate a uniform distributed random numbers ξ_2 from the interval $[0, 1]$;

7. Check whether $\xi_2 < y_1$;

8. If "yes" then $n_{new} = n_{old} - 1$, otherwise $n_{new} = n_{old} + 1$ for t_{new}.

The realization of the explained algorithm and the influence of the transition rates $w_-(n)$ and $w_+(n)$ are shown on Fig. 2.8. Finally, the probability density $p(n,t)$ is calculated by the same way as explained in Section 2.2.1.

2.3 Active Brownian Particles

We have already mentioned in Introduction that the object of our current investigations is the understanding of the nature of complex systems taking as an example the vehicular traffic. One main distinctive property of such a system is the fact that the system consists of so–called *driven particles* [29]. In this case, the system under consideration is open and dissipative. As a result, due to the influence of driving and friction contributions into the car dynamics, the energy of the system is not conserved.

For example, let us introduce here the active Brownian particle dynamics [91]. The motion of usual Brownian particles is given by the system of stochastic differential equations (2.18) – (2.19) with the friction constant γ and the diffusion term B. Taking into account the energy exchange with the environment, the influence of the energy depot function $e(t)$ should be added to the system of stochastic differential equations (2.18)–(2.19). The additional equation has the form

$$\frac{d}{dt}e(t) = q(x) - c\,e(t) - d(v)\,e(t) \tag{2.56}$$

with the following contributions:

- $q(x)$ is the energy flux into depot;

- $c\,e(t)$ is stored energy which is proportional to energy depot $e(t)$ with coefficient c;

- $d(v)\,e(t)$ is conversion of internal energy into motion and $d(v)$ is the rate of conversion of internal energy into kinetic energy.

Furtheron the simplest ansatz for $d(v) = d_2\,v^2$ with $d_2 > 0$ will be used.

The main idea of presented explanations is to introduce a nonlinear friction function $\Gamma(v)$ having in mind the energy depot effect. For this fact, let us remind the balance equation for the total energy $E(t)$ of the system. In our case the total energy $E(t)$ consists on two contributions, i. e. kinetic energy $T(t)$ and energy depot $e(t)$. Then,

$$\frac{d}{dt}E(t) = \frac{d}{dt}\left(T(t) + e(t)\right) = \frac{d}{dt}\left(\frac{1}{2}\,m\,v^2 + e(t)\right). \tag{2.57}$$

The temporal change of the kinetic energy $T(t)$ happens due to two facts. One of them is the influence of the friction term included in the equation (2.19). Another reason is the conversion of depot energy $e(t)$ into the kinetic energy $d_2\,v^2\,e(t)$ (2.56). Hence,

$$\frac{d}{dt}T(t) = (d_2\,e(t) - \gamma)\,v^2. \tag{2.58}$$

Using (2.57) and (2.58), the resulting balance equation reads as

$$\frac{d}{dt}E(t) = q(x) - c\,e(t) - \gamma\,v^2. \tag{2.59}$$

The extension of the equation (2.58)

$$\frac{d}{dt}\left(\frac{1}{2}\,m\,v^2\right) = m\,v\,\frac{dv}{dt} = (d_2\,e(t) - \gamma)\,v^2, \tag{2.60}$$

$$m\,\frac{dv}{dt} = -\,(\gamma - d_2\,e(t))\,v \tag{2.61}$$

provides the connection between equations (2.18) – (2.19) and (2.56). Finally, the system will be described by the following set of the stochastic differential equations

$$dx = v\,dt\,, \tag{2.62}$$

$$dv = -\Gamma(v)\,v\,dt + \sqrt{2\,B}\,dW(t)\,, \tag{2.63}$$

$$\frac{d}{dt}e(t) = q(x) - c\,e(t) - d_2\,v^2\,e(t)\,, \tag{2.64}$$

where $\Gamma(v) = \gamma - d_2\,e(t)$ is the velocity–depended friction function.

The corresponding Fokker–Planck equation to the system of equations (2.62) – (2.64) has the form

$$\frac{\partial p(x,v,t)}{\partial t} = -\frac{\partial}{\partial x}\left(v\,p(x,v,t)\right) - \frac{\partial}{\partial v}\left(F(v)\,p(x,v,t)\right) + B\,\frac{\partial^2}{\partial v^2}p(x,v,t)\,, \tag{2.65}$$

where $F(v) = -\Gamma(v)\,v$. We would like to find the stationary solution of the reduced probability density $p^{st}(v)$ given by the expression (2.40). Due to these assumptions, the following equation should be solved

$$-\frac{d}{dv}\left(F(v)\,p^{st}(v)\right) + B\,\frac{d^2}{dv^2}p^{st}(v) = 0 \tag{2.66}$$

or in the equivalent form

$$\frac{d}{dv}\left[-F(v)\,p^{st}(v) + B\,\frac{d}{dv}p^{st}(v)\right] = 0 \tag{2.67}$$

from which follows that

$$-F(v)\,p^{st}(v) + B\,\frac{d}{dv}p^{st}(v) = 0\,. \tag{2.68}$$

The transformation $u(v) = \ln(p^{st}(v))$ simplifies the integration. The transformed equation reads
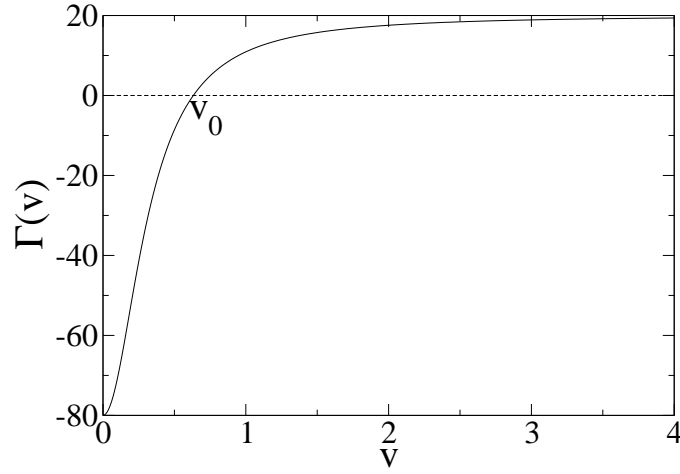
$$\frac{du}{dv} = \frac{1}{B}\,F(v) \tag{2.69}$$

and allows us to get the solution for $u(v)$ in the form

$$u(v) = \frac{1}{B}\int_0^v F(v)\,dv\,. \tag{2.70}$$

The stationary solution for the velocity distribution function $p^{st}(v)$ reads as

$$p^{st}(v) = \exp\left(\frac{1}{B}\int_0^v F(v)\,dv\right)\,. \tag{2.71}$$

Fig. 2.9: The velocity–depended friction function (2.72). The curve is shown for the following set of parameters: $\gamma = 20$ s^{-1}, $q_0 = 10$ m^2/s^3, $d_2 = 10$ s/m^2, $c = 1$ s^{-1}.

As an example, we consider the following ansatz for the friction function $\Gamma(v)$ [91]

$$\Gamma(v) = \gamma - d_2 \, e_{st} = \gamma - \frac{q_0 \, d_2}{c + d_2 \, v^2} \qquad (2.72)$$

using the stationary solution e_{st} of (2.64) with positive constants γ, q_0, c and d_2. The behaviour of the friction function (2.72) is presented is Fig. 2.9. The dotted line shows the zero axis. This line divides the plot domain on two regions, $\Gamma(v) < 0$ and $\Gamma(v) > 0$. The first case corresponds to the situation of the energy pumping to the system dynamics or, what the same, the acceleration of particle for $v < v_0$ where v_0 is defined by $\Gamma(v_0) = 0$. The second case is the opposite one and can be interpreted as the energy dissipation or the deceleration process for $v > v_0$.

The stationary solution $p^{st}(v)$ of the Fokker–Planck equation with the friction function (2.72) is calculated from (2.71) by using

$$\int_0^v F(v) \, dv = - \int_0^v v \, \Gamma(v) \, dv = -\frac{1}{2} \, \gamma \, v^2 + \frac{1}{2} \, q_0 \ln \left(c + d_2 \, v^2 \right) + F_0 \,, \qquad (2.73)$$

where the integration constant F_0 is equal to $\frac{1}{2} q_0 \ln(c)$. Finally, the stationary solution of Fokker–Planck equation for the velocity distribution (2.66) with the friction function $\Gamma(v)$ given by the expression (2.72) has the form

$$p^{st}(v) = p_0 \left(c + d_2 \, v^2 \right)^{\frac{q_0}{2B}} \exp \left(-\frac{1}{2B} \, \gamma \, v^2 \right) \qquad (2.74)$$

Julia Hinkel
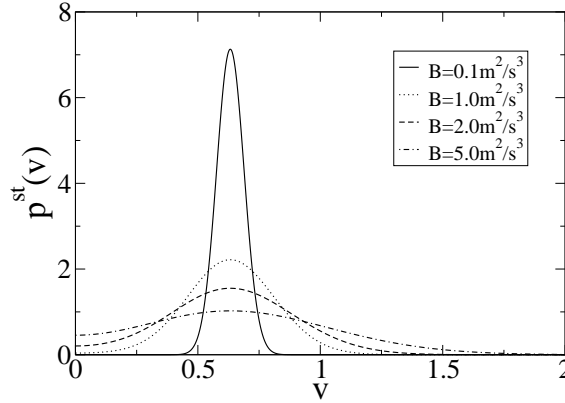
Fig. 2.10: The stationary solution (2.74) of the reduced Fokker–Planck equation (2.66) with velocity depended friction $\Gamma(v)$ according to (2.72). The results are shown for different value of the diffusion constant B. Other parameter are the same as in Fig. 2.9.

with normalisation constant p_0

$$p_0 = \left(\int_0^\infty \left(c + d_2\, v^2 \right)^{\frac{q_0}{2\,B}} \exp\left(-\frac{1}{2\,D}\, \gamma\, v^2 \right) dv \right)^{-1}. \qquad (2.75)$$

Fig. 2.10 illustrates the behaviour of the stationary solution given by (2.74).

In the context of this Chapter, the brief introduction to the theory of stochastic processes has been performed. The main topic of our subsequent explanations is the description of traffic flow. As it has been already mentioned before, the traffic flow has complex structure. The different approaches are proposed in order to analyze such a nontrivial behaviour in details. Therefore, the dynamics including nonlinearity is under consideration. In order to understand the cluster formation, the spatial temporary diagrams together with the velocity changing in time are derived from the corresponding governed equation. In this case, the analysis leads on microscopic level, and equations of motion can be given in the form of (2.14) with or without noise, i.e. stochastic or deterministic description respectively. To represent the general situation on the road, the probabilistic approach based on Fokker–Planck equation (2.22) or on master equation (2.52) should be applied. Such a common characteristic having the probabilistic nature is the *traffic breakdown*. It has been fixed from the empirical data [52], that when the jam reaches its critical size, the motion breaks. The cluster size is defined as a number of cars in jam. According to this fact, the growth or dissolution of cluster size can be investigated, see Fig. 2.7. Such processes are described by the one–step master equation (2.53).

3 Dynamics of Traffic Flow

3.1 Following the Leader Model

This Section is devoted to the description of the models used below. The car following model imitates real traffic on a one–lane road without crossroads. This model takes into account mainly the interaction of the neighboring cars governing their dynamics and ignores car overtakings. Despite this interaction being local in nature, it gives rise to cooperative phenomena that manifests the formation, dissolution and joining of large car clusters. The cooperative phenomena are rather intricate depending on specific values of the control parameters.

The basic element of this approach is the description of a car pair where the lead car moves at the given velocity (e. g. changing with time). The governing equation is written for the following car. Within the standard approximation, the motion of the following car is specified by its coordinate $x_n(t)$ and its velocity $v_n(t)$. Referring to analogy with Brownian motion given by the system of stochastic differential equations (2.16) – (2.17) discussed in Chapter 2, the equation for the acceleration including the deterministic force and Langevin source has the form

$$\frac{dx_n}{dt} \;=\; v_n \,, \tag{3.1}$$

$$m\,\frac{dv_n}{dt} \;=\; F_{det}(x_n, x_{n+1}, v_n, v_{n+1}) + F_{stoch}(x_n, v_n, t) \,, \tag{3.2}$$

where m is the mass of each car. The right hand side of the equation for the acceleration (3.2) contains the total force which represents the sum of all forces acting on the n-th vehicle. The driver collects information about the motion mainly through the visual perception. The information consists of car velocities, accelerations, vehicle spacings and relative velocities. It should be mentioned that the driver is sensitive only to some of these characteristics. According to the obtained information, the driver should make a decision about his driving strategy. In this manner, the equation for the acceleration (3.2) can be interpreted as a response–stimulus relationship. In other words, the driver responds according to a given stimulus derived from the current driving characteristics.

Usually, the deterministic force F_{det} is responsible for the optimal safe motion. Moreover, there are two stimuli affecting the driver's behaviour. One of them is the wish to move as fast as possible, i.e. with the speed v_{n+1} of the leading car. In this manner, the driver should control the velocity difference $v_{n+1} - v_n$. The other
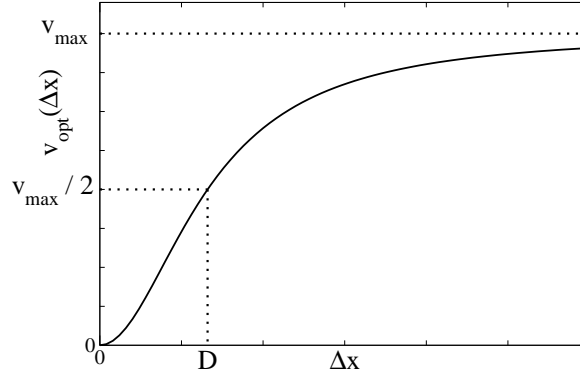
Fig. 3.1: The optimal velocity function $v_{opt}(\Delta x)$ vs headway Δx given by the expression (3.3).

is the necessity to maintain the headway distance $\Delta x_n = x_{n+1} - x_n$ between two neighboring cars with position x_n and x_{n+1} respectively. The headway depends, of course, on the velocity v_{n+1} of the leading car. In particular, the earliest *follow–the–leader* models [78,87] take into account the former stimulus only and leave out the headway Δx_n completely. In contrast to that, the *optimal velocity* model [3,4] directly relates the acceleration to the difference between the current velocity v_n and a certain optimal value $v_{opt}(\Delta x_n)$ at the current headway Δx_n. The dependence of the optimal motion of the headway can be written applying a rather general speculations:

- when the headway decreases $\Delta x_n \to 0$ the optimal velocity is a decreasing function of the headway and becomes zero: $v_{opt}(\Delta x_n \to 0) \to 0$;

- on the empty road, corresponding to the infinitely large headway, the car velocity reaches its maximum allowed velocity: $v_{opt}(\Delta x_n \to \infty) \to v_{max}$.

3.1.1 Bando's Optimal Velocity Model

The idea proposed by Bando et. al. [3,4] consists of the introduction of the smooth and sigmoid function $v_{opt}(\Delta x)$ satisfying the conditions described in the previous Section 3.1. The example of such a function extensively used by Mahnke et. al. [64–67] is given by the following ansatz

$$v_{opt}(\Delta x) = v_{max} \frac{(\Delta x)^2}{D^2 + (\Delta x)^2} \tag{3.3}$$

and shown in Fig. 3.1. The optimal velocity relationship (3.3) contains two parameters, i. e. the maximum velocity v_{max} and the interaction distance D.

In order to explain the structure of the right–hand side of the equation (3.2), let us, at first, consider the pure deterministic model where $F_{stoch}(x, v, t) = 0$.
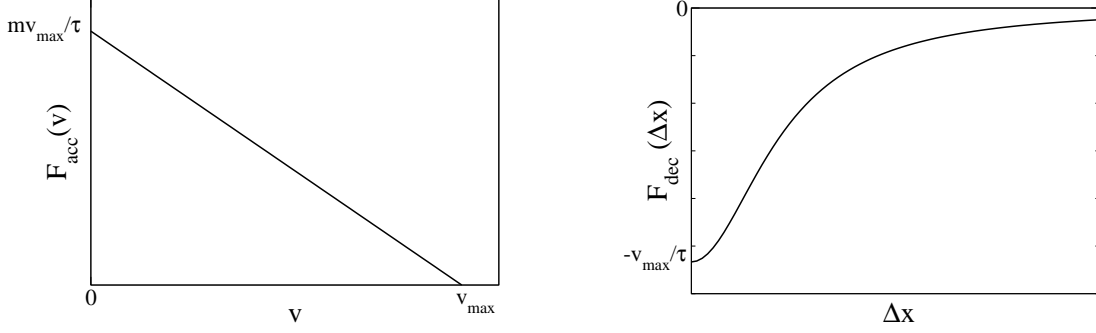
Fig. 3.2: The acceleration $F_{acc}(v)$ (left hand side) and deceleration $F_{dec}(\Delta x)$ (right hand side) forces described by expressions (3.5) and (3.6) respectively.

Under these conditions, the deterministic force $F_{det}(x, v, t)$ can be interpreted as the sum of the acceleration force $F_{acc}(v)$ depending on velocity v and the deceleration force $F_{dec}(\Delta x)$ as a function of headway distance Δx

$$F_{det}(v, \Delta x) = F_{acc}(v) + F_{dec}(\Delta x) \,. \tag{3.4}$$

The acceleration force $F_{acc}(v)$ is introduced as a linear function with the domain $v \in [0, v_{max}]$. When the velocity reaches its maximum value $v = v_{max}$ further acceleration is not possible and $F_{acc}(v = v_{max}) = 0$. That is why, the following expression has been proposed

$$F_{acc}(v) = m \frac{v_{max} - v}{\tau_1} \geq 0 \,, \tag{3.5}$$

where the time scale τ_1 characterizes the driver's response. Following similar arguments, the headway dependence of the deceleration is written as

$$F_{dec}(\Delta x) = m \frac{v_{opt}(\Delta x) - v_{max}}{\tau_2} \leq 0 \,. \tag{3.6}$$

Here, τ_2 is the breaking time. For simplicity, the case of $\tau = \tau_1 = \tau_2$ will be discussed further on. The functions (3.5) and (3.6) are shown in Fig. 3.2. Then, in the general case, the governing equations (3.1) – (3.2) become

$$\frac{dx_n}{dt} = v_n \,, \tag{3.7}$$

$$\frac{dv_n}{dt} = \frac{1}{\tau} \left(v_{opt}(\Delta x_n) - v_n \right) \,, \quad n = 1, \dots, N \,, \tag{3.8}$$

where N is the total number of cars. The sign of the term $v_{opt}(\Delta x_n) - v_n$ determines whether the driver will accelerate when $v_{opt}(\Delta x_n) > v_n$ or decelerate when $v_{opt}(\Delta x_n) < v_n$.

To complete the description of car dynamics $(3.7) - (3.8)$, we consider a circle road of length L or, which is equivalent, the periodic boundary conditions will be used such as

$$\sum_{i=1}^{N} \Delta x_n = 0 \,. \tag{3.9}$$

In order to analyse the system of equations $(3.7) - (3.8)$ in the dimensionless form, the new variables

$$u_n = \frac{v_n}{v_{max}} \,, \quad y_n = \frac{x_n}{D} \,, \quad T = \frac{t}{\tau} \tag{3.10}$$

are introduced and the governing equations becomes

$$\frac{dy_n}{dT} \;=\; \frac{1}{b}\, u_n \,, \tag{3.11}$$

$$\frac{du_n}{dT} \;=\; u_{opt}(\Delta y_n) - u_n \,, \tag{3.12}$$

where the dimensionless optimal velocity function has the form

$$u_{opt}(\Delta y) = \frac{(\Delta y)^2}{1 + (\Delta y)^2} \tag{3.13}$$

and the new control parameter b is defined as

$$b = \frac{D}{\tau \, v_{max}} \,. \tag{3.14}$$

3.1.2 Stability analysis

Let us rewrite the system of $2N$ differential equations of first order $(3.11) - (3.12)$ as

$$\frac{d^2 y_n}{dT^2} = \frac{1}{b}\, u_{opt}(\Delta y_n) - \frac{dy_n}{dT} \,, \quad n = 1, \ldots, N \,. \tag{3.15}$$

The stationary solution of (3.15) is a system of uniformly distributed vehicles with constant speed

$$\Delta y_n^{st} \;=\; \Delta y^{st} = \frac{\mathcal{L}}{N} \,, \tag{3.16}$$

$$u_n^{st} \;=\; u^{st} = u_{opt}(\Delta y^{st}) \,. \tag{3.17}$$

The stationary headway Δy^{st} can be discussed introducing the new parameter c given as

$$c = \frac{N}{\mathcal{L}} \tag{3.18}$$

representing the concentration on the road of length $\mathcal{L} = L/D$. In this case, the stationary headway (3.16) is

$$\Delta y^{st} = \frac{1}{c} \,. \tag{3.19}$$

In order to analyze the stability of the stationary solution (3.15), we consider small perturbations in the car dynamics in its vicinity [4, 29]

$$y_n = \frac{1}{b} u^{st} T + \Delta y^{st} n + \delta y_n \tag{3.20}$$

and

$$\frac{dy_n}{dT} = \frac{1}{b} u_{opt} \left(\Delta y^{st} \right) + \frac{d\delta y_n}{dT} \,. \tag{3.21}$$

The equation related to small perturbations δy_n has the form

$$\frac{d^2 \delta y_n}{dT^2} = \frac{1}{b} \left. \frac{du_{opt}}{d\Delta y} \right|_{\Delta y = \Delta y^{st}} + \frac{d\delta y_n}{dT} \,. \tag{3.22}$$

By virtue of the periodic boundary conditions, the solution of the wave equation (3.22) can be taken as

$$\delta y_n \propto \exp \left(i\,k\,n\,\Delta y^{st} + \gamma\,T \right) , \tag{3.23}$$

where k is the wave vector and γ is the frequency. After substituting of (3.23) into (3.22), the eigenvalue equation for γ gets the form

$$\gamma^2 + \gamma = \frac{1}{b} \left. \frac{du_{opt}}{d\Delta y} \right|_{\Delta y = \Delta y^{st}} \left[\exp \left(i\,\Delta y^{st}\,k \right) - 1 \right] . \tag{3.24}$$

The following situation will be discussed:

- the instability for $\Re(\gamma) > 0$;

- stability threshold for $\Re(\gamma) = 0$;

- stability for $\Re(\gamma) < 0$.

Let us calculate the stability threshold. Due to the vanishing real part, only the pure imaginary roots

$$\Re(\gamma) = 0 \quad \text{or} \quad \gamma = i\,z \tag{3.25}$$

have to be found. According to this assumption, from (3.24) we get

$$-z^2 + i\,z = \frac{1}{b} \left. \frac{du_{opt}}{d\Delta y} \right|_{\Delta y = \Delta y^{st}} \left[i\,\sin \left(\Delta y^{st}\,k \right) - 2\,\sin^2 \left(\frac{1}{2}\,\Delta y^{st}\,k \right) \right] . \tag{3.26}$$

The roots of equation (3.26) are given by

$$z^2 = 2\frac{1}{b}\left.\frac{du_{opt}}{d\Delta y}\right|_{\Delta y = \Delta y^{st}} \sin^2\left(\frac{1}{2}k\,\Delta y^{st}\right) \tag{3.27}$$

and

$$z = 2\frac{1}{b}\left.\frac{du_{opt}}{d\Delta y}\right|_{\Delta y = \Delta y^{st}} \sin\left(\frac{1}{2}k\,\Delta y^{st}\right)\cos\left(\frac{1}{2}k\,\Delta y^{st}\right). \tag{3.28}$$

Finally, the stability threshold reads as

$$b = 2\left.\frac{du_{opt}}{d\Delta y}\right|_{\Delta y = \Delta y^{st}} \cos^2\left(\frac{1}{2}k\,\Delta y^{st}\right) \tag{3.29}$$

and the instability condition for perturbation (3.23) is

$$b < b(c), \tag{3.30}$$

where the function $b(c)$ is given as a function of the car concentration c

$$b(c) = \left.\frac{du_{opt}}{d\Delta y}\right|_{\Delta y = 1/c}\left(1 + \cos\left(\frac{2\pi}{N}\right)\right) = \frac{2\,c^3}{(c^2+1)^2}\left(1 + \cos\left(\frac{2\pi}{N}\right)\right). \tag{3.31}$$

The maximum of $b(c)$ corresponds to the situation when

$$\left.\frac{d^2 u_{opt}}{d\Delta y^2}\right|_{\Delta y = 1/c} = 0. \tag{3.32}$$

The finite–size effect on the phase diagram, where the regions of stable and unstable homogeneous flow are separated by the curve $b(c)$, is illustrated in Fig. 3.3. The homogeneous stationary solution (3.16)–(3.17) transforms into a heterogeneous limit–cycle solution when entering the region below the $b(c)$ curve. The stability of the limit–cycle solution for $N = 60$ cars has been studied numerically, and we have found that it becomes unstable when exiting the region below the dashed curve shown in Fig. 3.3. In other words, like in many physical systems (e. g. supersaturated vapour), we observe a hysteresis effect which is a property of the first–order phase transition.

3.2 Phases of Traffic Flow

The system of equations (3.11) – (3.12) has been integrated numerically by using the Runge–Kutta method of 4–th order [79] with the fixed time step $\Delta T = 10^{-2}$. The ensemble of 150 cars has been considered. Due to the stability analysis presented in Section 3.1.2 and shown in Fig. 3.3, three regimes are under consideration. The following control parameters have been used: $b = 1.1$ and different values of the concentration c
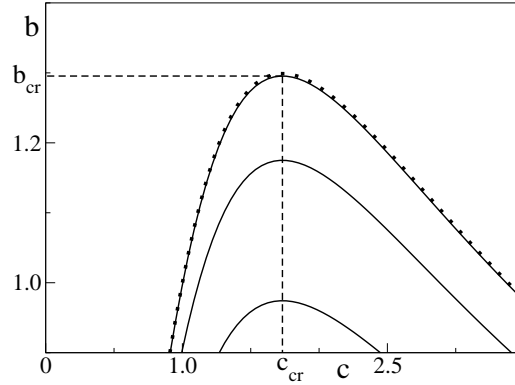
Fig. 3.3: Phase diagram as b-c-plane for a system with fixed different number of cars N. From the bottom to the top solid curves $b(c)$ show the stability border of the homogeneous traffic flow at $N = 6$, $N = 10$, and $N = 60$, respectively. The dotted curve is the function $b(c)$ when N tends to infinity. Each $b(c)$ plot has a maximum at the critical density $c_{cr} = \sqrt{3} \approx 1.732$. The maximum value at $N \to \infty$ is $b_{cr} = 3\sqrt{3}/4 \approx 1.299$.

1. $c = 0.5$ – stable case;

2. $c = 2$ – unstable case;

3. $c = 3.5$ – stable case.

   Initial conditions were specified in the following way: the vehicles are assumed to stand and their positions are randomly determined. This situation is marked in Fig.3.5 by star points. In order to visualize different stages of the car dynamics (3.11) – (3.12), the vehicle distributions is shown for different time intervals. The short–time behaviour is represented in Figs. 3.4 and 3.5 where cars accelerate very fast. Fig. 3.4 visualises the car motion within a time interval required for the one fixed car to run over the whole circle. During this phase typically several clusters form. Their number can be different for various implementations. It is found that the number of clusters is random due to the randomness in initializa-tion of the coordinates. Fig. 3.5 represents this process for different numerical realizations in phase space of velocity $u(T)$ and headway distance $\Delta y(T)$. It should be emphasized, that in spite of different number of clusters forming dur-ing this stage, the velocity of cars in the clusters is the same and rather low. The latter feature allows us to view these clusters as a phase state of traffic flow with specific parameters, in particular with characteristic velocity. Furtheron, the transient time is illustrated in Figs. 3.6 and 3.7. According to the value of the concentration c, two different kinds of the system behaviour have been observed. For small and significantly large concentrations, i. e. $c = 0.5$ and $c = 3.5$ respec-tively, dynamics starts to reach its stable mode. In this case, for $c = 0.5$ cars
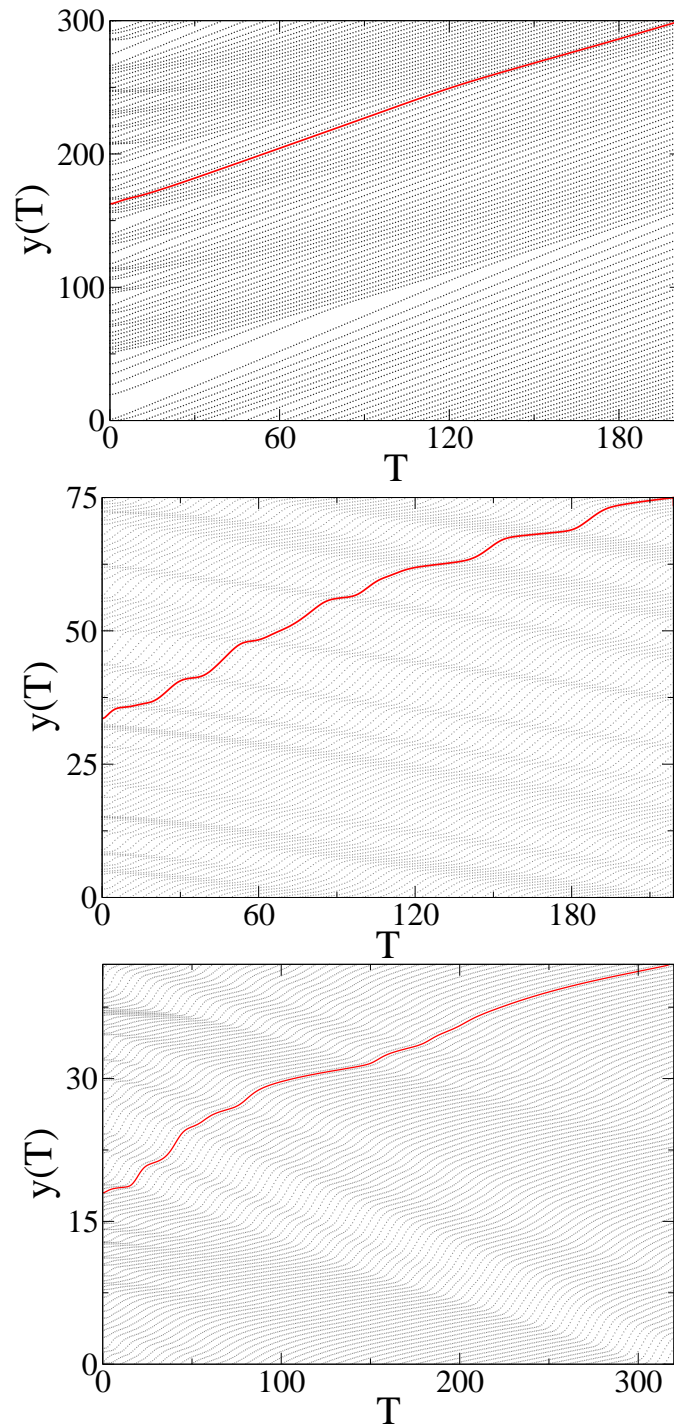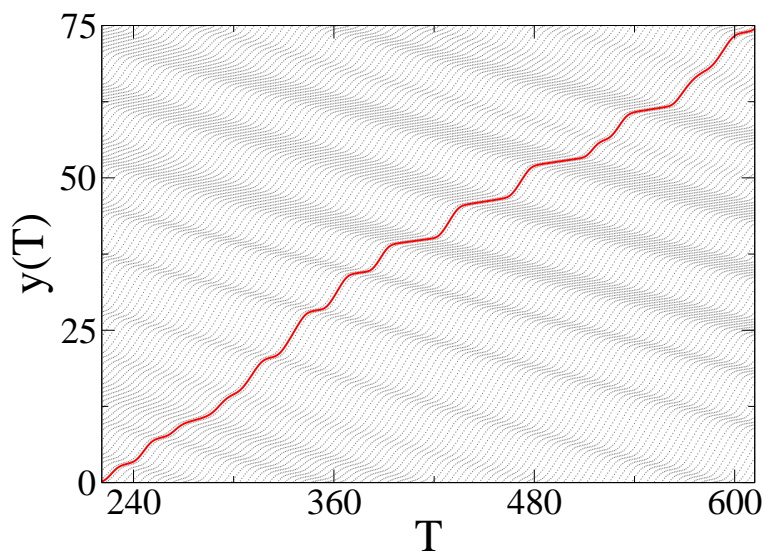
Fig. 3.4: The space time plot $y(T)$ described by the nonlinear dimensionless differential equations (3.11) – (3.12) for the different values of the car concentration c. From bottom to the top $c = 3.5$, $c = 2$, $c = 0.5$. The bold line represents the movement of one particular car.
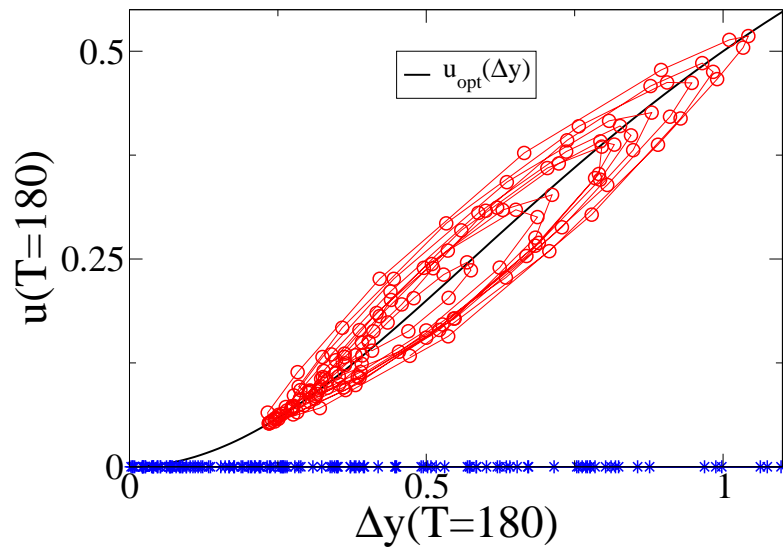
Fig. 3.5: The phase portrait $(\Delta y, u)$ (circles) of the car following model described by the system of equations (3.11) – (3.12) for the fixed time moment $T = 180$ and car concentration $c = 2$. The initial distribution is marked by star points. The bold line shows the dimensionless optimal velocity function (3.13).

Fig. 3.6: The space time plot $y(T)$ described by the differential equations (3.11) – (3.12) for the car concentration $c = 2$. The bold line presents the moving of one particular car.

move relative fast with the velocity $u_n(T) \approx u^{st} = 0.8$ and the headway distances $\Delta y_n(T) \approx \Delta y^{st} = 2$. Whereas, the traffic is so occupied for $c = 3.5$, that the vehicles are almost staying $u_n(T) \approx u^{st} = 0.07$ close to each other with the distance $\Delta y_n(T) \approx \Delta y^{st} = 0.286$. These two regimes are stable and can be interpreted as *free flow* and *heavy traffic*. Fig. 3.6 describes the contrary regime for $c = 2$ which is completely unstable. The system continues its development further on. In this case, the process is characterized by the motion of large numbers of small clusters. Some of them join other clusters and form larger congestions. The competition between clusters takes place. In order to show this effect, velocity $u_{75}(T)$ together with headway $\Delta y_{75}(t)$ have been plotted at $T = 600$ for one particular car. The results are illustrated in Fig. 3.8. The joining of a particle to the cluster can be observed by its velocity drop. The motion in a cluster is determined by low velocities and small headways. In the case of the stable motion, when the traffic is either free ($c = 0.5$) or very dense ($c = 3.5$), the system comes to its stable behaviour relative fast. The tendency of the dynamics has been already visible for the time interval $T \in [0, 600]$ (see Fig. 3.7). The system reaches its stationary point and stays there. Another situation has been observed for the unstable regime ($c = 2$). It takes infinitely long time until the motion can be stabilized and converged to the stable limit cycle. Then, all clusters should be reduced to a fixed number of moving cluster. Figs. 3.9, 3.10 and 3.11 show the long time behaviour. At this stationary regime, two phases of traffic flow occur. The movement of the particles is concentrated in two regions. The region in Fig. 3.12 where the velocity and headway values are close to zero represents the motion in the jam. When a particle leaves the cluster and starts to accelerate, it enters the free flow. After some time, the particle decelerates, the distance to the neighbour car decreases and it joins the jam once again. Such a periodic behaviour is known as *stop–and–go waves*. Both velocities in jam and in free flow have been calculated numerically. A car moves in a cluster with the speed $u_{cluster} = 3.677 \cdot 10^{-2}$. Whereas, the the motion in free flow takes place with the velocity $u_{free} = 0.545$.

3.3 Langevin Approach

Up to now the deterministic car following model has been discussed. In order to consider the stochastic description of traffic flow, the multiplicative Gaussian white noise has been added to the dynamics described by the set of equations (3.11) – (3.12) to the equation for acceleration (3.12)

$$dy_n = \frac{1}{b} u_n \, dT \,, \tag{3.33}$$

$$du_n = (u_{opt}(\Delta y_i) - u_i) \, dT + \sigma u_i \, dW_i(T) \quad n = 1, \dots, N. \tag{3.34}$$
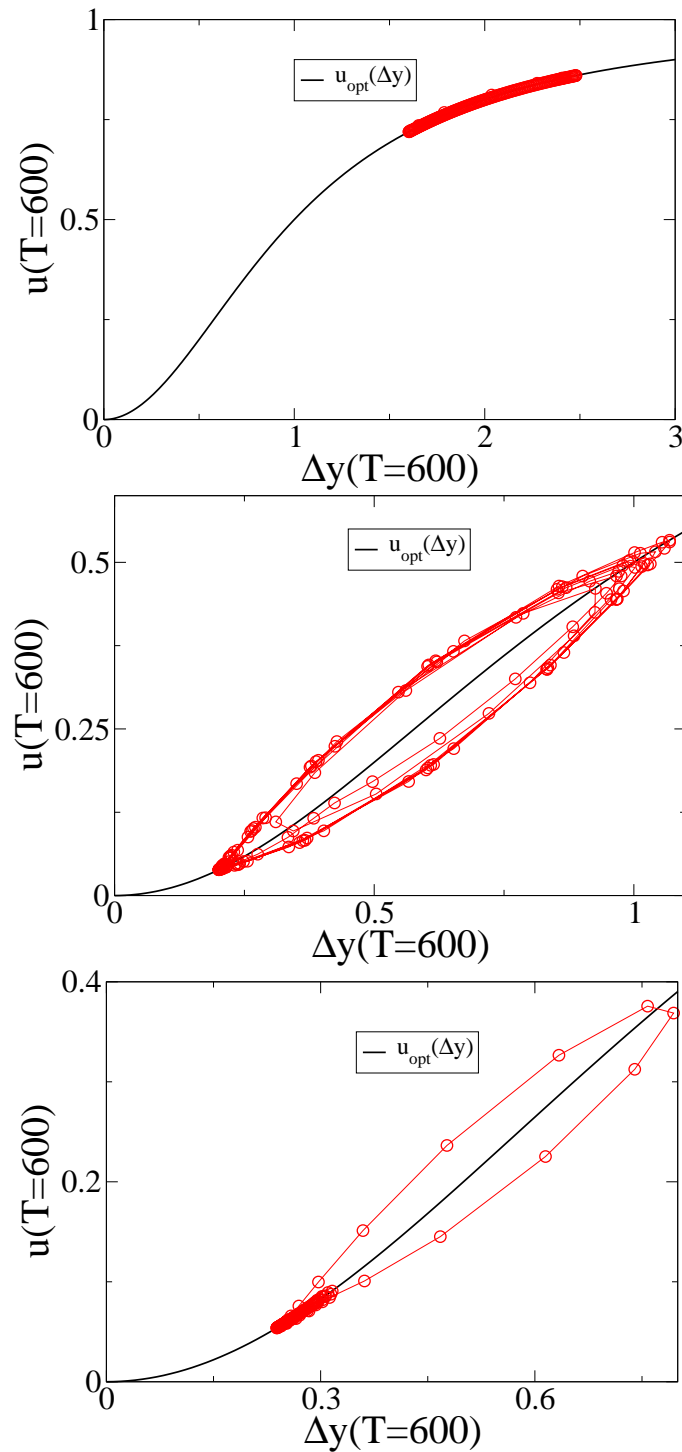
Fig. 3.7: The phase portrait $(\Delta y, u)$ obtained from the car following model described by the system of stochastic differential equations (3.11) – (3.12) for the fixed time moment $T = 600$ for different car concentrations. From bottom to top $c = 3.5$, $c = 2$, $c = 0.5$. The bold line shows the dimensionless optimal velocity function (3.13).
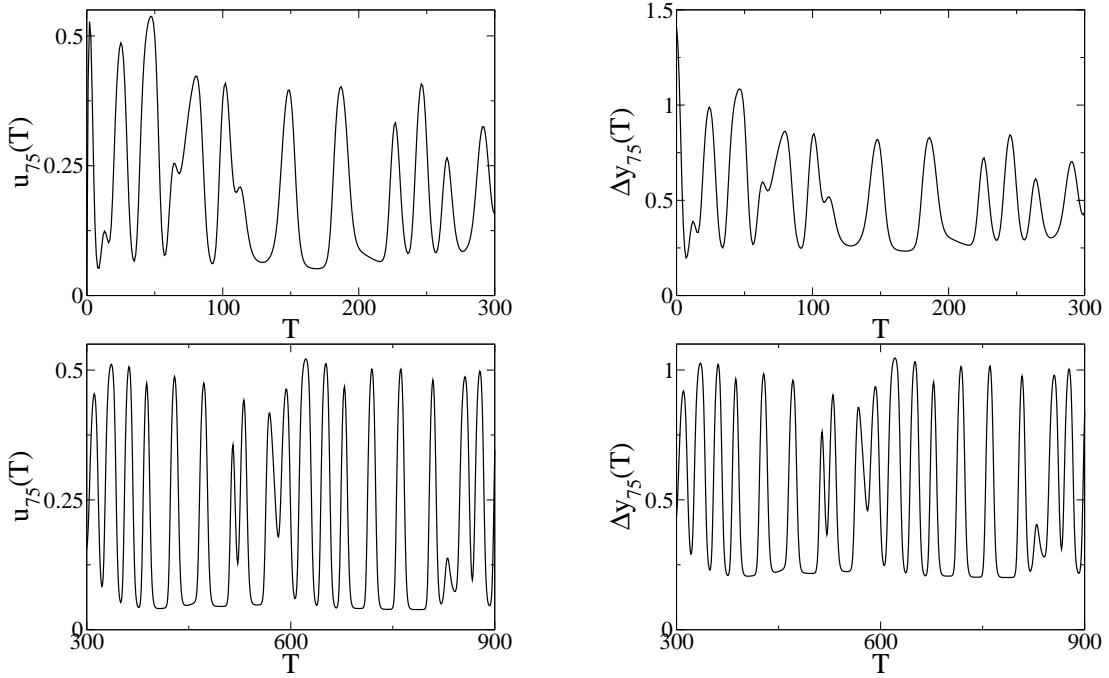
Fig. 3.8: The temporal variation of the velocity $u_{75}(T)$ (left side) and headway $\Delta y_{75}(T)$ (right side) for one particular car $n = 75$ and given concentration $c = 2$.

Here, the new parameter σ is the dimensionless noise amplitude. Such a description is similar to the description of the stochastic differential equations introduced in Chapter 2. For our case, the system (3.33) – (3.34) can be also written in the vector form, compare with (2.14), as

$$dr(T) = A(r, T)\, dT + B(r, T)\, dW(T)\,, \tag{3.35}$$

where $r(T) \in \mathbb{R}^{2N}$ and $A(r, T) \in \mathbb{R}^{2N}$ dimensional vectors

$$r(T) = \begin{pmatrix} y_1(T) \\ \dots \\ y_N(T) \\ u_1(T) \\ \dots \\ u_N(T) \end{pmatrix}, \qquad A(r, T) = \begin{pmatrix} u_1(T) \\ \dots \\ u_N(T) \\ u_{opt}(\Delta y_1) - u_1 \\ \dots \\ u_{opt}(\Delta y_N) - u_N \end{pmatrix}. \tag{3.36}$$

The diffusion $2N \times 2N$ matrix $B(r, T) \in \mathbb{R}^{2N \times 2N}$ has the block structure

$$\mathcal{B}(r) = \begin{bmatrix} \mathcal{O} & \mathcal{O} \\ \mathcal{O} & \mathcal{U}(r) \end{bmatrix}, \tag{3.37}$$

where each block is a $N \times N$ matrix. The matrix $\mathcal{O} \in \mathbb{R}^{N \times N}$ consists of zero elements due to the fact that the stochasticity term accounts for acceleration
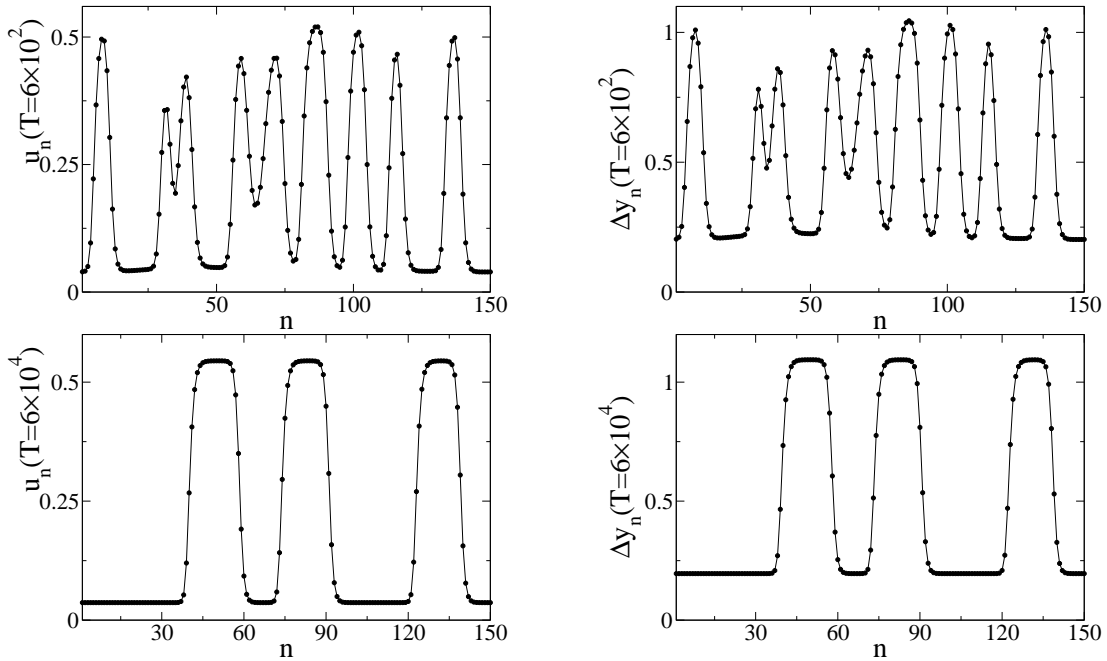
Fig. 3.9: Velocities $u_n(T)$ (left side) and headway distances $\Delta y_n(T)$ (right side) for all particles $n = 1, \ldots, N$ for the concentration $c = 2$ for different time moments.
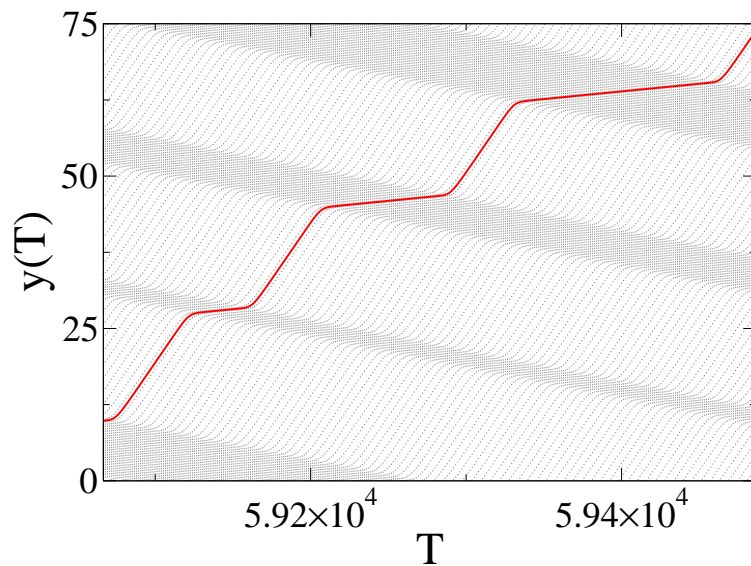
Fig. 3.10: The space time plot $y(T)$ described by the differential equations (3.11) – (3.12) for the car concentration $c = 2$. The bold line presents the moving of one particular car..
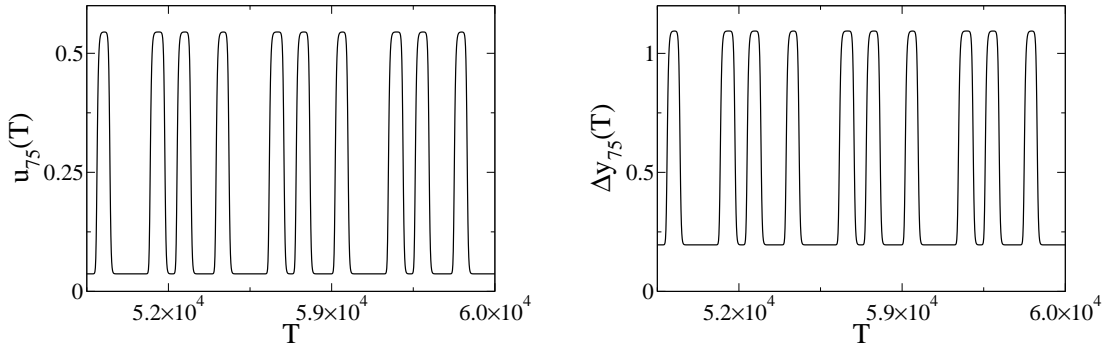
Fig. 3.11: The long time behaviour of the velocity $u_{75}(T)$ (left side) and headway $\Delta y_{75}(T)$ (right side) for one particular car and for the concentration $c = 2$.
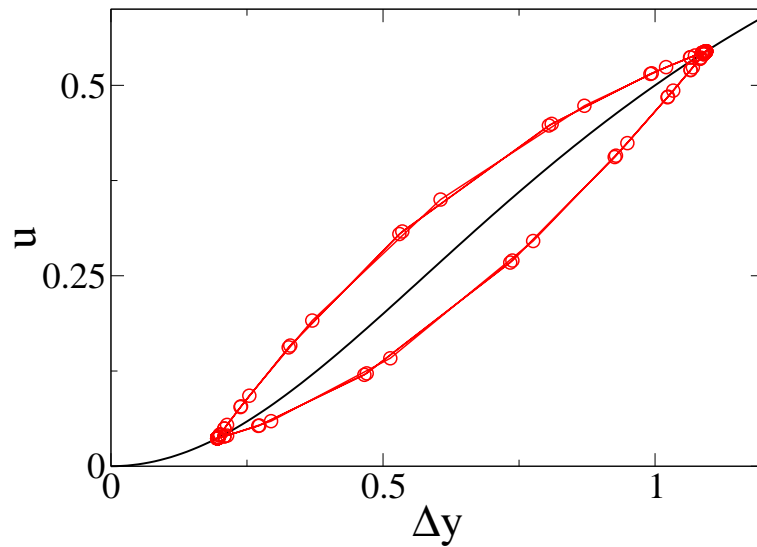
Fig. 3.12: The limit cycle regime for $c = 2$. The circles show the calculated velocities vs headway distances. The solid line presents the theoretical ansatz for the optimal velocity $u_{opt}(\Delta y)$ given by expression (3.13).

only. Hence, the block $\mathcal{U} \in \mathbb{R}^{N \times N}$ is the diagonal matrix and has the form

$$
\mathcal{U}(r) = \begin{bmatrix}
\sigma\, u_1(T) & 0 & \dots & 0 \\
0 & \sigma\, u_2(T) & \dots & 0 \\
\dots & \dots & \dots & \dots \\
\dots & \dots & \dots & \dots \\
0 & 0 & \dots & \sigma\, u_N(T)
\end{bmatrix}. \tag{3.38}
$$

The multiplicative noise has been included to the equation for the acceleration and has been considered in order to control the velocity and to neglect its negative value.

It has been already introduced in Chapter 2 that there is an equivalent probabilistic form of the microscopic stochastic description (3.33) – (3.34) in terms of the probability density $P(u, \Delta y, T)$. In order to obtain the stationary distribution function $P(u, \Delta y)$, the system (3.33) – (3.34) has been simulated by usage of the explicit strong schemes of the 1.5 order [48] for the three values of the car concentration c. We have fixed the control parameter $b = 1.1$ and noise amplitude $\sigma = 0.1$. The integration has been done with the time step $\Delta T = 5 \cdot 10^{-3}$ for the time interval $T \in [0, 10^4]$. Fig. 3.13 shows the stationary probability densities in terms of velocity $P(u)$ and headway distance $P(\Delta y)$ distributions. The unimodal distributions have been obtained for the case of $c = 0.5$ and $c = 3.5$. The maximum of the functions $P(u)$ and $P(\Delta y)$ locates near the stationary point $u^{st} = u_{opt}(y^{st})$ and $\Delta y^{st} = 1/c$ respectively. The one–maximum distributions represent the existence of one phase in traffic flow which can be either free ($c = 0.5$) or dense ($c = 3.5$) traffic. The probability density function for the velocity as well as for the headway becomes a bimodal distributions for the concentration $c = 2$. Each maximum is responsible for the specific scenarios. Thus, one peak corresponds to low velocity and small headway describing the motion in the jam. The second maximum is related to the free flow and defined by high velocity and large headway distance.

Both deterministic and stochastic approaches of the car following model have been carried out. The analysis shows the existence of two phases of traffic flow, i. e. either free or congested. The free flow is characterized by high velocities which are approximately equal to the maximal allowed speed. The congested traffic occurs with the increase of the car concentration. Such a movement is represented by the different numbers of moving clusters with the same velocity close to zero. In this sense, the probability densities of velocities and headway distances have been calculated for the different values of the concentration. The distribution function can become bimodal according to the occupation on the road.
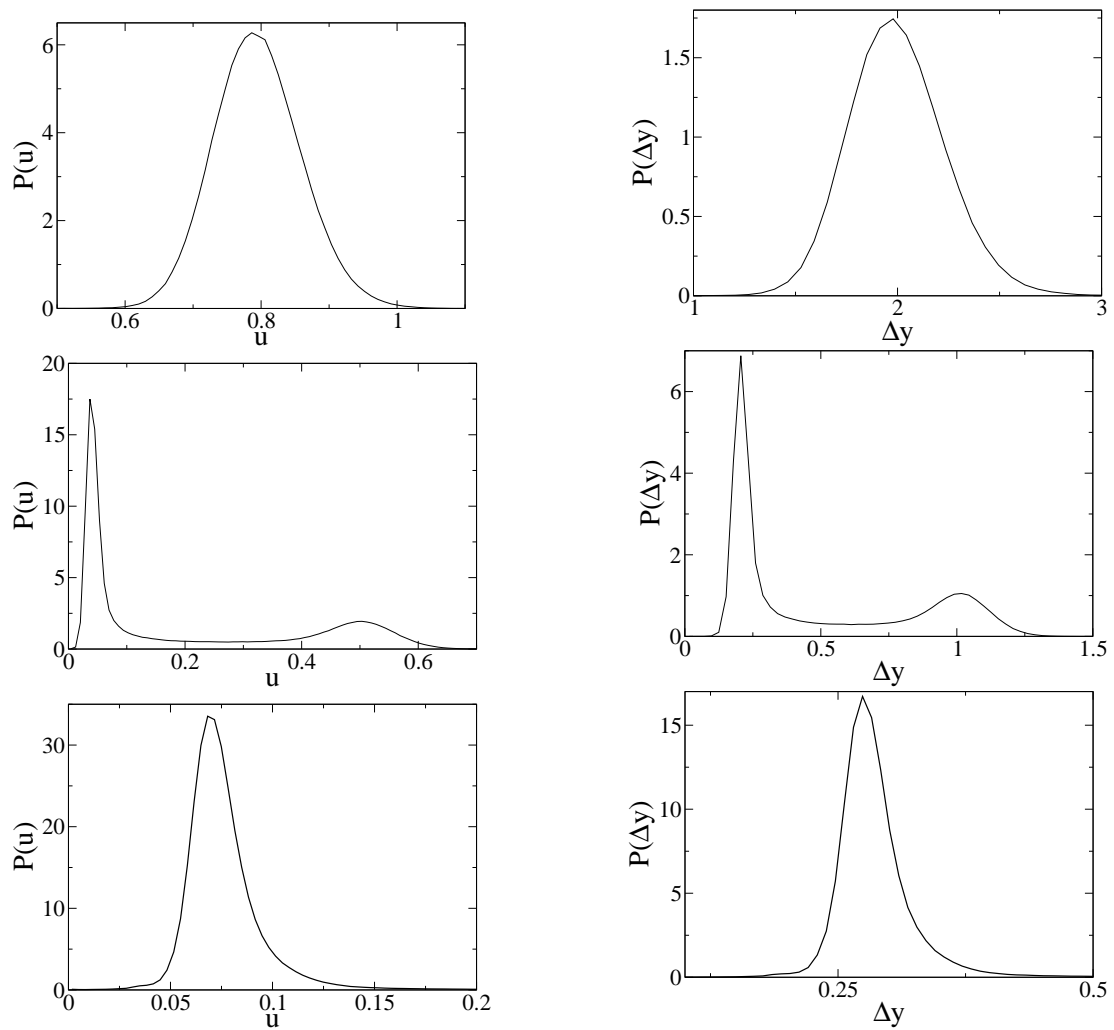
Fig. 3.13: The distribution functions $P(u)$ (left) and $P(\Delta y)$ (right) for the stochastic car following model described by equations (3.33) – (3.34) for different values of the concentration c. From bottom to the top $c = 3.5$, $c = 2$, $c = 0.5$.

3.4 Energy Balance Equation

It has been shown in Section 3.1.1 that on a microscopic level traffic flow can be described by the optimal velocity model (3.7) – (3.8) with the sigmoid optimal velocity function (3.3). In this case the equations of motion have been written as Newton's law with accelerating and decelerating forces which can be interpreted as the dissipative and interacting contributions to the car dynamics

$$m \frac{dv_n}{dt} = \underbrace{F_{acc}(v_n)}_{dissipative\,force} + \underbrace{F_{dec}(\Delta x_n)}_{interacting\,force}, \quad n = 1, \ldots, N. \tag{3.39}$$

The total energy E of the system is defined as a sum of the kinetic energy T and the potential energy U.

$$E = T + U. \tag{3.40}$$

We focus on the fact, that since traffic flow is a dissipative system of driven or active particles the total energy E is not conserved

$$\frac{dE}{dt} \neq 0. \tag{3.41}$$

As a result, the energy balance equation should be held

$$\frac{dE}{dt} + \Phi = 0, \tag{3.42}$$

where the new quantity Φ is the energy flux following from the equations of motion (3.39) and consisting of dissipation (due to friction) and energy input (due to burning of petrol). We would like to constract the total energy E of the car system together with the energy flux function Φ.

The kinetic energy of the many particle system is equal to the sum of kinetic energies of all particles

$$T = \sum_{n=1}^{N} T(v_n) \qquad \text{where} \qquad T(v_n) = \frac{1}{2} m \, v_n^2. \tag{3.43}$$

The potential energy U of the system under consideration is defined as

$$U = \sum_{n=1}^{N} U(\Delta x_n) \qquad \text{with} \qquad U(\Delta x_n) = -\int^{\Delta x_n} F_{dec}(\Delta x_n) \, dx_n + C, \tag{3.44}$$

where C is an integration constant and should be found from the normalization condition. The potential $U(\Delta x_n)$ is the interaction potential of the n-th car with the car ahead $n + 1$, which is given by

$$F_{dec}(\Delta x_n) = -\frac{\partial U(x_{n+1} - x_n)}{\partial x_n} = \frac{dU(\Delta x_n)}{d\Delta x_n}. \tag{3.45}$$

Julia Hinkel

By integrating this equation we get

$$U(\Delta x) = v_{max} \frac{D\,m}{\tau} \left[\frac{\pi}{2} - \arctan\left(\frac{\Delta x}{D}\right) \right] , \qquad (3.46)$$

where the integration constant is chosen in such a way that $U(\Delta x \to \infty) = 0$. For comparison, the interaction potential of the form $U(\Delta x) \propto (\Delta x)^{-\alpha}$ has been considered in [49]. Note that $F_{dec}(\Delta x_n)$ is not given by $-\partial U/\partial x_n$, since the latter quantity includes an additional term $-\partial U(x_n - x_{n-1})/\partial x_n$. This term is absent in our definition of the force because the car behind does not influence the motion of the actual n–th vehicle. It reflects the fact that, unlike in physical systems, the third Newton's law does not hold.

By multiplying both parts of the equation of motion (3.39) with v_n we get

$$\frac{d}{dt}\left(\frac{m\,v_n^2}{2}\right) = F_{acc}(v_n)\,v_n + F_{dec}(\Delta x_n)\,v_n , \quad n = 1, \ldots, N. \qquad (3.47)$$

Taking into account the definition of the kinetic energy (3.43) and the connection between the potential $U(\Delta x_n)$ with the conservative force $F_{dec}(\Delta x_n)$ (3.45) the following equality should be held

$$\frac{d}{dt}T(v_n) = F_{acc}(v_n)\,v_n + \frac{dU(\Delta x_n)}{d\Delta x_n}\frac{dx_n}{dt} , \quad n = 1, \ldots, N. \qquad (3.48)$$

Furthermore, the following mathematical treatment should be performed

$$\begin{aligned}
\frac{dU(\Delta x_n)}{d\Delta x_n}\frac{dx_n}{dt} &= \frac{dU(\Delta x_n)}{d\Delta x_n}\frac{dx_{n+1}}{dt} - \frac{dU(\Delta x_n)}{d\Delta x_n}\frac{d\Delta x_n}{dt} \\
&= F_{dec}(\Delta x_n)\,v_{n+1} - \frac{dU(\Delta x_n)}{dt} , \quad n = 1, \ldots, N.
\end{aligned} \qquad (3.49)$$

Substituting the derived result (3.49) to the equality (3.48), we obtain

$$\frac{d}{dt}\left[T(v_n) + U(\Delta x_n)\right] = F_{acc}(v_n)\,v_n + F_{dec}(\Delta x_n)\,v_{n+1} , \quad n = 1, \cdots, N. \qquad (3.50)$$

Summing the latter equality over n and taking into account relationships (3.40), (3.43) and (3.44) the following energy balance equation is obtained

$$\frac{d}{dt}E + \Phi = 0 , \qquad (3.51)$$

where the energy flux Φ has the form

$$\Phi = -\sum_{n=1}^{N} \left[F_{acc}(v_n)\,v_n + F_{dec}(\Delta x_n)\,v_{n+1}\right] . \qquad (3.52)$$

The energy flux function (3.52) includes both energy dissipation due to friction and energy input from the engine.

Equation (3.51) shows that, in distinction to closed mechanical systems, the total energy is not conserved in traffic flow. Nevertheless, as it has been shown in Section 3.2, it approaches a constant value in the long–time limit. In this case the system converges to one of two possible stationary states: either to the fixed point $\Delta x_n = \Delta x_{st}$, $v_n = v_{opt}(\Delta x_{st})$ (where $\Delta x_{st} = L/N$ is the distance between homogeneously distributed N cars over the road of length L), or to the limit cycle in the phase space of headways and velocities. Both situations are illustrated in Fig. 3.14. The presented results have been obtained numerically for an ensemble of $N = 60$ vehicles by using the same simulation method as in Section 3.2. Here, we have solved the equation of motion (3.7) – (3.8) in the original phase space $(\Delta x_n, v_n)$. Drawing the analogy to the dimensionless case (3.11) – (3.12) discussed in Section 3.2, the simulation parameters for the case of original variables correspond to the dimensionless values in the following way

$$b = \frac{D}{v_{max}\,\tau} = 1.1\,, \tag{3.53}$$

$$c = D\,\rho \quad \text{where} \quad \rho = \frac{N}{L}\,,$$

$$\Longrightarrow c_1 = D\,\rho_1 = 1\,, \quad c_2 = D\,\rho_2 = 2\,. \tag{3.54}$$

At a small enough concentration (ρ_1 or c_1) of cars there is a stable fixed point (solid circle), which lies on the optimal velocity curve (dotted line). An unstable fixed point (empty circle) exists at a larger concentration (ρ_2 or c_2). In the latter case any small perturbation of the initially homogeneous fixed point situation leads to the limit cycle (solid line) in the long–time limit.

The total energy has a certain value in any one of the stationary states. The temporal behaviour of E for the same sets of parameters as in Fig. 3.14 is shown in Fig. 3.15. In the case of the convergence to the limit cycle (solid line) for $\rho_2 = 0.0606$ m^{-1}, one can distinguish 6 plateau in the energy curve. The first one represents the short–time behaviour when starting from an almost homogeneous initial condition with zero velocities, and the second plateau is the unstable fixed point situation. Further on, 4 car clusters have been formed in the actual simulation, and this temporal situation is represented by the third relatively small plateau. The next three plateaus with 3, 2, and finally 1 car clusters reflect the coarse graining or Ostwald ripening process. The dashed line shows the convergence to the stable fixed point value at $\rho_1 = 0.0303$ m^{-1}.

To summarize this Chapter, the following comments should be done: in the long–time limit the many car system tends to certain stationary state. In the microscopic description it is either the fixed–point or the limit cycle in the phase space of velocities and headways depending on the overall car concentration and control parameters. The stationary state is characterised by the specific internal energy.
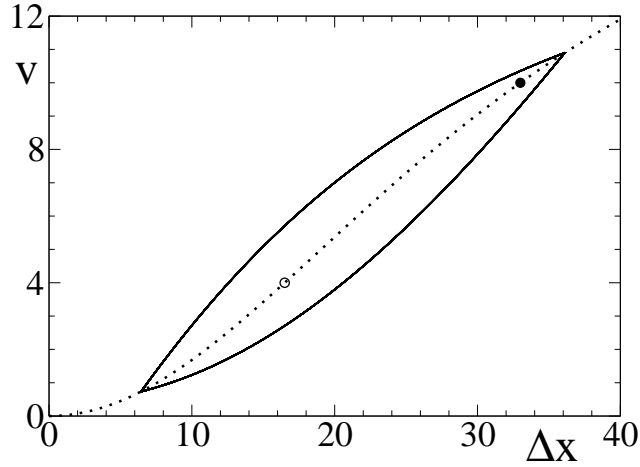
Fig. 3.14: Fixed points (circles) and limit cycle (solid line) in the space of headways Δx and velocities v of cars. The solid circle represents the stable fixed point at the car concentration $\rho_1 = 0.0303$ m^{-1}. The empty circle is the unstable fixed point at a larger concentration $\rho_2 = 0.0606$ m^{-1}, where the long–time trajectory for any car is the limit cycle shown. The fixed points lie on the optimal velocity curve (dotted line) given by (3.3). The parameters are chosen as $N = 60$, $D = 33$ m, $v_{max} = 20$ m/s, $\tau = 1.5$ s, and $m = 1000$ kg.
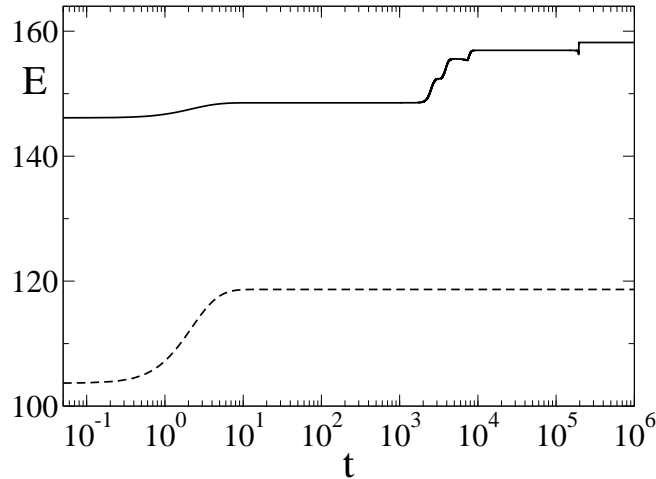
Fig. 3.15: The total energy E of the car system, measured in units of $mv_{max}^2/2$, depending on time t given in seconds. The same sets of parameters have been used as in Fig. 3.14. The upper solid line corresponds to a larger concentration $\rho_2 = 0.0606$ m^{-1} where the limit cycle forms, whereas the lower dashed line — to a smaller concentration $\rho_1 = 0.0303$ m^{-1} where the convergence to stable fixed point is observed.

4 Phase Transitions Caused by Anomalies in Kinetic Coefficient

4.1 Fundamental Diagram

The Bando model (3.7) – (3.8) based on the optimal velocity ansatz (3.3) has been examined in Chapter 3. During the model analyzing, the different states of traffic flow have been observed. By way of the numerical integration of both deterministic (3.7) – (3.8) and stochastic (3.33) – (3.34) approaches, it was found that traffic can be either free or congested. Each traffic phase is characterized by the car concentration c and the average velocity V which can be defined for some fixed observation time as

$$V = \frac{1}{N} \sum_{i=1}^{N} v_i \,. \tag{4.1}$$

By this means, the states of traffic flow can be specified in term of the functional dependence $V(c)$. Applying to the general notion about the driver behaviour, we can suppose that the average velocity V attains its maximum at small concentrations

$$V(c \to 0) = v_{max} \,, \tag{4.2}$$

whereas the motion of cars for large concentrations on the road characterizes by very low velocity

$$V(c = c_{max}) = 0 \,. \tag{4.3}$$

As a result, we can also represent the traffic flow rate q as a function of the contration c

$$q(c) = c \, V(c) \,. \tag{4.4}$$

as the product of the average velocity V and vehicle concentration c. The visualisation of this function (4.4) is called the *fundamental diagram* and characterizes the possible phases of traffic flow. Fig. 4.1 represents schematically the behaviour of the fundamental diagram (4.4) in terms of $V = V(c)$ and $q = q(c)$ dependencies.
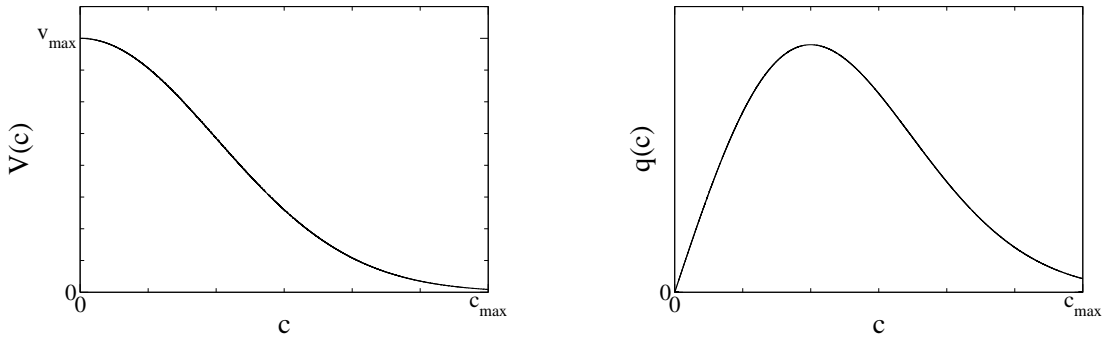
Fig. 4.1: Schematic view of mean velocity V (left) and flux q (right) as functions of vehicular density c.

4.2 Motivations

Turning back to the optimal velocity model discussed in Chapter 3, the following comments should be done. Such a model gives precise separation into two phases of the motion. The traffic can be

- free (small concentration);

- congested (large concentration).

Fig. 4.2 presents the empirical data collected at the German highway A 1 and analyzed by Lubashevsky et. al. [60]. The data shows very complex and heterogeneous structure.

Kerner et. al. [43–47] have explaned such a complexity. The hypothesis proposed by them implies the existence of the three traffic states:

- free flow;

- synchronized flow;

- wide moving jams.

In contrast to the free and congested flow, the synchronized regime is characterized by a not unique correspondence on c–q plane. This effect is shown in Fig. 4.2. According to this fact, the synchronized mode is also referred to as widely scattered states. Following the classification proposed by Kerner and Rehborn there are three distinctive kinds of synchronized flow

1. stationary and homogeneous states where both the average speed V and flow rate q are approximately constant during a fairly long time interval;

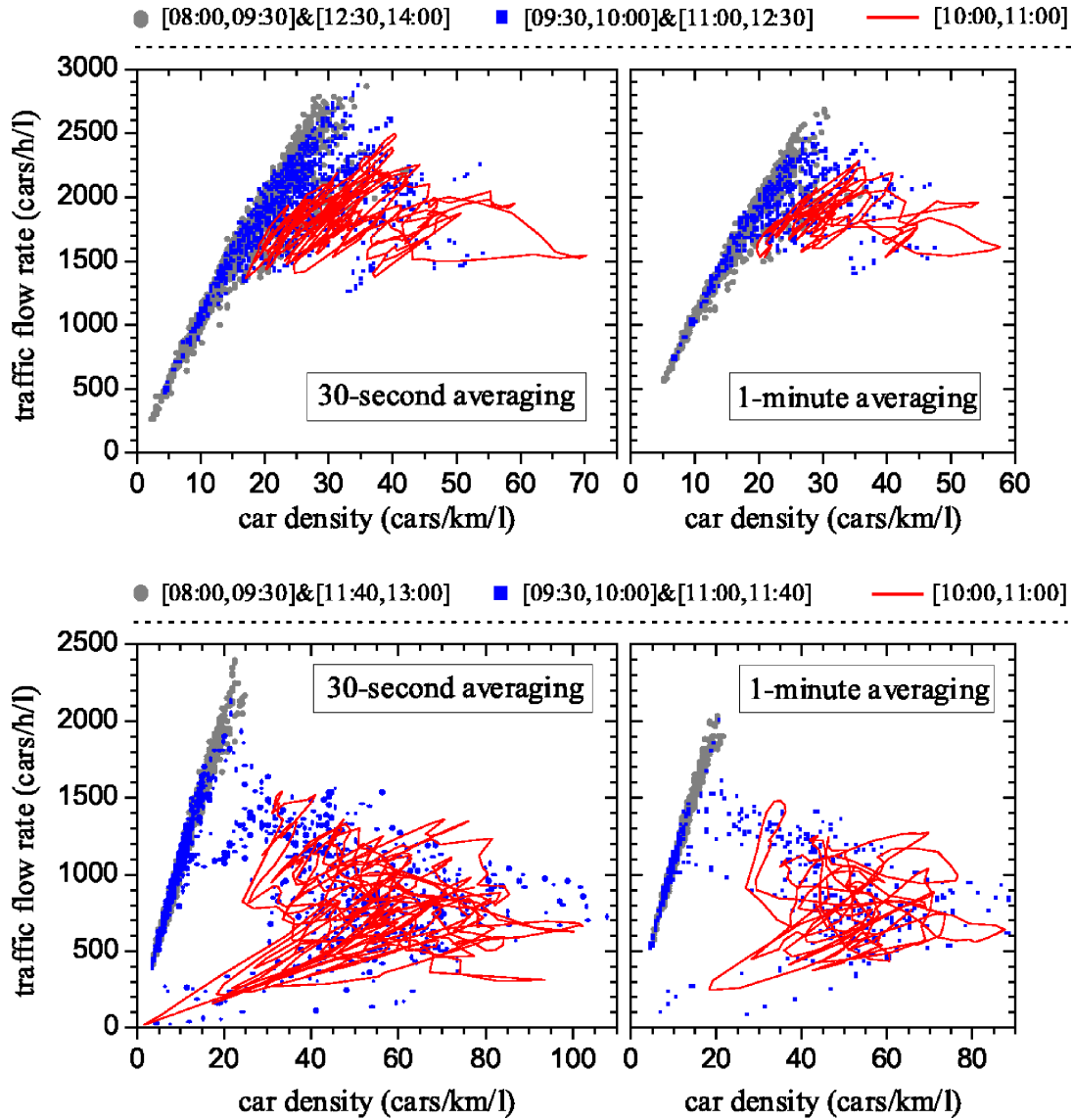2. states where only the average vehicle speed V is stationary;

Fig. 4.2: The fundamental diagram showing the possible states of traffic flow [60].

3. nonstationary and nonhomogeneous states.

Kerner has formulated his hypothesis about the synchronized mode to explain the properties of the widely scattered states [40–42]. In particular, regarding the synchronized traffic of first and second type he has assumed it to contain a whole multitude continuum of possible congested traffic states. This leads to continuous spatial–temporal transitions between these states. However, theoretical description and further empirical evidence for this hypothesis are still to be found. In order to understand such a phenomenon, the following questions have to be asked:

- What is the macroscopic mechanism of this phase?

- Whence these states appear?

The physical properties of drivers play the fundamental role. The driver can not control the relative velocity (velocity difference) and headway equally. Since the relative velocity is the more important factor for the safe motion, the driver response to its variation is much faster than its reaction to the headway change. In this case, after getting the region of small relative velocities the system stays for long time. Such a fragment of the motion can be regarded as a long–lived state.

4.3 The Concept of Dynamical Traps

The notion of dynamical traps is currently worked out in physics of nonlinear Hamiltonian systems by Zaslavsky [101] in 2002. The dynamical trap can be defined as a relatively small domain in phase space where a particle can spend a long time. In Hamiltonian systems it is due to the particle performs almost deterministic motion located in the region of dynamical trap and cannot leave it practically just after having come into it. Up to know the formation of such regions and their properties is a challenging problem of nonlinear physics.

The classical theory of phase transitions [77] is based on the properties of the energy functional and, in particular, on the analysis of its local minimum. Nevertheless, the calculation of potential energy poses many problems in the systems with the complex energy exchange. Making the qualitative description requires the developing of new methods. The new approach is based on study of dynamical states controlled by kinetic coefficients of the system under consideration taking into account their anomalous properties and their dependence on position in phase space. For this purpose, the dynamical trap concept is introduced.

The essential characteristics of the dynamical trap effect is the fact that the deterministic force F_{det} does not change the sign in its passage through the dynamical trap region. The influence of the dynamical trap just depressed the

action the deterministic force. When the effect of dynamical traps is substantial, the system motion in this region is determinded mostly by stochastic forces.

Dynamical traps induce the formation of the macroscopic states. Their characteristics are not determined by stationary points of the deterministic force F_{det} but by complex and continuous movement of particles. In this connection, it is natural to call such structures *dynamical* states which can be also interpreted as phase transions of a new type. Therewith, the phase transions between the states take place at a nonzero deterministic force F_{det}. That is the reason why the present description is different from the classical theory of phase transitions.

4.4 Description of the Dynamical Trap

It is suggested that as result of the cooperative interaction of particles, the deterministic force F_{det} becomes the complex dependence. As a consequence, several stationary states appear. Therewith, the homogeneous state becomes to be an unstable one and the transition of the system to one of stable states takes place. In this case, the effect of the stochastic forces is reduced to random motion in the vicinity of stable stationary states or in stochastic transitions between stable states if they locate sufficient close to each other.

Within the framework of such a schematic view, noise induced phase transitions can be treated also within this approach. The theoretical approximation of such phenomena following the classical approach meets certain problems. The deterministic force F_{det} must have very complex structure. There is an alternative approach proposed by Klimontovich for the description of the system with a continuum of long–lived states. He has assumed that nonequilibrium phase transitions can be caused not only by change of the forces but also via anomalies in kinetic coefficients as well. In this case, the force can have a simple structure with one stationary state which corresponds to the stable state.

It is suggested that there is some unrestricted domain in phase space where all states characterize by special behaviour. This domain is called the domain of dynamical trap. In this region the motion of the system slows down essentially and the system stays in some small vicinity of the entrance point to the domain for some long time. This fragment of the motion can be considered as a long–lived state. When the system leaves the domain of the dynamical traps, its dynamics is again controlled by deterministic force F_{det} until the system gets the domain of dynamical traps once again but in another point. By virtue of the influence of stochastic forces, the dynamics of the system develops an appearance of the consequence of stochastic transitions between long–lived states. Since, any small fragment of the domain of dynamical trap can induce the appearance of long–lived state, all such states has to form a continuum.

In mathematical terms, dynamical traps can be introduced in terms of anoma-

lies of kinetic coefficients and, for example, for one particular particle as

$$dx = v\,dt\,, \tag{4.5}$$

$$dv = \Omega(x,v)\,F_{det}(x,v)\,dt + \varepsilon\,dW(t)\,, \tag{4.6}$$

where x and v are coordinate and velocity of the particle respectively, $F_{det}(x,v)$ is deterministic force. The equation for acceleration (4.6) contains the additive white noise represented by the increment of the Wiener process $dW(t)$ (see Chapter 2) with noise intensity ε. The factor $\Omega(x,v)$ is the function of dynamical trap. In the domain of dynamical traps this factor is small and the process evolution is determined by stochastic properties.

The theory of nonequilibrium systems with dynamical traps is still in its infancy. It is necessary to perform the detailed analysis of the properties of phase transitions. In framework of such an analysis, the formation mechanism of long–lived macroscopic states for the elucidation of the fundamental properties of the cooperative motion in systems with dynamical traps should be done.

4.5 The Model Description

The notion of dynamical traps has been applied to the follow the leader model. The main argument for the present investigation is the fact that a driver cannot control all motion parameters to the same degree. Since the relative velocity is of high importance in preventing collisions the driver response to its variations is very fast. By contrast, when the relative velocity is below its threshold in the driver perception, the driver control over the headway is delayed essentially. In this way we get a new model for dynamical traps. Here the region of dynamical traps is a rather narrow layer containing the headway excise. Its thickness is about the relative velocity threshold in the driver perception. When the car velocity comes into this region the driver response is delayed substantially and, as a result, the car dynamics is stagnated.

A pair of cars is under consideration. The car ahead is assumed to move at a fixed constant speed v_l. Dynamics of the following car, i.e. time variations in its velocity v and position x are described practically within the optimal velocity model (3.7) – (3.8)

$$dx = v\,dt\,, \tag{4.7}$$

$$dv = \frac{1}{\tau}\Big[v_{opt}(\Delta x) - v\Big]\,dt + \varepsilon\,dW(t)\,, \tag{4.8}$$

where the optimal velocity function $v_{opt}(\Delta x)$ is represented by the headway dependence (3.3) introduced in Chapter 3. The relaxation time τ evaluates the characteristic delay in the driver response. The proposed system of equations

(4.7) – (4.8) can be rewritten in terms of the headway $\Delta x = x_l - x$ and the velocity difference $\Delta v = v_l - v$ as

$$d\Delta x \quad = \quad \Delta v\, dt\,, \tag{4.9}$$

$$d\Delta v \quad = \quad -\frac{1}{\tau}\Big[v_{opt}(\Delta x) - v_l + \Delta v\Big]\, dt + \varepsilon\, dW(t)\,. \tag{4.10}$$

Without noise $\varepsilon = 0$ this system has only one stationary point

$$\Delta x^{st} \quad = \quad D\,\sqrt{\frac{v_l}{v_{max} - v_l}}\,, \tag{4.11}$$

$$\Delta v \quad = \quad 0\,. \tag{4.12}$$

which is always stable. As already noted in Section 3.2, the system, starting from any initial condition, comes to its stable mode and stays there for long time. By including of a noise to the car dynamics, the motion does not differs essentially from the noiseless situation.

The physical properties of a driver have a dominant role in the traffic dynamics. The driver can not equally control the relative velocity Δv and the headway distance Δx. Since the relative velocity of the car is the most important criterion for the safe driving, the reaction time of the driver on its changing vastly more than the reaction time for controlling of dinstance between two cars. Therefore, the domain of small relative velocity $\Delta v \ll 0$ plays the role of the dynamical trap. On this basic, the modified equations of motion have the form

$$d\Delta x \quad = \quad \Delta v\, dt\,, \tag{4.13}$$

$$d\Delta v \quad = \quad -\frac{\Omega(\Delta v)}{\tau}\Big[v_{opt}(\Delta x) - v_l + \Delta v\Big]\, dt + \varepsilon\, dW(t)\,. \tag{4.14}$$

The factor $\Omega(\Delta v)$ allows for difference in the driver control over the relative velocity Δv and the headway Δx. Based upon properties discussed in previous Section 4.4, the following ansatz for the dynamical trap function

$$\Omega(\Delta v) = \frac{(\Delta v)^2 + \theta^2 v_t^2}{(\Delta v)^2 + v_t^2} \tag{4.15}$$

is used, where v_t denotes the driver threshold for recognizing small relative speeds. Besides, the velocity threshold v_t will be estimated as $v_t \sim 1$–2 m/s taking into account the empirical data on driver action points [7]. The parameter $\theta \leq 1$ evaluates the increase in the delay τ of the driver response when the relative velocity Δv is rather small, $|\Delta v| \lesssim v_t$, and calm driving is possible in comparison with that of driving in tension caused by the remarkable relative velocity, $|\Delta v| \gg v_t$. In other words, the parameter θ measures the effect of dynamical traps due to the bounded rationality of drivers. The influence of trap to dynamics is neglected for $\theta = 1$. For $\theta = 0$, the effect of dynamical trap is most strong. The main
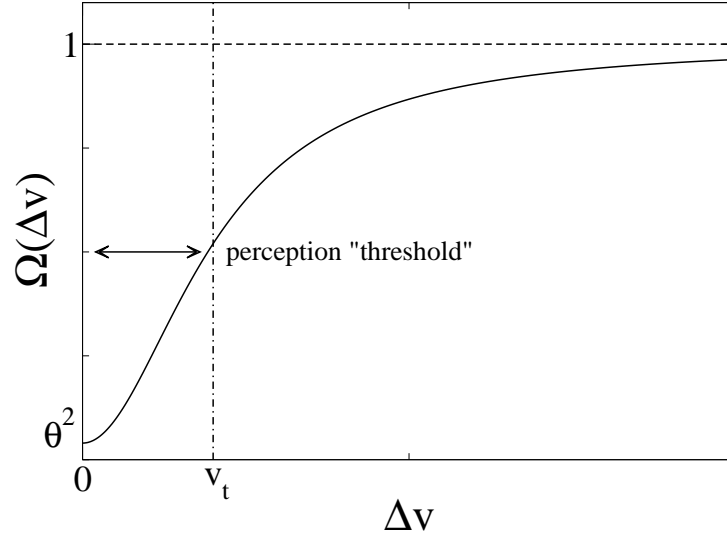
Fig. 4.3: The dynamical trap function $\Omega(\Delta v)$ described by equation (4.15).

properties of dynamical trap function $\Omega(\Delta v)$ are shown in Fig. 4.3. When the relative velocity Δv tends to zero, the deterministic force $F_{det}(\Delta x, \Delta v)$ is suppressed. In this case, the dynamical trap function $\Omega(\Delta v = 0) = \theta^2 \ll 1$ and the car dynamics is determined only by stochastic force. Beyond the domain of dynamicall trap $\Delta v > v_t$ the motion of the system takes place in usual way without the perceptible influence of factor $\Omega(\Delta v)$.

The given system (4.13) – (4.14) has been analyzed numerically. For this purpose it was converted into the dimensionless form using the same scaling relations as in Section 3.1.1

$$\Delta y \;=\; \frac{\Delta x}{D}, \tag{4.16}$$

$$\Delta u \;=\; \frac{\Delta v}{v_{max}}, \tag{4.17}$$

$$T \;=\; \frac{t}{\tau}. \tag{4.18}$$

In these terms the system of equations (4.13) – (4.14) reads

$$d\Delta y \;=\; \frac{1}{b}\,\Delta u\,dT\,, \tag{4.19}$$

$$d\Delta u \;=\; -\,\Omega(\Delta u)\,[u_{opt}(\Delta y) - u_l + \Delta u]\,dT + \zeta\,dW(T) \tag{4.20}$$

with the new set of dimensionless control parameters:

$$u_l = v_l/v_{max}, \tag{4.21}$$

$$u_t = v_t/v_{max}, \tag{4.22}$$

$$b = \frac{D}{\tau \, v_{max}}, \tag{4.23}$$

$$\zeta = \varepsilon \frac{\sqrt{\tau}}{v_{max}}. \tag{4.24}$$

Due to the variable transformation (4.16) – (4.17), dimensionless trap and optimal velocity functions are specified as

$$\Omega(\Delta u) = \frac{(\Delta u)^2 + \theta^2 \, u_t^2}{(\Delta u)^2 + u_t^2}, \tag{4.25}$$

$$u_{opt}(\Delta y) = \frac{(\Delta y)^2}{1 + (\Delta y)^2}. \tag{4.26}$$

The latter is due to system (4.19) – (4.20) being absolutely stable without noise. This conclusion follows directly from the existence of the Lyapunov function $\mathcal{L}(\Delta y, \Delta u)$. The Lyapunov function $\mathcal{L}(\Delta y, \Delta u)$ will be constructed in the form

$$\mathcal{L}(\Delta y, \Delta u) = \mathcal{G}(\Delta y) + \mathcal{V}(\Delta u). \tag{4.27}$$

Let us assume, that there are no dissipations. Then,

$$\frac{\partial \mathcal{L}(\Delta y, \Delta u)}{\partial T} = 0 \tag{4.28}$$

and the following identity is valid

$$\frac{d\mathcal{G}(\Delta y)}{d\Delta y} \, d\Delta y + \frac{d\mathcal{V}(\Delta u)}{d\Delta u} \, d\Delta u = 0. \tag{4.29}$$

Hence, using the set of equations (4.19) – (4.20) we obtain

$$\frac{d\mathcal{G}(\Delta y)}{d\Delta y} \left[\frac{1}{b} \Delta u\right] + \frac{d\mathcal{V}(\Delta u)}{d\Delta u} \left[-\Omega(\Delta u) \, (u_{opt}(\Delta y) - u_l)\right] = 0 \tag{4.30}$$

or, what is the same,

$$\frac{d\mathcal{G}(\Delta y)}{d\Delta y} \left[\frac{1}{u_{opt}(\Delta y) - u_l}\right] = \frac{d\mathcal{V}(\Delta u)}{d\Delta u} \left[b \frac{\Omega(\Delta u)}{\Delta u}\right] = 1. \tag{4.31}$$

By integration of both contributions in (4.31)

$$\frac{d\mathcal{G}(\Delta y)}{d\Delta y} = u_{opt}(\Delta y) - u_l, \tag{4.32}$$

$$\frac{d\mathcal{V}(\Delta u)}{d\Delta u} = \frac{1}{b} \frac{\Delta u}{\Omega(\Delta u)} \tag{4.33}$$

we derive the expression for functions $\mathcal{G}(\Delta y)$ and $\mathcal{V}(\Delta u)$

$$\mathcal{G}(\Delta y) = \Delta y\,(1 - u_l) - \arctan(\Delta y)\,, \tag{4.34}$$

$$\mathcal{V}(\Delta u) = \frac{1}{2}\frac{1}{b}\left[(\Delta u)^2 + u_t^2\left(1 - \theta^2\right)\ln\left(1 + \frac{(\Delta u)^2}{\theta^2\,u_t^2}\right)\right] \tag{4.35}$$

respectively. Finally, the Lyapunov function $\mathcal{L}(\Delta y, \Delta u) = \mathcal{G}(\Delta y) + \mathcal{V}(\Delta u)$ gets the unique mininum at $\left\{\Delta y^{st} = \sqrt{\dfrac{u_l}{1 - u_l}}, \Delta u^{st} = 0\right\}$ and obeys the inequality

$$\frac{\partial \mathcal{L}(\Delta y, \Delta u)}{\partial T} = -\frac{1}{b}\,(\Delta u)^2 < 0 \quad \text{for} \quad \Delta u \neq 0\,. \tag{4.36}$$

4.6 Numerical results

The effect of dynamical traps on car dynamics has been considered for various values of the dimensionless parameters θ, b, and ζ. Beforehand it is possible to declare that the less the parameter θ, the more pronounced the dynamical trap effect. The analysis has been performed numerically with explicit strong schemes of the 1.5 order for the integration of stochastic differential equations [48]. The simulation results have been calculated with the computer time step $\Delta T = 2 \cdot 10^{-2}$ for the relative long time interval $T \in [0, T_{max}]$ with $T_{max} = 5 \cdot 10^5$. The following dimensionless parameters have been fixed

- $u_l = 0.5$;

- $u_t = 0.03$;

- $\zeta = 10^{-1}$.

and the behaviour of the system (4.19) – (4.20) has been analysied with respect to the influence of the dynamical trap value θ and the parameter b. The initial situation for all simulations has been chosen by the same way

$$\Delta y = \Delta y^{st} = 1\,, \tag{4.37}$$

$$\Delta u = \Delta u^{st} = 0\,. \tag{4.38}$$

The phase portrait in terms of headway and velocity difference $(\Delta y, \Delta u)$ is shown in Fig. 4.4. Two situations are presented: the dynamics with strong dynamical trap effect $\theta = 0.1$ (main figure) and without it $\theta = 1$ (internal plot). Without dynamical trap, due to stochaticity, the system fluctuates in small vicinity of its stationary point (4.37) – (4.38). The opposite effect is illustrated for the case of strong influence of the dynamical trap with trap intensity $\theta = 0.1$. The phase portrait becomes asymmetrical and complex. It is shown precise phase
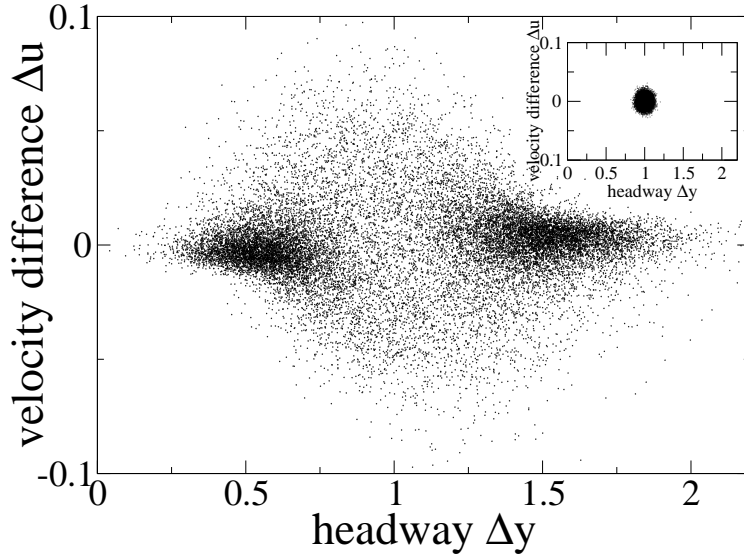
Fig. 4.4: The phase portrait $(\Delta y, \Delta u)$ for the car following model described by the system of stochastic differential equations (4.19) –(4.20) with dynamical trap effect ($\theta = 0.1$) and without ($\theta = 1$, internal plot). The results have been obtained for the control parameter $b = 0.05$.

separation into two regions in the phase space of headway and velocity difference $(\Delta y, \Delta u)$. Each region is located in some small vicinity of zero values of velocity difference $\Delta u \in [-u_t, +u_t]$. One of the congested area corresponds to headway distance $\Delta y \approx 0.5$, another one to $\Delta y \approx 1.5$. To show the influence of the dynamical trap in more detail, the fragment of the time evolution for the headway distance $\Delta y(T)$ and velocity difference $\Delta u(T)$ has been plotted in Fig. 4.5.

Figs. 4.4 and 4.5 show that the relizations $\Delta y(T)$ and $\Delta u(t)$ of the process described by set of stochastic differential equations (4.19) –(4.20) has very complex structure. In order to understand the nature of such a complexity and to analyse the memory of the process, the autocorrelation functions for the headway distance $\Delta y(T)$
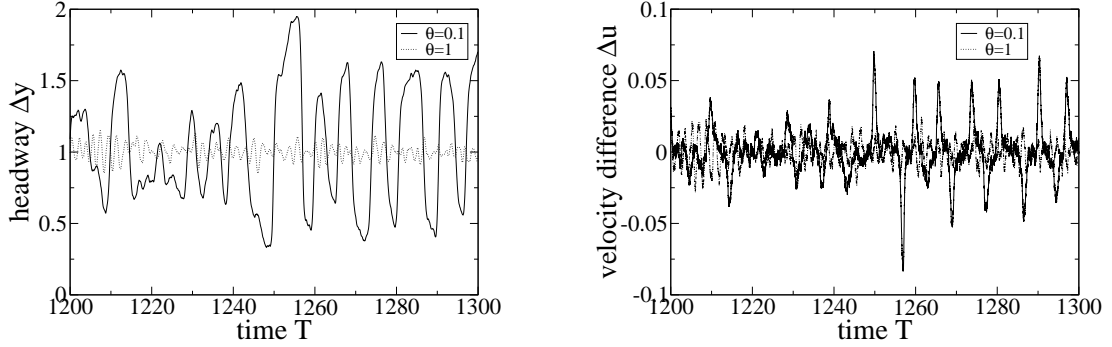
$$\langle \Delta y(T)\,\Delta y(T+T')\rangle = \frac{1}{\int_0^\infty \Delta y(T)^2\,dT}\int_0^\infty \Delta y(T)\,\Delta y(T+T')\,dT \qquad (4.39)$$

as well as for velocity difference $\Delta u(t)$

$$\langle \Delta u(T)\,\Delta u(T+T')\rangle = \frac{1}{\int_0^\infty \Delta u(T)^2\,dT}\int_0^\infty \Delta u(T)\,\Delta u(T+T')\,dT \qquad (4.40)$$

have been calculated. The prefactors in formulae (4.39) and (4.40) are chosen in a way to normalize the autocorrelation function. The normalization conditions

Fig. 4.5: The fragment of the time evolution $T \in [1200, 1300]$ of headway $\Delta y(T)$ and velocity difference $\Delta u(t)$ with (solid curve) dynamical trap effect ($\theta = 0.1$) and without (dashed curve) dynamical trap effect ($\theta = 1$). The results have been obtained for the control parameter $b = 0.05$.

are

$$\langle \Delta y(T)\, \Delta y(T + T' = 0)\rangle \;=\; 1\,, \qquad (4.41)$$

$$\langle \Delta u(T)\, \Delta u(T + T' = 0)\rangle \;=\; 1\,. \qquad (4.42)$$

The autocorrelation functions (4.39) and (4.40) have been calculated numerically by using the certain discrete approximation [19]. Fig. 4.6 shows the behaviour of the autocorrelation functions (4.39) and (4.40) under influence of the dynamical trap effect and without it. Unlike deterministic processes, where each value of their realizations is well defined from the given equation of motion and the initial condition, the information about the memory of stochastic process is hidden and distorted after some time. In terms of the autocorrelation functions (4.39) and (4.40), such an effect means, that

$$\langle \Delta y(T)\, \Delta y(T + T')\rangle \;\rightarrow\; 0\,, \qquad (4.43)$$

$$\langle \Delta u(T)\, \Delta u(T + T')\rangle \;\rightarrow\; 0 \qquad (4.44)$$

with time increasing $T' \rightarrow \infty$. Exactly this situation is visualized by the dashed curve in Fig. 4.6 and gives the autocorrelation functions (4.39) and (4.40) in the case, when the dynamical trap effect is absent. The functions (4.39) and (4.40) have their maximum in $T' = 0$ and decay very fast for $T' > 0$. The quite opposite situation has been seen under the influence of the dynamical trap effect. The dynamical traps induce very long correlations in the car dynamics.

As it has been shown in Fig. 4.4 the dynamical traps induce the phase separation which can be explaines as the phase transition. In this sense, the probability distribution function $P(\Delta y, \Delta u)$ becomes bimodal. In order to show this effect, the probability distribution $P(\Delta y, \Delta u)$ has been calculated as the average distribution according to the time T, i. e. how oft the system is located in some
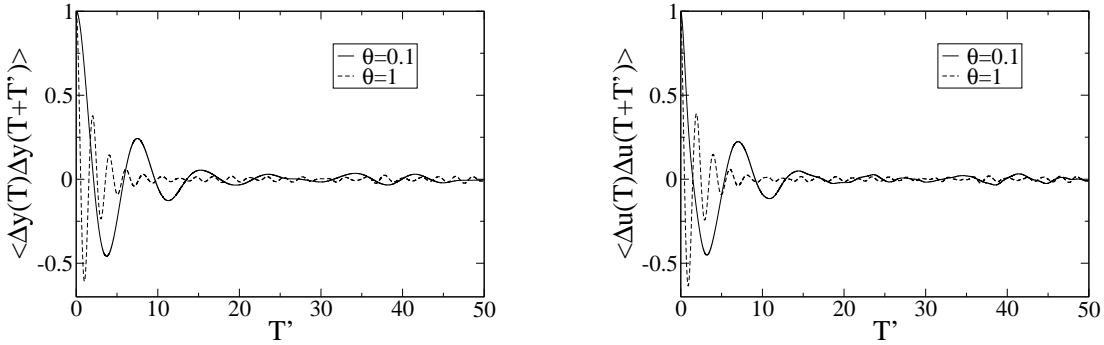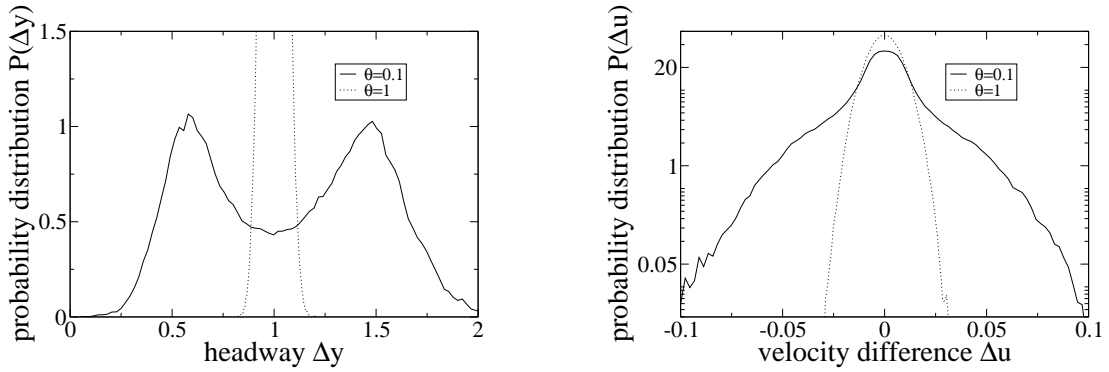
Fig. 4.6: Autocorrelation functions for headway Δy and velocity Δu difference for the car following model with dynamical traps described by equations (4.19) – (4.20) with (solid curve) dynamical trap effect ($\theta = 0.1$) and without (dashed curve) dynamical trap effect ($\theta = 1$). The results have been obtained for the control parameter $b = 0.05$.

cell of space phase of headway distance $\Delta y(T)$ and velocity difference $\Delta u(t)$ for a sufficiently long time $T \in [0, T_{max}]$. The results are presented as one–dimensional plots. Fig. 4.7 illustrates the headway $P(\Delta y)$ and velocity difference $P(\Delta u)$ distributions. The dashed curve corresponds to the situation when the effect of dynamical trap is absent, i. e. $\theta = 1$. In this case the distribution functions are unimodal and have the Gaussian form. The influence of the dynamical trap is represented in Fig. 4.7. The headway distribution $P(\Delta y)$ becomes bimodal. The maximum of the distribution $P(\Delta y)$ corresponds to headway values $\Delta y = 0.5$ and $\Delta y = 1.5$ (see Fig. 4.4). Under the influence of dynamical traps, the probability distribution of the velocity difference $P(\Delta u)$ becomes the Laplacian form.

Figs. 4.8 and 4.9 show the role of the dynamical trap effect on car dynamics in response to control parameter b. This parameter can be interpreted as a dissipation factor. The probability density distributions of the headway $P(\Delta y)$ and the velocity difference $P(\Delta u)$ are demonstrated in Fig. 4.8. It is shown that with decreasing of the parameter b, the effect of the trap is more pronounced. In this case the phase separation in terms of headway distribution $P(\Delta y)$ becomes more evident. The probability distribution for the velocity difference $P(\Delta u)$ changes under influence of parameter b as well. The distribution $P(\Delta u)$ is characterized by long tails. Fig. 4.9 gives the dependence of the autocorrelation functions (4.39) and (4.40) on the control parameter b. As it has been already mentioned in Fig. 4.6 the dynamical traps induce very long correlations in the car dynamics. With decreasing of the parameter b the correlation scales increase. Such an effect can be explained by the fact, that the dynamical traps produce the dynamical states in car dynamics which can be specified as the long–lived states.

In order to answer questions asked in Section 4.2, follow the leader model based on optimal velocity ansatz and including the dynamical trap effect has

Fig. 4.7: The distribution functions $P(\Delta y)$ and $P(\Delta u)$ for the car following model with dynamical traps described by equations (4.19) – (4.20) with (solid curve) dynamical trap effect ($\theta = 0.1$) and without (dashed curve) dynamical trap effect ($\theta = 1$). The results have been obtained for the control parameter $b = 0.05$.
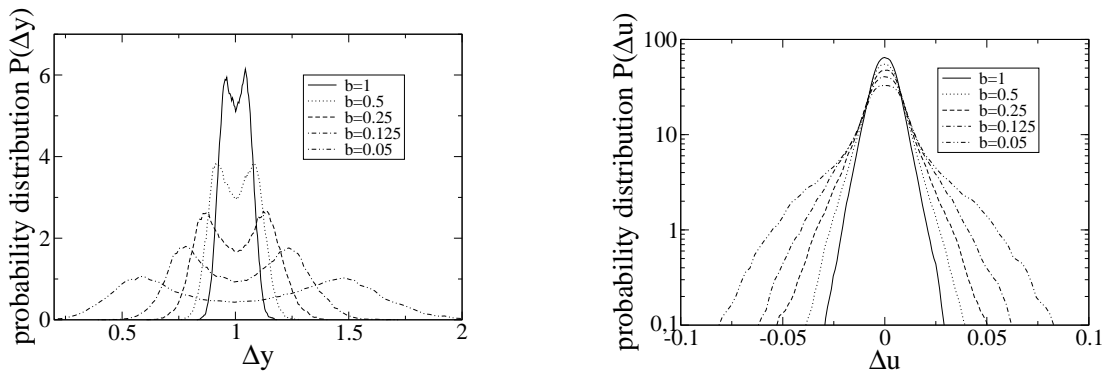
Fig. 4.8: The distribution functions $P(\Delta y)$ and $P(\Delta u)$ for the car following model with dynamical traps described by equations (4.19) – (4.20) for different values of the control parameter b with the dynamical trap efficacy $\theta = 0.1$.
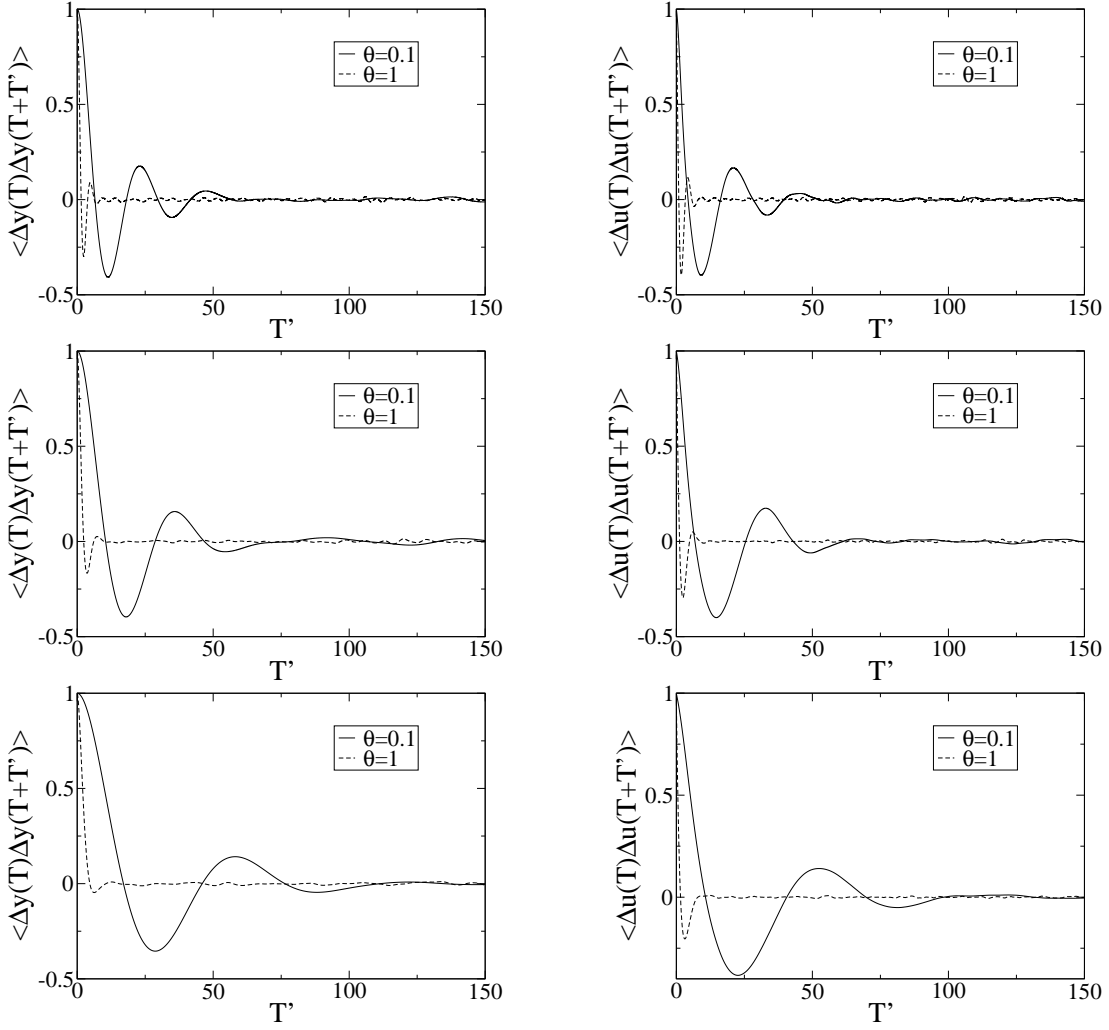
Fig. 4.9: Autocorrelation functions for headway $\Delta y(t)$ and velocity difference $\Delta u(t)$ for the dynamical trap efficacy $\theta = 0.1$ (solid curve) and different values of the parameter b, i. e. from bottom to the top $b = 1$, $b = 0.5$, $b = 0.25$. Dashed curve visualizes the autocorrelation function for headway $\Delta y(t)$ and velocity difference $\Delta u(t)$ for the case when the dynamical trap effect is absent.

been proposed and developed. The dynamical states of one particular car which equation of motion contains the dynamical trap function have been examined by way of the numerical modeling of corresponding stochastic differential equations including additive white noise. The detailed analysis of the car dynamics reveals the following anomalies caused by the interaction between the noise and the dynamical trap:

- the headway distribution $P(\Delta y)$ becomes bimodal;

- the probability distribution of the velocity difference $P(\Delta u)$ has a Laplace form which is characterized by fat tails;

- the long correlations appear in the system with strong dissipation. This fact manifests the long–lived states in the car dynamics;

- the phase portrait $(\Delta y, \Delta u)$ becomes asymmetrical and complex. Such an unusual structure gives a possibility to describe widely scattered states.

5 Understanding of Traffic Breakdown

5.1 What is a Breakdown?

Observations from different freeways around the world analysed by Daganzo et al. [17], Elefteriadou et al. [54,58], by Brilon and Zurlinden [10,104] indicate that traffic breakdowns do not necessary occur at maximum flow. It has been shown, that breakdown can occur at flows lower or higher than those traditionally accepted as capacity value. The *traffic breakdown* can be specified as a transition from an uncongested traffic state to a congested state. Such a definition is comparable with a phase transition in nature between different states of matter. Due to the fact that the traffic breakdown has been observed at very different flows, this phenomena has a probabilistic nature. Therefore, the traffic breakdown is specified as a stochastic event and, in order to analyze this quantity, the probability $W(q)$ of traffic breakdown as a function of vehicular flows q should be calculated. For this purpose, it is necessary to introduce the stochastic approach for the description of the traffic breakdown $W(q)$. It has been shown in Chapter 2, that the dynamical equations in terms of Fokker–Planck (2.22) and master equations (2.52) give the probabilistic description of such a stochastic process.

The congested state of traffic is characterized by the jam formation or, by drawing the analogy to the nucleation [90], by the *cluster formation*. It is possible to analyse the process of cluster formation in terms of its size n. The schematic definition of the cluster formation is illustrated in Fig. 5.1. Similarly to the nucleation process, the cluster formation is specified by two contributions called *inflow or attachment* rate and *discharge or detachment* rate. Furthermore, the case of constant attachment and detachment rates will be analysed in detail.

In order to describe the traffic breakdown, let us underline the main properties of the cluster size. The cluster size n is a discrete stochastic variable

$$n = 0, 1, 2, \ldots \quad \text{or} \quad n \geq 0 \,. \tag{5.1}$$

We define the traffic breakdown appearance with the help of a critical or escape value of cluster size n_{esc}. If the cluster size n is less than n_{esc} then no breakdown is detected. If the cluster size reaches the escape value $n = n_{esc}$ then the motion slows down and the traffic breakdown occurs. In other word, the domain of the
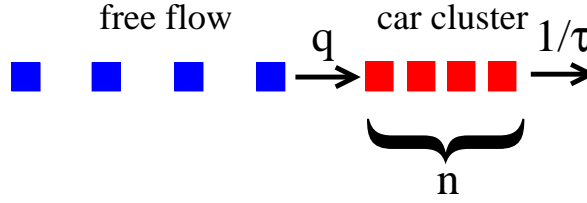
Fig. 5.1: The schematic definition of cluster formation: q [veh/h] = traffic flow or traffic volume; n = cluster size or queue length (number of congested vehicles) as stochastic variable; τ [$\tau \approx 1.5 \ldots 2.0$ s] = characteristic time needed for the first car leaving the cluster to become free.

cluster size is restricted by the interval $0 \leq n < n_{esc}$ and the parameter n_{esc} controls and defines the traffic breakdown.

It has been shown in Chapter 2 that the dynamics of the stochastic variable n which takes the discrete states and can change only by ± 1 per time unit is governed by the one–step master equation (2.53) which has been introduced in Chapter 2 [24, 34, 52, 66]

$$\frac{\partial p(n,t)}{\partial t} = w_+(n-1)\,p(n-1,t) + w_-(n+1)\,p(n+1,t)$$
$$- \ [w_+(n) + w_-(n)]\,p(n,t) \tag{5.2}$$

including the initial condition

$$p(n, t = 0) = \delta_{n,n_0}\,, \tag{5.3}$$

where $n_0 = n(t = 0)$, $w_+(n)$ and $w_-(n)$ attachment and detachment rates respectively (see Fig. 2.7). As it has been already mentioned above and illustrated in Fig. 5.1, the present investigations are carried out for the case of

$$w_+(n) = q \tag{5.4}$$
$$w_-(n) = \frac{1}{\tau}\,, \tag{5.5}$$

where q and τ are constant. These parameters refer to the inflow rate and to the characteristic time needed for the first car in the cluster to leave it respectively. According to the above–mentioned properties of the cluster size n, it is necessary to specify the boundary conditions at $n = 0$ and $n = n_{esc}$ for the probability density $p(n,t)$ given by master equation (5.2). Due to (5.1), $n = 0$ is specified as the reflecting boundary [24, 34]. It means that

$$w_-(0) = 0\,. \tag{5.6}$$

The boundary at $n = n_{esc}$ is absorbing [24, 34] and
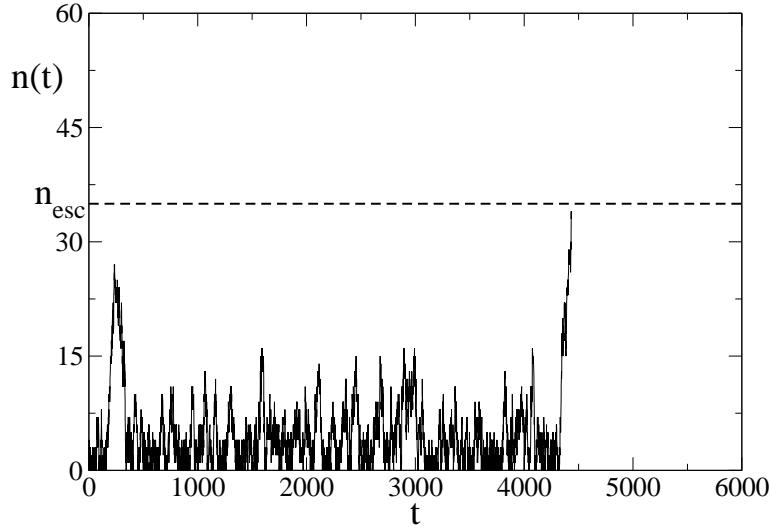
Fig. 5.2: Example of the stochastic trajectory $n(t)$ which imitates the time evolution of the cluster size n. with the initial condition $n(t=0) = 0$, reflecting boundary at $n = 0$ veh and absorbing boundary at $n_{esc} = 35$ veh.

$$w_-(n_{esc} + 1) = 0 \,. \tag{5.7}$$

Fig. 5.2 shows an example of cluster evolution $n(t)$ taking into account boundary conditions (5.6) – (5.7). Under these conditions, the master equation (5.2) takes the special form at $n = 0$ and $n = n_{esc}$ [24]. Namely,

$$w_-(0)\, p(0, t) - w_+(-1)\, p(-1, t) = 0 \tag{5.8}$$
$$p(n_{esc} + 1) = 0 \,. \tag{5.9}$$

The probability $p(n, t)$ of finding that the cluster size equals to value n at fixed time t is the solution of the master equation (5.2) taking into account the initial (5.3) and boundary conditions (5.8) – (5.9). It has been discussed in Chapter 2 that it is rather difficult to integrate directly the equation (5.2). Therefore, taking into account the equivalence between the master equation and Fokker–Planck equation, our future investigations will be carried out with the help of the corresponding to the initial–boundary–value–problem (5.2), (5.8) – (5.9) Fokker–Planck equation [24, 38]. For this purpose, the diffusion approximation of the master equation (5.2) has been used. Using the deterministic approach [66], the potential can be introduced by

$$-\frac{dU(n)}{dn} = w_+(n) - w_-(n) \tag{5.10}$$

and, due to the fact, that $w_+(n) = q$ and $w_-(n) = 1/\tau$ are assumed to be constant, the following relationship takes place

$$U(n) = -\,v\,n \,. \tag{5.11}$$
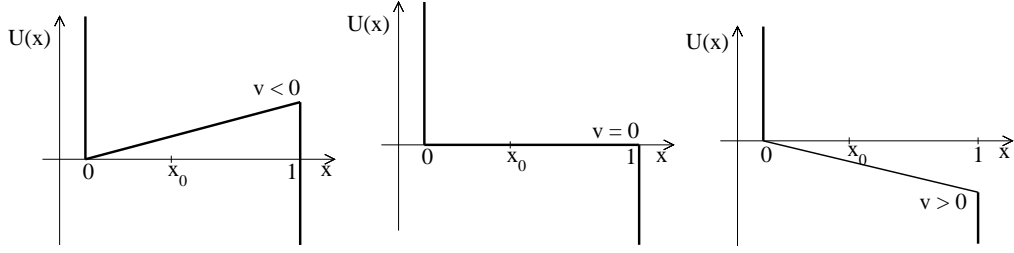
Fig. 5.3: The linear potential $U(n)$ for three different scenarios [52].

The quantity $v = q - 1/\tau$ is constant and interpreted as a drift velocity term. The drift $v \in \mathbb{R}$ can take various values. Fig. 5.3 illustrates the linear dependence of the potential $U(n)$ for three different situations:

- negative drift $v < 0$: $q < 1/\tau \implies$ cluster dissolves;

- zero drift $v = 0$: $q = 1/\tau \implies$ no tendency;

- positive drift $v > 0$: $q > 1/\tau \implies$ cluster grows.

Then, the initial–boundary–value–problem (shown schematically in Fig. 5.4) with constant diffusion coefficient D and constant drift coefficient v is under consideration. Our task is to calculate the probability density $p(x,t)$ to find the system in state x (exact in interval $[x; x + dx]$) at time moment t. The dynamics of $p(x,t)$ is given by the forward drift–diffusion–equation as well as initial and boundary conditions [24] by following dynamics

$$\frac{\partial p(x,t)}{\partial t} = -v \, \frac{\partial p(x,t)}{\partial x} + D \, \frac{\partial^2 p(x,t)}{\partial x^2} \ , \tag{5.12}$$

$$\text{or} \quad \frac{\partial p(x,t)}{\partial t} + \frac{\partial j(x,t)}{\partial x} = 0 \tag{5.13}$$

$$\text{with flux} \quad j(x,t) = v \, p(x,t) - D \, \frac{\partial p(x,t)}{\partial x} \tag{5.14}$$

with the initial condition

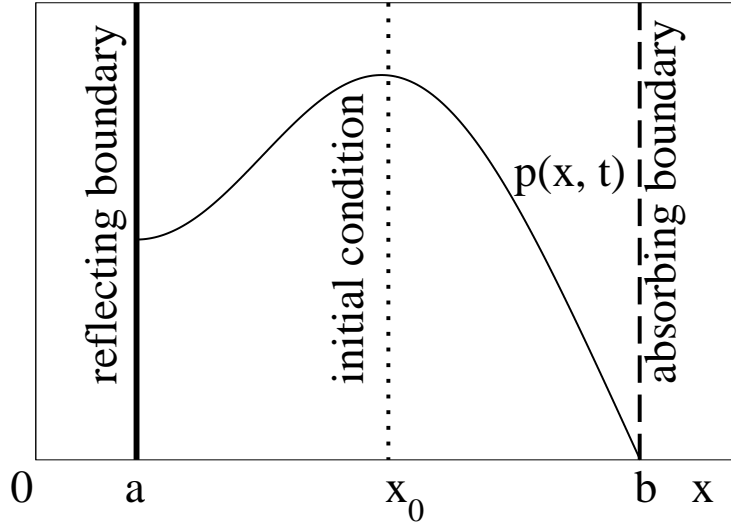$$p(x, t = 0) = \delta(x - x_0) \ , \tag{5.15}$$

and two boundary conditions [24], i. e. reflecting boundary at $x = a$

$$j(x = a, t) = v \, p(x = a, t) - D \, \left. \frac{\partial p(x,t)}{\partial x} \right|_{x=a} = 0 \ , \tag{5.16}$$

and absorbing boundary at $x = b$

$$p(x = b, t) = 0 \ . \tag{5.17}$$

Fig. 5.4: Schematic picture of the boundary–value problem showing the probability density $p(x,t)$ in the interval $a \leq x \leq b$.

It is convenient to formulate the drift–diffusion problem in dimensionless variables. For this purpose we define new variables y and T by

$$y = \frac{x-a}{b-a} \qquad \text{and} \qquad T = \frac{D}{(b-a)^2}\, t\,. \tag{5.18}$$

As a result, the system of partial differential equations (5.12) – (5.17) can be rewritten as

$$\frac{\partial P(y,T)}{\partial T} = -\Omega\, \frac{\partial P(y,T)}{\partial y} + \frac{\partial^2 P(y,T)}{\partial y^2}\,, \tag{5.19}$$

with initial condition

$$P(y,T=0) = \delta(y-y_0)\,, \tag{5.20}$$

reflecting boundary at $y=0$

$$J(y=0,T) = \Omega\, P(y=0,T) - \left.\frac{\partial P(y,T)}{\partial y}\right|_{y=0} = 0\,, \tag{5.21}$$

and absorbing boundary at $y=1$

$$P(y=1,T) = 0\,. \tag{5.22}$$

Hence, our problem has only one dimensionless control parameter $\Omega = \frac{v}{D}\,(b-a)$ (scaled drift v which may have positive, zero, or negative values). The parameter Ω has the same meaning as Péclet number which has been used in [82].

The system of equations (5.19) – (5.22) will be solved exactly by applying the forward technique [24]. The main idea is to obtain the solution of Fokker–Planck equation and after that the first passage time distribution in terms of probability density. Both quantities will be presented as eigenfunction expansion. The survival probability and moments of first passage time can be calculated differently by using backward drift–diffusion equation. These results shown in [13, 22,82] do not give the complete solution of the problem under consideration. Our presented analysis of the reference system (5.19) – (5.22) is the key result in order to study more complicated situations with nonlinear drift function $\Omega(y)$.

5.2 Solution in Terms of Orthogonal Eigenfunctions

To find the solution of the well–defined drift–diffusion problem, first we take the dimensionless form (5.19) – (5.22) and use a transformation to a new function Q by

$$Q(y, T) = e^{-\frac{\Omega}{2} y} P(y, T) . \tag{5.23}$$

This results in a dynamics without first derivative called reduced Fokker–Planck–equation

$$\frac{\partial Q(y, T)}{\partial T} = -\frac{\Omega^2}{4} Q(y, T) + \frac{\partial^2 Q(y, T)}{\partial y^2} . \tag{5.24}$$

According to (5.23) the initial condition is transformed to

$$Q(y, T = 0) = e^{-\frac{\Omega}{2} y_0} P(y, T = 0) , \tag{5.25}$$

whereas the reflecting boundary condition at $y = 0$ becomes

$$\frac{\Omega}{2} Q(y = 0, T) - \left. \frac{\partial Q(y, T)}{\partial y} \right|_{y=0} = 0 , \tag{5.26}$$

and the absorbing boundary condition at $y = 1$ now reads

$$Q(y = 1, T) = 0 . \tag{5.27}$$

The solution of reduced equation (5.24) can be found by the method of separation of variables [92]. Making a separation ansatz $Q(y, T) = \chi(T)\psi(y)$, we obtain

$$\frac{1}{\chi(T)} \frac{d\chi(T)}{dT} = -\frac{\Omega^2}{4} + \frac{1}{\psi(y)} \frac{d^2\psi(y)}{dy^2} . \tag{5.28}$$

Both sides should be equal to a constant. This constant is denoted by $-\lambda$, where λ has the meaning of an eigenvalue. The eigenvalue λ should be real and nonnegative.

Integration of the left hand side gives exponential decay

$$\chi(T) = \chi_0 \exp\{-\lambda T\} \tag{5.29}$$

with $\chi(T = 0) = \chi_0$ and setting $\chi_0 = 1$.

Let us now define the dimensionless wave number k as $k^2 = \lambda$. The right–hand side of equation (5.28) then transforms into the following wave equation

$$\frac{d^2\psi(y)}{dy^2} + \left(k^2 - \frac{\Omega^2}{4}\right)\psi(y) = 0 \ . \tag{5.30}$$

Further on, we introduce a modified wave number $\tilde{k}^2 = k^2 - \Omega^2/4$. Note that $\tilde{k} = +\sqrt{k^2 - \Omega^2/4}$ may be complex (either pure real or pure imaginary).

First we consider the case where $\tilde{k}$ is real. A suitable complex ansatz for the solution of the wave equation (5.30) reads

$$\psi(y) = C^* \exp\{+i\tilde{k}y\} + C \exp\{-i\tilde{k}y\} \tag{5.31}$$

with complex coefficients $C = A/2 + i\,B/2$ and $C^* = A/2 - i\,B/2$ chosen in such a way to ensure a real solution

$$\psi(y) = A\cos(\tilde{k}y) + B\sin(\tilde{k}y) \ . \tag{5.32}$$

The two boundary conditions (5.26) and (5.27) can be used to determine the modified wave number $\tilde{k}$ and the ratio A/B. The particular solutions are eigenfunctions $\psi_m(y)$, which form a complete set of orthogonal functions. As the third condition, we require that these eigenfunctions are normalised

$$\int\limits_0^1 \psi_m^2(y)dy = 1 \ . \tag{5.33}$$

In this case all three parameters $\tilde{k}$, A and B are defined.

The condition for the left boundary (5.26) reads

$$\frac{\Omega}{2}\psi(y = 0) - \frac{d\psi(y)}{dy}\bigg|_{y=0} = 0 \ . \tag{5.34}$$

After a substitution by (5.31) it reduces to

$$\frac{\Omega}{2}(C^* + C) = i\tilde{k}\,(C^* - C) \tag{5.35}$$

or

$$\frac{\Omega}{2}A = \tilde{k}B \ . \tag{5.36}$$

The condition for the right boundary (5.27)

$$\psi(y = 1) = 0 \tag{5.37}$$

gives us

$$C^* \exp\{+i\tilde{k}\} + C \exp\{-i\tilde{k}\} = 0 \tag{5.38}$$

or

$$A \cos\left(\tilde{k}\right) + B \sin\left(\tilde{k}\right) = 0 . \tag{5.39}$$

By putting both equalities (5.36) and (5.39) together and looking for a non-trivial solution, we arrive at a transcendental equation

$$i\frac{\Omega}{2}\left(\exp\{+i\tilde{k}\} - \exp\{-i\tilde{k}\}\right) = \tilde{k}\left(\exp\{+i\tilde{k}\} + \exp\{-i\tilde{k}\}\right) \tag{5.40}$$

or

$$\frac{\Omega}{2}\sin\left(\tilde{k}\right) + \tilde{k}\cos\left(\tilde{k}\right) = 0 , \tag{5.41}$$

respectively

$$\tan\left(\tilde{k}\right) = -\frac{2}{\Omega}\tilde{k} , \tag{5.42}$$

which gives the spectrum of values $\tilde{k}_m$ with $m = 0, 1, 2, \ldots$ (numbered in such a way that $0 < \tilde{k}_0 < \tilde{k}_1 < \tilde{k}_2 < \ldots$) and the discrete eigenvalues $\lambda_m > 0$.

Due to (5.32) and (5.39), the eigenfunctions can be written as

$$\psi_m(y) = R_m \left[\cos\left(\tilde{k}_m y\right) \sin\left(\tilde{k}_m\right) - \cos\left(\tilde{k}_m\right) \sin\left(\tilde{k}_m y\right)\right] , \tag{5.43}$$

where $R_m = A_m / \sin\left(\tilde{k}_m\right) = -B_m / \cos\left(\tilde{k}_m\right)$. Taking into account the identity $\sin(\alpha - \beta) = \sin\alpha\cos\beta - \cos\alpha\sin\beta$, equation (5.43) reduces to

$$\psi_m(y) = R_m \sin\left[\tilde{k}_m(1-y)\right] . \tag{5.44}$$

The normalisation constant R_m is found by inserting (5.44) into (5.33). Calculation of the normalisation integral by using the transcendental equation (5.41) gives us

$$R_m^2 \int_0^1 \sin^2\left[\tilde{k}_m\left(1-y\right)\right] dy = R_m^2 \left[\frac{1}{2} - \frac{1}{4\tilde{k}_m}\sin\left(2\tilde{k}_m\right)\right]$$
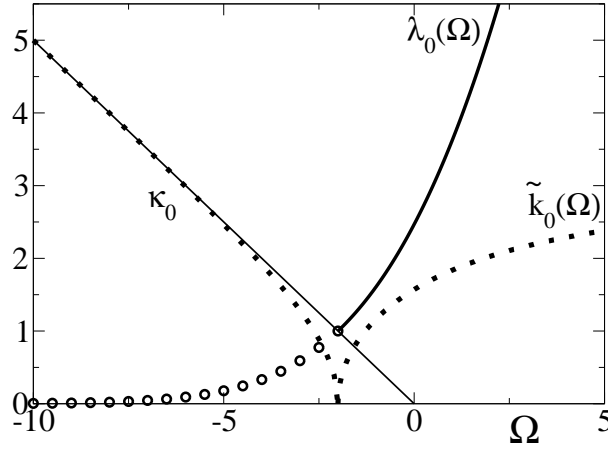$$= \frac{R_m^2}{2}\left(1 + \frac{\Omega}{2}\frac{1}{\tilde{k}_m^2 + \Omega^2/4}\right) = 1 , \tag{5.45}$$

and hence (5.44) becomes

$$\psi_m(y) = \sqrt{\frac{2}{1 + \frac{\Omega}{2}\frac{1}{\tilde{k}_m^2 + \Omega^2/4}}}\, \sin\left[\tilde{k}_m(1-y)\right] \tag{5.46}$$

or

$$\psi_m(y) = \sqrt{\frac{2}{1 + \frac{\Omega}{2}\frac{1}{k_m^2}}}\, \sin\left[\sqrt{k_m^2 - \Omega^2/4}\,(1-y)\right] . \tag{5.47}$$

Fig. 5.5: The wave number $\tilde{k}_0$ ($\Omega \geq -2$) respectively κ_0 ($\Omega \leq -2$) and eigen-value λ_0 for ground state $m = 0$. The thin straight line shows the approximation $\kappa_0 \approx -\Omega/2$ valid for large negative $\Omega < -5$.

This calculation refers to the case $\Omega > -2$ where all wave numbers k_m or $\tilde{k}_m = \sqrt{k_m^2 - \Omega^2/4}$ are real and positive.

However the smallest or ground–state wave vector $\tilde{k}_0$ vanishes when Ω tends to -2 from above, and no continuation of this solution exists on the real axis for $\Omega < -2$. A purely imaginary solution $\tilde{k}_0 = i\kappa_0$ appears instead, where κ_0 is real, see Fig. 5.5. In this case (for $\Omega < -2$) a real ground–state eigenfunction $\psi_0(y)$ can be found in the form (5.31) where $C = A/2 + B/2$ and $C^* = A/2 - B/2$, i. e.,

$$\psi_0(y) = A \cosh(\kappa_0 y) + B \sinh(\kappa_0 y) . \tag{5.48}$$

The transcendental equation for the wave number $\tilde{k}_0 = i\kappa_0$ can be written as the following equation for κ_0

$$\frac{\Omega}{2} \sinh\left(\kappa_0\right) + \kappa_0 \cosh\left(\kappa_0\right) = 0 . \tag{5.49}$$

As compared to the previous case $\Omega > -2$, trigonometric functions are replaced by the corresponding hyperbolic ones. Similar calculations as before yield

$$\psi_0(y) = \sqrt{-\frac{2}{1 + \frac{\Omega}{2} \frac{1}{-\kappa_0^2 + \Omega^2/4}}} \sinh\left[\kappa_0(1 - y)\right] . \tag{5.50}$$

Note that $\kappa_0 = -i\tilde{k}_0$ is the imaginary part of $\tilde{k}_0$ and $\kappa_0^2 = -\tilde{k}_0^2$. As regards other solutions of (5.41) called excited states, i. e., those for $\tilde{k}_m$ with $m > 0$, nothing special happens at $\Omega = -2$, so that these wave numbers are always real. The situation for ground state $m = 0$ at different values of dimensionless drift parameter Ω is summarized in Table 5.1 which presents the solutions κ_0

Tab. 5.1: The ground–state wave number κ_0 (for $\Omega \leq -2$) and $\tilde{k}_0$ (for $\Omega \geq -2$) and eigenvalue λ_0 depending on the dimensionless drift parameter Ω.

Ω	κ_0	λ_0		Ω	$\tilde{k}_0$	λ_0
-9.00	4.499	0.010		-2.00	0.000	1.000
-8.50	4.248	0.015		-1.50	0.845	1.276
-8.00	3.997	0.021		-1.00	1.165	1.608
-7.50	3.745	0.031		-0.50	1.393	2.004
-7.00	3.493	0.045		0.00	1.571	2.468
-6.50	3.240	0.064		0.50	1.715	3.005
-6.00	2.984	0.091		1.00	1.836	3.623
-5.50	2.726	0.128		1.50	1.939	4.325
-5.00	2.464	0.178		2.00	2.028	5.116
-4.50	2.195	0.245		2.50	2.106	5.999
-4.00	1.915	0.333		3.00	2.174	6.979
-3.50	1.617	0.446		3.50	2.235	8.058
-3.00	1.288	0.591		4.00	2.288	9.239
-2.50	0.888	0.774		4.50	2.337	10.525
-2.00	0.000	1.000		5.00	2.381	11.917

from transcendental equation (5.49) together with $\lambda_0 = -\kappa_0^2 + \Omega^2/4$ and $\tilde{k}_0$ from transcendental equation (5.41) together with eigenvalues $\lambda_0 = \tilde{k}_0^2 + \Omega^2/4$. Table 5.2 shows the behaviour of lowest wave numbers $\tilde{k}_m$ with $m = 0, 1, \ldots, 5$. The results are plotted in Fig. 5.6.

In general (for arbitrary Ω), the eigenfunctions are orthogonal and normalised, i. e.,

$$\int_0^1 \psi_l(y)\psi_m(y)dy = \delta_{ml} \ . \tag{5.51}$$

Fig. 5.7 shows the ground eigenstate ($m = 0$) for different parameter values Ω, whereas Fig. 5.8 gives a collection of eigenstate functions ($m = 0, 1, \ldots, 5$) for $\Omega = -5.0$ and $\Omega = 3.0$.

In the following, explicit formulae (where $\psi_m(y)$ is specified) are written for the case $\Omega > -2$.

In order to construct the time–dependent solution for $Q(y, t)$, which fulfils the initial condition, we consider the superposition of all particular solutions with different eigenvalues λ_m

$$Q(y, T) = \sum_{m=0}^{\infty} C_m e^{-\lambda_m T} \psi_m(y) \ . \tag{5.52}$$

Tab. 5.2: The wave numbers $\tilde{k}_m$ ($m = 0, 1, \ldots, 5$) depending on the dimensionless drift parameter Ω.

| Ω	-10.0	-5.0	-2.0	-1.0	0.0	1.0	2.0	5.0	10.0
$m = 0$	4.999	2.464	0.000	1.165	1.571	1.836	2.028	2.381	2.653
$m = 1$	3.790	4.172	4.493	4.604	4.712	4.816	4.913	5.163	5.454
$m = 2$	7.250	7.533	7.725	7.789	7.854	7.917	7.979	8.151	8.391
$m = 3$	10.553	10.767	10.904	10.949	10.995	11.040	11.085	11.214	11.408
$m = 4$	13.789	13.959	14.066	14.101	14.137	14.172	14.207	14.310	14.469
$m = 5$	16.992	17.133	17.220	17.249	17.279	17.308	17.336	17.421	17.556
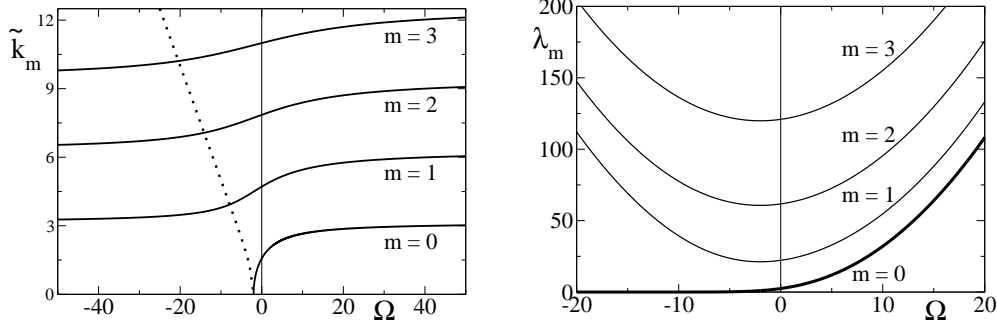
Fig. 5.6: The parameter dependence of wave numbers $\tilde{k}_m(\Omega)$ and eigenvalues $\lambda_m(\Omega)$ for ground state $m = 0$ and excited states $m = 1, 2, 3$.
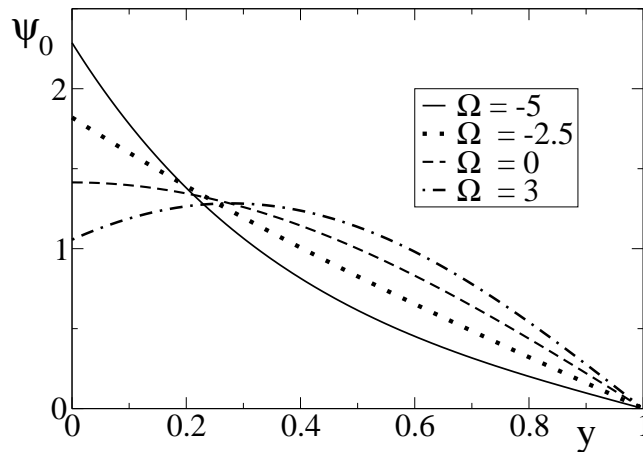
Fig. 5.7: The eigenfunction $\psi_0(y)$ for different values of control parameter Ω.
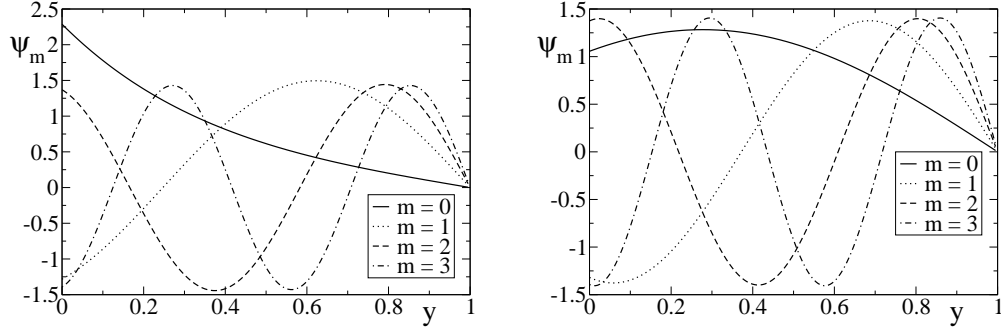
Fig. 5.8: The eigenfunctions $\psi_m(y)$ for $m = 0, 1, 2, 3$ and for $\Omega = -5.0$ (left) and $\Omega = 3.0$ (right).

By inserting the initial condition

$$P(y, T = 0) = e^{\frac{\Omega}{2}y}Q(y, T = 0) = \delta(y - y_0) \tag{5.53}$$

into (5.52) we obtain

$$\sum_{m=0}^{\infty} C_m\psi_m(y) = e^{-\frac{\Omega}{2}y}\delta(y - y_0) . \tag{5.54}$$

Now we expand the right hand side of this equation by using the basis of orthonormalised eigenfunctions (5.46) and identify C_m with the corresponding coefficient at ψ_m, i. e.,

$$C_m = \int e^{\frac{\Omega}{2}y}\delta(y - y_0)\psi_m dy = e^{-\frac{\Omega}{2}y_0}\psi_m(y_0) . \tag{5.55}$$

This allows us to write the solution for $P(y, T)$ as

$$P(y, T) = e^{\frac{\Omega}{2}(y - y_0)} \sum_{m=0}^{\infty} e^{-\lambda_m T}\psi_m(y_0)\psi_m(y) , \tag{5.56}$$

with eigenfunctions (5.46) and (5.50) of ground state ($m = 0$)

$$\psi_0(y) = \begin{cases} \sqrt{\dfrac{2}{1 + \frac{\Omega}{2}\frac{1}{\tilde{k}_0^2 + \Omega^2/4}}} \sin\left[\tilde{k}_0(1 - y)\right] , & \Omega > -2 \\[20pt] \sqrt{3}\,(1 - y) , & \Omega = -2 \\[20pt] \sqrt{-\dfrac{2}{1 + \frac{\Omega}{2}\frac{1}{-\kappa_0^2 + \Omega^2/4}}} \sinh\left[\kappa_0(1 - y)\right] , & \Omega < -2 \end{cases} \tag{5.57}$$

and all other eigenfunctions (5.46)

$$\psi_m(y) = \sqrt{\frac{2}{1 + \frac{\Omega}{2}\frac{1}{\tilde{k}_m^2 + \Omega^2/4}}} \ \sin\left[\tilde{k}_m(1-y)\right] \quad m = 1, 2, \ldots . \tag{5.58}$$

The eigenvalue of ground state $(m = 0)$ is given by

$$\lambda_0 = \begin{cases} \tilde{k}_0^2 + \Omega^2/4\,, & \Omega > -2 \\[2mm] 1\,, & \Omega = -2 \\[2mm] -\kappa_0^2 + \Omega^2/4\,, & \Omega < -2 \end{cases} \tag{5.59}$$

and all others are

$$\lambda_m = \tilde{k}_m^2 + \Omega^2/4 \qquad m = 1, 2, \ldots , \tag{5.60}$$

where the wave numbers are calculated from transcendental equation (5.42)

$$\tilde{k}_0 \ : \qquad \tan \tilde{k}_0 = -\frac{2}{\Omega}\,\tilde{k}_0 \qquad \Omega > -2 \tag{5.61}$$

$$\kappa_0 \ : \qquad \tanh \kappa_0 = -\frac{2}{\Omega}\,\kappa_0 \qquad \Omega < -2 \tag{5.62}$$

$$\tilde{k}_m \ : \qquad \tan \tilde{k}_m = -\frac{2}{\Omega}\,\tilde{k}_m \qquad m = 1, 2, \ldots . \tag{5.63}$$

The set of Figs. 5.9 illustrates the time evolution of probability density (5.56) choosing different parameter values Ω.

5.3 First Passage Time Probability Density

It has been shown in previous Sections that the probability density $P(y, T)$ is not normalized under given restrictions, i. e. reflected at $y = 0$ and absorbed at $y = 1$. Due to that fact, let us apply here the balance equation in the open system given in dimensionless variables by

$$\overline{\mathcal{P}}(T, y = 1) = -\frac{\partial}{\partial T} \int\limits_0^1 P(y, T)\,dy \tag{5.64}$$

which relates the probability $P(y, T)$ that the system is still in a state $y \in [0, 1]$ with the probability flux $\overline{\mathcal{P}}(T, y = 1)$ out of this interval at the right absorbing boundary $y = 1$ at time moment T. Hence, $\overline{\mathcal{P}}(T, y = 1)$ is the first passage time probability density [13, 22, 82]. It can be calculated by using obtained results of previous Section. The first passage time probability density distribution $\overline{\mathcal{P}}$ (breakdown probability density) depending on Ω reads as follows
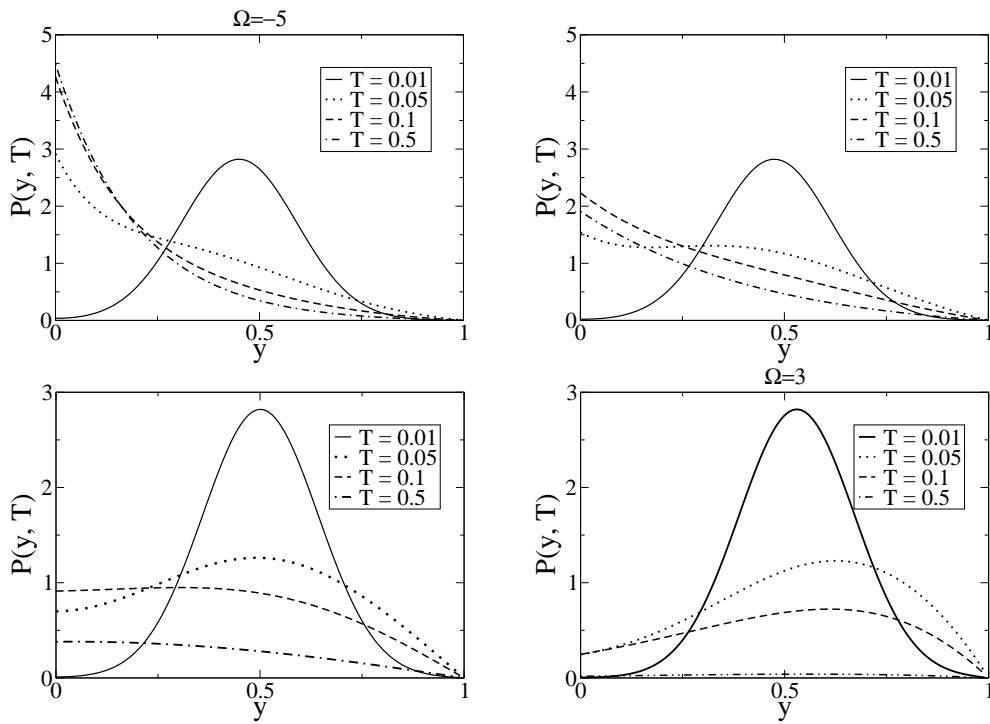
Fig. 5.9: The solution of drift–diffusion Fokker–Planck equation with initial condition $y_0 = 0.5$ for different values of the control parameter Ω, i. e. $\Omega = -5.0$ (top left), $\Omega = -2.5$ (top right), $\Omega = 0.1$ (bottom left), $\Omega = 3.0$ (bottom right).
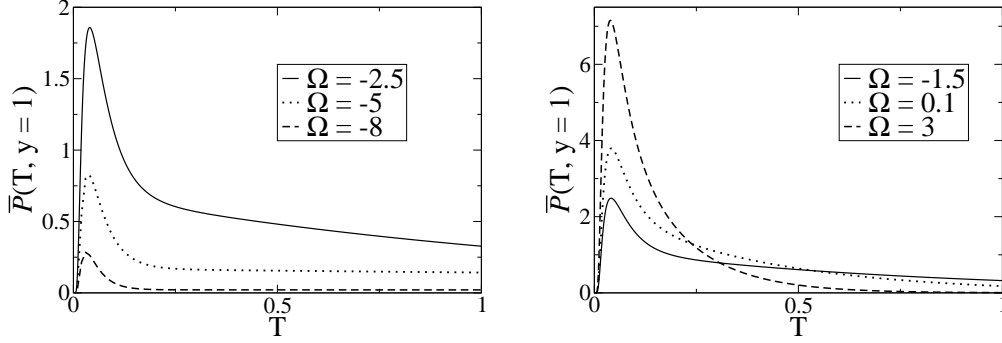
Fig. 5.10: The first passage time probability density distribution $\overline{\mathcal{P}}(T, y = 1)$ for $\Omega < -2$ (left) and $\Omega > -2$ (right) obtained for the fixed initial condition $y_0 = 0.5$.

1. $\Omega > -2$

$$\overline{\mathcal{P}}(T, y = 1) = 2e^{\frac{\Omega}{2}(1-y_0)} \sum_{m=0}^{\infty} \frac{e^{-\left(\tilde{k}_m^2 + \Omega^2/4\right)T}}{1 + \frac{\Omega}{2}\frac{1}{\tilde{k}_m^2 + \Omega^2/4}} \tilde{k}_m \sin\left[\tilde{k}_m(1 - y_0)\right] \qquad (5.65)$$

2. $\Omega = -2$

$$\begin{aligned}
\overline{\mathcal{P}}(T, y = 1) &= e^{-(1-y_0)}\Bigg[3\left(1 - y_0\right)e^{-T} \\
&\quad + 2\sum_{m=1}^{\infty} \frac{e^{-\left(\tilde{k}_m^2 + 1\right)T}}{1 - \frac{1}{\tilde{k}_m^2 + 1}} \tilde{k}_m \sin\left[\tilde{k}_m(1 - y_0)\right]\Bigg]
\end{aligned} \qquad (5.66)$$

3. $\Omega < -2$

$$\begin{aligned}
\overline{\mathcal{P}}(T, y = 1) &= 2e^{\frac{\Omega}{2}(1-y_0)} \\
&\quad \times \Bigg[-\frac{e^{-\left(-\kappa_0^2 + \Omega^2/4\right)T}}{1 + \frac{\Omega}{2}\frac{1}{-\kappa_0^2 + \Omega^2/4}} \kappa_0 \sinh\left[\kappa_0(1 - y_0)\right] \\
&\quad + \sum_{m=1}^{\infty} \frac{e^{-\left(\tilde{k}_m^2 + \Omega^2/4\right)T}}{1 + \frac{\Omega}{2}\frac{1}{\tilde{k}_m^2 + \Omega^2/4}} \tilde{k}_m \sin\left[\tilde{k}_m(1 - y_0)\right]\Bigg]
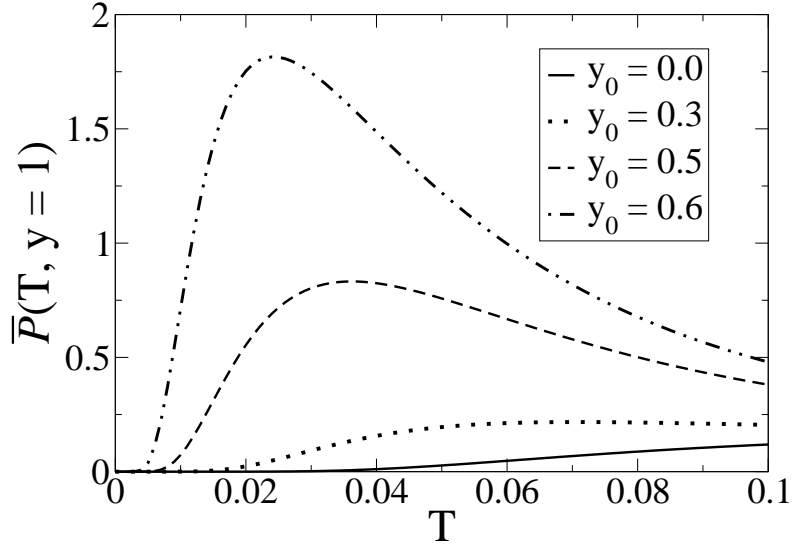\end{aligned} \qquad (5.67)$$

The outflow distribution $\overline{\mathcal{P}}(T, y = 1)$ is shown in Fig. 5.10 (with different values of dimensionless drift Ω) as well as in Fig. 5.11 (with different values of initial condition y_0).

Fig. 5.11: Short time behaviour of first passage time probability density distribution $\overline{\mathcal{P}}(T, y = 1)$ for $\Omega = -2$ and different initial conditions $0 \leq y_0 \leq 1$ showing time lag.

5.4 Cumulative Breakdown Probability

The probability that the absorbing boundary $y = 1$ is reached within certain observation time interval $0 \leq T \leq T_{obs}$ is given by the cumulative (breakdown) probability

$$W\left(\Omega, T = T_{obs}\right) = \int\limits_{0}^{T_{obs}} \overline{\mathcal{P}}(T, y = 1)\, dT \tag{5.68}$$

with $\overline{\mathcal{P}}(T, y = 1)$ from (5.64). For $T_{obs} \to \infty$ we have $W \to 1$. Generally, we obtain
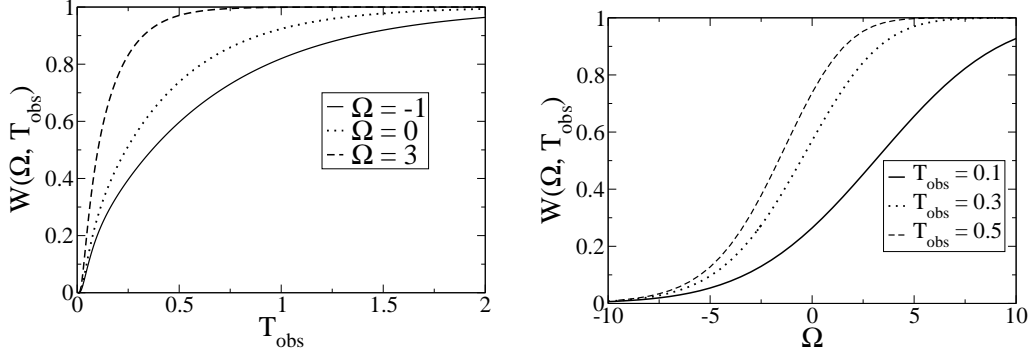
1. $\Omega > -2$

$$W\left(\Omega, T_{obs}\right) = 2e^{\frac{\Omega}{2}(1-y_0)} \sum_{m=0}^{\infty} \frac{1 - e^{-\left(\tilde{k}_m^2 + \Omega^2/4\right)T_{obs}}}{\tilde{k}_m^2 + \Omega^2/4 + \Omega/2} \tilde{k}_m \sin\left[\tilde{k}_m(1 - y_0)\right] \tag{5.69}$$

2. $\Omega = -2$

$$
\begin{aligned}
W\left(\Omega, T_{obs}\right) &= e^{-(1-y_0)}\Bigg[3\left(1 - e^{-T_{obs}}\right)(1 - y_0) \\
&\quad + 2\sum_{m=1}^{\infty} \frac{1 - e^{-\left(\tilde{k}_m^2 + 1\right)T_{obs}}}{\tilde{k}_m} \sin\left[\tilde{k}_m(1 - y_0)\right] \Bigg].
\end{aligned}
\tag{5.70}
$$

Fig. 5.12: The probability $W(\Omega, T_{obs})$ (5.68) as function of observation time T_{obs} with fixed Ω (left) and vice versa (right).

3. $\Omega < -2$

$$
\begin{aligned}
W\left(\Omega, T_{obs}\right) &= 2\, e^{\frac{\Omega}{2}(1-y_0)} \\
&\quad \times \Bigg[-\frac{1 - e^{-\left(-\kappa_0^2 + \Omega^2/4\right)T_{obs}}}{-\kappa_0^2 + \Omega^2/4 + \Omega/2}\kappa_0 \sinh\left[\kappa_0(1 - y_0)\right] \\
&\quad + \sum_{m=1}^{\infty} \frac{1 - e^{-\left(\tilde{k}_m^2 + \Omega^2/4\right)T_{obs}}}{\tilde{k}_m^2 + \Omega^2/4 + \Omega/2}\tilde{k}_m \sin\left[\tilde{k}_m(1 - y_0)\right] \Bigg] \quad (5.71)
\end{aligned}
$$

Fig. 5.12 shows $W\left(\Omega, T_{obs}\right)$ as a function of observation time T_{obs} (left) as well as parameter dependence Ω (right).

5.5 Limit Case for Large Positive Values of the Control Parameter

Consider parameter limit $\Omega \to +\infty$ which corresponds either to large positive drift v and/or large interval $b - a$, or to a small diffusion coefficient D. In this case, for a given m, the solution of the transcendental equation can be found in the form $\tilde{k}_m = \pi(m + 1) - \varepsilon_m$, where ε_m is small and positive. From the periodicity property we obtain

$$
\cos\tilde{k}_m = \cos(\pi(m + 1) - \varepsilon_m) = -(-1)^m \cos(\varepsilon_m) = -(-1)^m + \mathcal{O}\left(\varepsilon_m^2\right)
$$

$$
\sin\tilde{k}_m = \sin(\pi(m + 1) - \varepsilon_m) = (-1)^m \sin(\varepsilon_m) = (-1)^m\varepsilon_m + \mathcal{O}\left(\varepsilon_m^3\right) \ .
$$

By inserting this into the transcendental equation (5.41), we obtain

$$
\varepsilon_m = \frac{2}{\Omega}\pi(m + 1) + \mathcal{O}\left(\Omega^{-2}\right) , \tag{5.72}
$$

$$
\sin(\tilde{k}_m) = \frac{2}{\Omega}(-1)^m\pi(m + 1) + \mathcal{O}\left(\Omega^{-2}\right) \ . \tag{5.73}
$$

In this approximation the normalisation integral for large Ω and with the initial condition $y_0 \to 0$ can be written as

$$
\begin{aligned}
I &= \int\limits_0^\infty \overline{\mathcal{P}}(T, y = 1)\, dT = 2e^{\Omega/2} \sum_{m=0}^\infty \frac{\tilde{k}_m \sin\left(\tilde{k}_m\right)}{\lambda_m + \Omega/2} \\[2mm]
&\simeq e^{\Omega/2} \sum_{m=1}^\infty \frac{-4}{\Omega} \frac{(-1)^m (\pi m)^2}{\pi^2 m^2 + \Omega^2/4} = e^{\Omega/2} \sum_{m=-\infty}^\infty \frac{-2}{\Omega} \frac{(-1)^m (\pi m)^2}{\pi^2 m^2 + \Omega^2/4}\ .
\end{aligned}
\tag{5.74}
$$

Further on we set $(-1)^m = e^{i\pi m}$ and, in a continuum approximation, replace the sum by the integral

$$
I \simeq e^{\Omega/2} \int\limits_{-\infty}^\infty \frac{-2}{\Omega} \frac{e^{i\pi m}(\pi m)^2}{\pi^2 m^2 + \Omega^2/4} dm\ .
\tag{5.75}
$$

Now we make an integration contour in the complex plane, closing it in the upper plane ($\Im(m) > 0$) at infinity where $|e^{i\pi m}|$ is exponentially small. According to the residue theorem, it yields

$$
I = 2\pi i \sum_i \text{Res}(m_i) = 2\pi i\, \text{Res}(m_0)\ ,
\tag{5.76}
$$

where $m_0 = \frac{i\Omega}{2\pi}$ is the location of the pole in the upper plane, found as a root of the equation $\pi^2 m^2 + \Omega^2/4 = 0$. According to the well–known rule, the residue is calculated by setting $m = m_0$ in the enumerator of (5.75) and replacing the denominator with its derivative at $m = m_0$. It gives the desired result $I = 1$, i. e., the considered approximation gives correct normalisation of outflow probability density $\overline{\mathcal{P}}(T, y = 1)$ at the right boundary.

The probability distribution function $P(y, T)$ given by (5.56) can also be calculated in such a continuum approximation. In this case the increment of wave numbers is

$$
\Delta \tilde{k}_m = \tilde{k}_{m+1} - \tilde{k}_m = \pi + \varepsilon_m - \varepsilon_{m+1} \simeq \pi \left(1 - \frac{2}{\Omega}\right) \simeq \frac{\pi}{1 + 2/\Omega}\ .
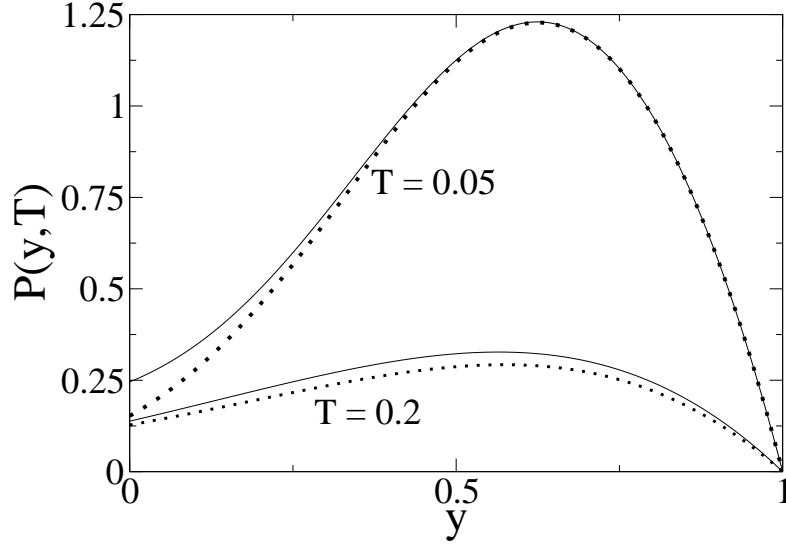\tag{5.77}
$$

Note that in this approximation for $\Omega \to \infty$ the normalisation constant R_m in (5.45) is related to the increment $\Delta \tilde{k}$ via

$$
R_m^2 = \frac{2}{1 + \frac{\Omega}{2}\frac{1}{\tilde{k}_m^2 + \Omega^2/4}} \simeq \frac{2}{1 + 2/\Omega} \simeq \frac{2}{\pi}\Delta \tilde{k}_m\ .
\tag{5.78}
$$

Hence, the equation (5.56) for the probability density can be written as

$$
P(y, T) = 2e^{\frac{\Omega}{2}(y - y_0)} \sum_{m=0}^\infty R_m^2 e^{-\lambda_m T} \sin\left[\tilde{k}_m (1 - y_0)\right] \sin\left[\tilde{k}_m (1 - y)\right]
\tag{5.79}
$$

$$
\simeq \frac{2}{\pi} e^{\frac{\Omega}{2}(y - y_0)} \sum_{m=0}^\infty e^{-\left(\tilde{k}_m^2 + \Omega^2/4\right)T} \sin\left[\tilde{k}_m (1 - y_0)\right] \sin\left[\tilde{k}_m (1 - y)\right] \Delta \tilde{k}_m\ .
$$

Fig. 5.13: Comparison of probability density $P(y, T)$ in drift–diffusion–dynamics with finite boundaries for two time moments. Parameter value is $\Omega = 3.0$; initial condition is $y_0 = 0.5$. The solid lines represent the exact result (5.56); dotted lines display the approximation (5.81).

In the continuum approximation we replace the sum by the integral

$$P(y, T) \simeq \frac{2}{\pi} e^{\frac{\Omega}{2}(y - y_0)} \int\limits_0^\infty e^{-\left(\tilde{k}^2 + \Omega^2/4\right)T} \sin\left[\tilde{k}\left(1 - y_0\right)\right] \sin\left[\tilde{k}\left(1 - y\right)\right] d\tilde{k} \quad (5.80)$$

$$= \frac{1}{\pi} e^{\frac{\Omega}{2}(y - y_0)} \int\limits_0^\infty e^{-\left(\tilde{k}^2 + \Omega^2/4\right)T} \left(\cos\left[\tilde{k}\left(y - y_0\right)\right] - \cos\left[\tilde{k}\left(2 - y - y_0\right)\right]\right) d\tilde{k} \; .$$

In the latter transformation we have used the identity $\sin\alpha \sin\beta = \frac{1}{2}\left(\cos(\alpha - \beta) - \cos(\alpha + \beta)\right)$. The resulting known integrals yield

$$P(y, T) \simeq \frac{1}{\sqrt{4\pi T}} e^{\frac{\Omega}{2}\left(y - y_0 - \frac{\Omega}{2}T\right)} \left[e^{-\frac{(y - y_0)^2}{4T}} - e^{-\frac{(2 - y - y_0)^2}{4T}}\right] \; . \quad (5.81)$$

The approximation (5.81) is shown in Fig. 5.13. For short enough times $4T \ll (2 - y - y_0)^2$ the second term is very small. Neglecting this term, equation (5.81) reduces to the known exact solution for natural boundary conditions.

Based on (5.81), it is easy to calculate the probability flux

$$J(y, T) = \Omega P(y, T) - \frac{\partial}{\partial y} P(y, T) \quad (5.82)$$

and the first passage time distribution $\overline{\mathcal{P}}(T) = J(y = 1, T)$ which takes a particularly simple form

$$\overline{\mathcal{P}}(T) = \frac{1 - y_0}{\sqrt{4\pi T^3}} e^{-\frac{(1-y_0-\Omega T)^2}{4T}} .$$

(5.83)

The cumulative breakdown probability (5.68) is then

$$W(\Omega, T = T_{obs}) = \int\limits_0^{T_{obs}} \frac{1 - y_0}{\sqrt{4\pi T^3}} e^{-\frac{(1-y_0-\Omega T)^2}{4T}} dT .$$

(5.84)

The given explanations show the analytical method how to solve drift–diffusion initial–boundary–value problem for the case of reflecting and absorbing boundaries [13, 22, 55, 56, 82]. On the basis of Sturm–Liouville theory, the set of eigenvalues with corresponding eigenfunctions has been found. Here we have paid our attention to wave number calculations from transcendental equations. The equations have been solved numerically by Newton method [79]. The main problem which has been solved was the dependence of obtained results on drift value, i. e. different cases of control parameter $\Omega < -2$, $\Omega = -2$ and $\Omega > -2$. First case of $\Omega < -2$ corresponds to the situation when it is difficult and probably impossible, with significant small probability and for long times only, to leave the interval due to the large negative value of drift. The case of $\Omega = -2$ has been considered as limit case and the corresponding solution has been found. The opposite case of $\Omega > -2$ shows the usual situation when the system reaches the right border relatively fast. As application, the first passage time distribution as well as the cumulative probability have been calculated. The case of large positive values of Ω has been investigated in detail and has been obtained as approximation.

5.6 Relationship to Sturm–Liouville Theory

The particular drift–diffusion–problem over a finite interval with reflecting (left) and absorbing (right) boundaries belongs to the following general mathematical theory named after Jacques Charles Francois Sturm (1803–1855) and Joseph Liouville (1809–1882).

The classical Sturm–Liouville theory considers a real second–order linear differential equation of the form [103]

$$-\frac{d}{dx}\left[p(x)\frac{d\psi}{dx}\right] + q(x)\psi = \lambda\, w(x)\psi$$

(5.85)

together with boundary conditions at the ends of interval $[a, b]$ given by

$$\alpha_1\psi(x = a) + \alpha_2 \left.\frac{d\psi}{dx}\right|_{x=a} = 0 ,$$

(5.86)

$$\beta_1\psi(x = b) + \beta_2 \left.\frac{d\psi}{dx}\right|_{x=b} = 0 .$$

(5.87)

The particular functions $p(x), q(x), w(x)$ are real and continuous on the finite interval $[a, b]$ together with specified values at the boundaries. The aim of the Sturm–Liouville problem is to find the values of λ (called eigenvalues λ_n) for which there exist non–trivial solutions of the differential equation (5.85) satisfying the boundary conditions (5.86) and (5.87). The corresponding solutions (for such λ_n) are called eigenfunctions $\psi_n(x)$ of the problem.

Defining the Sturm–Liouville differential operator over the unit interval $[0, 1]$ by

$$\mathcal{L}\psi = -\frac{d}{dx}\left[p(x)\frac{d\psi}{dx}\right] + q(x)\psi \tag{5.88}$$

and putting the weight $w(x)$ to unity $(w = 1)$ the general equation (5.85) can precisely be written as eigenvalue problem

$$\mathcal{L}\psi = \lambda\psi \tag{5.89}$$

with boundary conditions (5.86)$(a = 0)$ and (5.87) $(b = 1)$ written as

$$\mathcal{B}_0\psi = 0 \qquad \mathcal{B}_1\psi = 0 . \tag{5.90}$$

Assuming a differentiable positive function $p(x) > 0$ the Sturm–Liouville operator is called regular and it is self–adjoint to fulfil

$$\int_0^1 \mathcal{L}\psi_1 \cdot \psi_2 = \int_0^1 \psi_1 \cdot \mathcal{L}\psi_2 . \tag{5.91}$$

Any self–adjoint operator has real nonnegative eigenvalues $\lambda_0 < \lambda_1 < \ldots < \lambda_n < \ldots \to \infty$. The corresponding eigenfunctions $\psi_n(x)$ have exact n zeros in $(0, 1)$ and form an orthogonal set

$$\int_0^1 \psi_n(x)\psi_m(x)dx = \delta_{mn} . \tag{5.92}$$

The eigenvalues λ_n of the classical Sturm–Liouville problem (5.85) with positive function $p(x) > 0$ as well as positive weight function $w(x) > 0$ together with separated boundary conditions (5.86) and (5.87) can be calculated by the following expression

$$\lambda_n \int_a^b \psi_n(x)^2 w(x)dx = \int_a^b \left[p(x)\left(d\psi_n(x)/dx\right)^2 + q(x)\psi_n(x)^2\right]dx$$
$$- \left|p(x)\psi_n(x)\left(d\psi_n(x)/dx\right)\right|_a^b . \tag{5.93}$$

The eigenfunctions are mutually orthogonal $(m \neq n)$ and usually normalized $(m = n)$

$$\int_a^b \psi_n(x)\psi_m(x)w(x)dx = \delta_{mn} \tag{5.94}$$

known as orthogonality relation (similar to (5.92)).

Comming back to the original drift–diffusion problem written in dimensionless variables over unit interval $0 \leq y \leq 1$ and recalling (5.28) the separation constant λ appears in the following differential equation

$$-\frac{d^2\psi(y)}{dy^2} + \frac{\Omega^2}{4}\psi(y) = \lambda\psi(y) \tag{5.95}$$

which can be related to the regular Sturm–Liouville eigenvalue problem via $p(y) = 1 > 0$; $w(y) = 1 > 0$ and $q(y) = \Omega^2/4$.

The boundary conditions given by (5.34) and (5.37) can be expressed as

$$\frac{\Omega}{2} \cdot \psi(y = 0) + (-1) \cdot \left.\frac{d\psi}{dy}\right|_{y=0} = 0 \, , \tag{5.96}$$

$$1 \cdot \psi(y = 1) + 0 \cdot \left.\frac{d\psi}{dy}\right|_{y=1} = 0 \tag{5.97}$$

in agreement with (5.86) and (5.87).

The up–to–now unknown separation constant λ has a spectrum of real positive eigenvalues which can be calculated using (5.93) from

$$\lambda_n = \int_0^1 \left[\left(\frac{d\psi_n(y)}{dy}\right)^2 + \frac{\Omega^2}{4}\psi_n(y)^2\right] dx - \left|\psi_n(y)\frac{d\psi_n(y)}{dy}\right|_0^1 \tag{5.98}$$

taking into account normalized orthogonal eigenfunction (5.94)

$$\int_0^1 \psi_n(y)\psi_m(y)dy = \delta_{mn} \, . \tag{5.99}$$

5.7 Comparison with Empirical Data

This Section presents the comparison of empirical data with the analytical solution obtained for the cumulative breakdown probability (5.69) – (5.71). The empirical data taken from German autobahn A2 and A3 have been obtained for the three–lane road and have been processed by Brilon and Regler [9, 83]. The data have been carried out by the application of the Product Limit Method based on the statistics of lifetime data analysis [39]. The measurements have been collected for the observation time interval $t_{obs} = 5$ min. As result, the cumulative breakdown probability $W(q)$ as a function of flow rate q have been calculated. Intuitively, the following asymptotic behaviour of the probability $W(q)$ can be expected

$$W(q) = \begin{cases} 0 & : \quad q \to 0 \\ 1 & : \quad q \to \infty \end{cases} \, . \tag{5.100}$$

In order to compare the empirical data with the analytical calculations presented in Section 5.12, the following transformations relating the parameters in our equations to the physical observables have been used

$$x = l_{eff}\, n \tag{5.101}$$

$$v = \left(q - \frac{1}{\tau}\right) l_{eff} \tag{5.102}$$

$$D = \frac{1}{2}\left(q + \frac{1}{\tau}\right) l_{eff}^2\,, \tag{5.103}$$

where n is the cluster size, q is the inflow rate being identical to the attachment rate $w_+(n)$. The parameter τ is specified as the relaxation time. The quantity $1/\tau$ is related to the detachment rate. These quantities have been introduced in Section 5.1. The value l_{eff} is the effective length of car. Then, some other control parameters are calculated from

$$\text{initial value:} \quad x_0 = l_{eff}\, n_0 \tag{5.104}$$

$$\text{reflecting boundary:} \quad a = l_{eff}\, n_0 \tag{5.105}$$

$$\text{absorbing boundary:} \quad b = l_{eff}\, n_{esc}\,. \tag{5.106}$$

Due to the given definition of traffic breakdown as a car cluster formation, the only parameter which allows fitting the empirical data is the escape cluster size n_{esc}. All other parameters like inverse discharge rate τ are fixed within a narrow range due to elementary definitions. The escape size n_{esc} defines the number of vehicles within a cluster to discriminate congested $(n > n_{esc})$ from non-congested $(n < n_{esc})$ traffic and summarize therefore the thresholds for a breakdown in comparison with statistical undulations. The value of n_{esc} is about 40% higher in case of a traffic control system switched on along the regarded road section and shows the effects of traffic control systems by stabilizing traffic flow. It leads to an onset of the breakdown at higher critical traffic volumes in comparison to situation without a traffic control system. The range n_{esc} is limited to realistic cluster sizes. Very small values like $n_{esc} = 2$ veh make no sense as well as too large values $n_{esc} = 1000$. Such extremes can be omitted.

The shape of cumulative breakdown probability (5.69) – (5.71) shown in Fig. 5.12 reminds to the stochastic distributions used in reliability assessment [83]. This function is called *Weibull distributions* and has been used as a fitting function of the empirical data analyzed by Regler et. al. [83]. The Weibull function is defined as [11, 71]

$$F_{weibull}(q) = 1 - \exp\left[-\left(\frac{q}{\beta}\right)^{\alpha}\right]. \tag{5.107}$$

The distribution $F_{weibull}(q)$ given by (5.107) has two control parameters. The shape of the function (5.107) is controlled by the parameter α. The parameter β
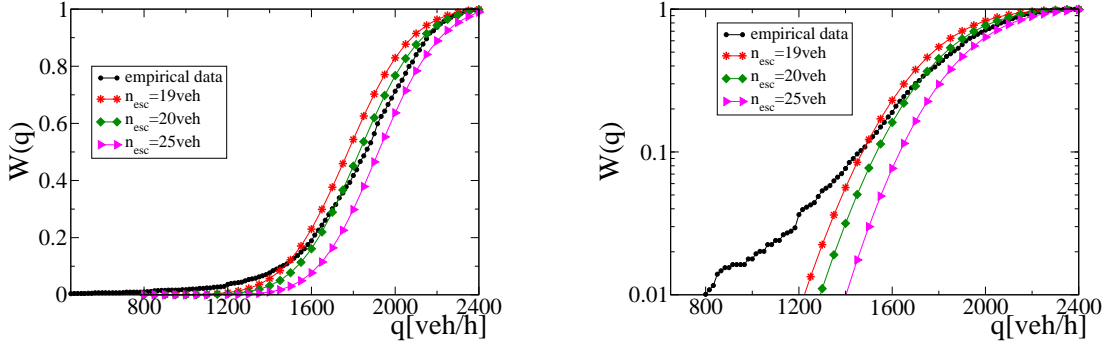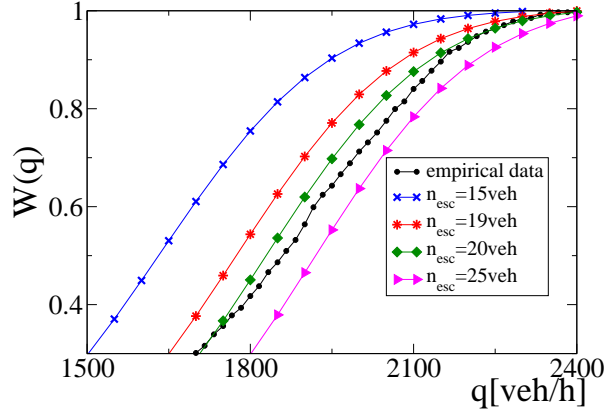
Fig. 5.14: Cumulative breakdown probability $W(q)$ obtained analytically and given by formulae (5.69) – (5.71) for the time interval $t_{obs} = 5$ min taking into account the transformation (5.101) – (5.103) (left plot). Black circles represent the empirical data from German autobahn A2 [83]. Other points are analytical results (5.69) – (5.71) for the different values of absorbing barrier $b = n_{esc}\,l_{eff}$. The parameters have been chosen as $l_{eff} = 7$ m, $\tau = 2$ s, $x_0 = 10^{-2}$ m ($n_0 \approx 0$). Cumulative breakdown probability $W(q)$ represented in the logarithmic scale is shown in right plot.

is responsible for the scaling of the distribution $F_{weibull}(q)$ towads the q–axis. The analytical solutions (5.69) – (5.71) derived by the technique of the first passage time are given by infinite series. This fact makes the application of the obtained analytical results to empirical data analysis difficult. For this reason, we have examined the applied method not only by the comparison with the real data but with the theoretical curve given in terms of the Weibull distribution and presented by finite formula (5.107) as well.

Keeping in mind the transformations (5.101) – (5.103), the cumulative breakdown probability has been calculated as a function $W(q)$ of the inflow rate q. The empirical data have been provided for the three-lane road. In order to compare these data with analytical solution, we have divided each empirical value of q by factor of 3. Fig. 5.14 presents the analytical curves for the cumulative breakdown probability $W(q)$ which have been calculated for the observation time $t_{obs} = 5$ min and for different values of the escape cluster size n_{esc}. The influence of escape value n_{esc} on the behaviour of the function $W(q)$ manifests itself in the displacement of $W(q)$ towards the q–axis. Fig. 5.14 shows, that the empirical curve represented by black circles grows more smoothly and not so rapidly than the functions obtained analytically. This effect is illustrated in the left plot of Fig. 5.14 which presents the behaviour of both analytical and empirical curves in the logarithmic scale. Moreover, it seems to be, that the nature of the empirical curve is rather different from the analytical solution (5.69) – (5.71). In order to understand such a behaviour in details, Fig. 5.14 has been zoomed for the range space of the function $W(q) \geq 0.3$. The zoomed version is presented in Fig. 5.15.
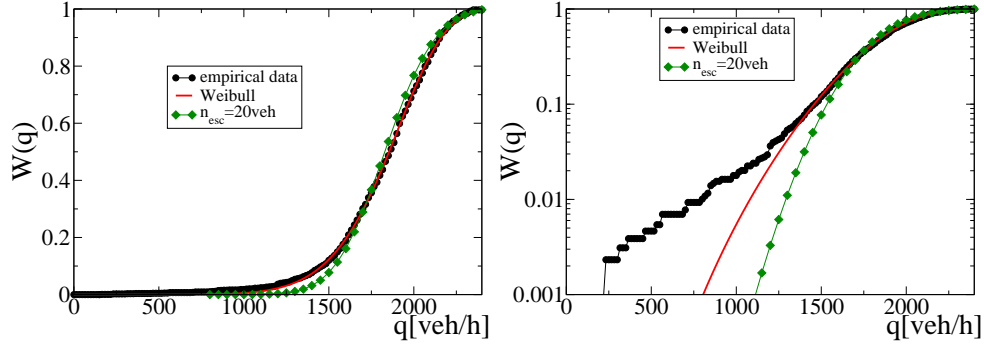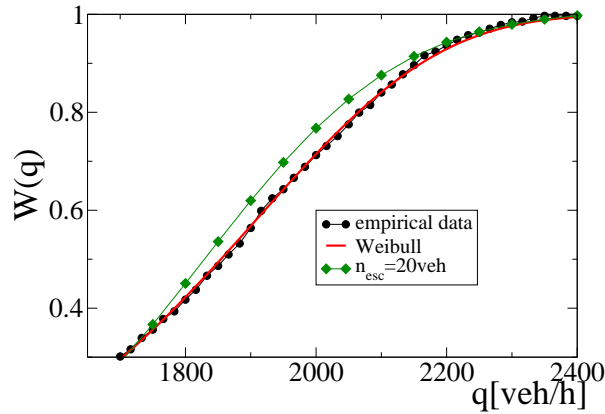
Fig. 5.15: Detailed picture of Fig. 5.14 for cumulative breakdown probability $W(q)$ given by formulae (5.69) – (5.71) for the value range $W(q) \geq 0.3$.

The theoretical curve calculated for $n_{esc} = 20$ veh shows the best agreement with the empirical breakdown function. Therefore, the analytical solution for $n_{esc} = 20$ veh has been plotted separately and compared with the both empirical curve and Weibull distribution given by the expression (5.107). The result is illustrated in Fig. 5.16 in original (right hand side) and logarithmic scales (left hand side). The analysis shows that for the inflow domain $q : q \leq 1650$ veh the agreement between analytical (5.69) – (5.71), empirical [83] and fitting curves [9,71,83] is rather week. Whereas, the functions are comparable favourably for larger inflow values $q : q \leq 1650$ veh (see Fig. 5.17). Fig. 5.18 shows the comparison of the cumulative breakdown probability $W(q)$ given by formulae (5.69) – (5.71) with the measurements taken from the German autobahn A3 [83]. In this case, the empirical data represent the behaviour of the cumulative breakdown probability in the region $W(q) \lesssim 0.5$. In order to verify the given measurements, the analytical solution (5.69) – (5.71) has been calculated for the different values of the control parameters n_{esc} and τ. The performed analysis shows that the analytical solution (5.69) – (5.71) of the drift–diffusion equation (5.19) including initial (5.20) and boundary conditions (5.21) – (5.22) does not completely agree with the empirical data. The empirical data shows rather different behaviour. The obtained discrepancy between the derived analytical solution and real data can be explained by the fact, that the technique of the first passage time has been applied for the case of constant inflow and outflow rates and, therefore, for the constant drift and diffusion terms. It seems, that there is rather sophisticated dependence for these functions. However, in this case, it is almost impossible to get the strong analytical result.

We have considered the traffic breakdown phenomenon regarded as a random process developing via the nucleation mechanism. The origin of critical jam nuclei proceeds in a metastable phase of traffic flow and seems to be located
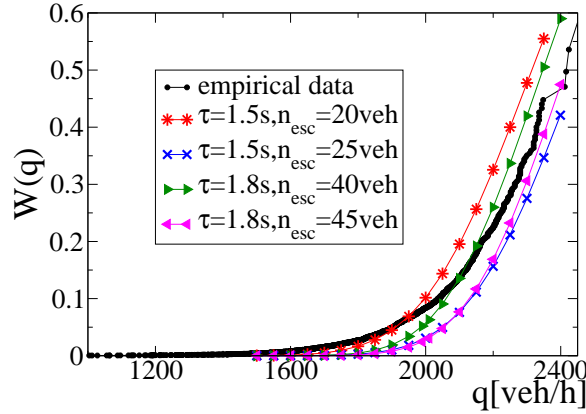
Fig. 5.16: Cumulative breakdown probability $W(q)$ and given by formulae (5.69) – (5.71) (diamond points) calculated for $n_{esc} = 20$ veh and $t_{obs} = 5$ min taking into account the transformation (5.101) – (5.103). Empirical data are marked by circles. Weibull distribution $F_{weibull}$ given by (5.107) presented by smooth curve (left plot). Parameters of the Weibull distribution have been chosen as $\alpha = 7.84$ and $\beta = 1943$. The plot on the right represents the obtained results in logarithmic scale.

Fig. 5.17: Detailed picture of Fig. 5.16 for cumulative breakdown probability $W(q)$ given by formulae (5.69) – (5.71) for the value range $W(q) \geq 0.3$.

Fig. 5.18: Cumulative breakdown probability $W(q)$ given by formulae (5.69) – (5.71) obtained for the observation time interval $t_{obs} = 5$ min. Black circles are empirical data taken from German autobahn A3 [83]. Another points are analytical result (5.69) – (5.71) for the different values of the escape value n_{esc} and relaxation time τ. The parameters have been chosen as $l_{eff} = 7$ m, $\tau = 2$ s, $x_0 = 10^{-2}$ m ($n_0 \approx 0$).

inside a not too large region on a highway, for example, in the close proximity of a highway bottleneck. The induced complex structure of the congested traffic phase is located upstream of the bottleneck. Keeping these properties in mind, we have applied the probabilistic model regarding the jam emergence as the development of a large car cluster on highway. In these terms the traffic breakdown proceeds through the formation of a certain car cluster of overcritical size in the metastable vehicular flow, which enables us to confine ourselves to the single cluster model. A method how to calculate the traffic breakdown in this simple physical model has been discussed and developed. The results have been compared with real empirical data [83].

6 Summary and Outlook

The application of physics of stochastic processes to vehicular traffic problems has been done within the framework of this thesis. The main objective of this work was to provide the detailed analysis of the possible states of traffic flow dynamics by way of the thorough study of the cooperative motion phenomenon. For this purpose, both analytical and numerical approaches have been performed. The following directions of investigation and results should be underlined:

1. The microscopic description of vehicular ensemble governed by Bando's optimal velocity model for the motion on a circle one lane road has been examined in detail. The both approaches of the car following model deterministic and stochastic have been carried out. The detailed analysis has shown the Bando's model admits the existence of two phases of traffic flow only, i. e. either free or congested. The free flow is characterized by high velocities which are approximately equal to the maximal allowed speed. The congested traffic occurs with the increase of the car concentration. Such a movement is represented by the different numbers of moving clusters with the same velocity close to zero. In this sense, the probability densities of velocities and headway distances have been calculated for the different values of the car concentration. The headway distribution function can become bimodal according to the occupation on the road. In the long–time limit the many car system tends to certain stationary state. In the microscopic description it is either the fixed–point or the limit cycle in the phase space of velocities and headways depending on the overall car concentration and control parameters. The stationary state is characterised by certain internal energy. The analysis has shown that during the cluster formation process the internal energy increases as a step–like function.

2. In view of the fact that there is a hypothesis about three phases of traffic flow, the problem of understanding and description of the intermediate states has been addressed within the framework of this thesis. The new approach is based on study of dynamical states controlled by kinetic coefficients taking into account their anomalous properties and their dependence on position in phase space. The physical properties of a driver have a dominant role in the traffic dynamics. The driver can not equally control the relative velocity and the headway distance. Since the relative velocity of the car is the most important criterion for the safe driving, the reaction time of the driver on its changing vastly more than the reaction time for controlling of dinstance between two cars. Therefore, the

domain of small relative velocity plays the role of the dynamical trap. For this purpose, follow the leader model based on optimal velocity ansatz and including the dynamical trap effect has been proposed and developed. It has been shown that mutual effect of stochastic and deterministic forces governing the motion of the following car can give rise to the nonequilibrium phase transition of new type. It manifests itself that the headway distribution becomes bimodal and the distribution of the velocity difference has a Laplace form which is characterized by fat tails. In addition it has been demonstrated that the dynamical traps induce long time correlations in the car dynamics.

3. The traffic breakdown phenomenon regarded as a random process developing via the nucleation mechanism has been analyzed in detail. The origin of critical jam nuclei proceeds in a metastable phase of traffic flow and has been assumed to be located inside a not too large region on a highway, for example, in the close proximity of a highway bottleneck. The induced complex structure of the congested traffic phase is located upstream of the bottleneck. Keeping these properties in mind, the probabilistic model regarding the jam emergence as the development of a large car cluster on highway has been applied. In these terms the traffic breakdown proceeds through the formation of a certain car cluster of overcritical size in the metastable vehicular flow, which enable us to confine ourselves to the single cluster model. A method how to calculate the traffic breakdown in this simple physical model has been discussed and developed. The results have been compared with real empirical data. The empirical data shows rather different behaviour. The obtained discrepancy between the derived analytical solution and real data can be explained by the fact, that the technique of the first passage time has been applied for the case of constant inflow and outflow rates and, therefore, for the constant drift and diffusion terms. It seems, that there is rather sophisticated dependence for these functions. However, in this case, it is almost impossible to get the strong analytical result.

In view of the above mentioned results obtained within the framework of this thesis, the following outlooks for the future investigations can be underlined:

1. The concept of the dynamical trap can be applied to the vehicular ensemble governed by car following model. It is possible to expect that the dynamical traps caused by human bounded rationality can endow the system with a number of anomalous properties.

2. The empirical data presented the probability of traffic breakdown show rather different behaviour according to the obtained analytical results. In this sense, the theoretical approach should be improved. For this purpose, it is necessary to consider the multi lane model with a lane changing effect. Such a process can not be described by the one–step master equation meaning that more complex description should be introduced.

Bibliography

[1] P. W. Anderson, K. J. Arrow, D. Pines, *The economy as an evolving complex system*, Addison-Wesley, Redwood City, 1988

[2] L. Arnold, *Random dynamical systems*, Springer, Berlin, 1998

[3] M. Bando, K. Hasebe, A. Nakayama, A. Shibata and Y. Sugiyama, Japan. J. Ind. Appl. Math. **11**, 203, 1994

[4] M. Bando, K. Hasebe, A. Nakayama, A. Shibata and Y. Sugiyama, Phys. Rev. E **51**, 1035, 1995

[5] R. B. Banks, *Growth and diffusion phenomena*, Springer, Berlin, 1994

[6] A. N. Borodin, *Handbook of brownian motion – facts and formulae*, Birkhäuser, Berlin, 2002

[7] M. Brackstone, B. Sultan, M. McDonald, Transp. Res. Part F, **5**, 31, 2002

[8] N. V. Brilliantov, Th. Pöschel, *Kinetic theory of granular gases*, Oxford University Press, 2004

[9] W. Brilon, J. Geistefeldt, M. Regler, Reliability of Freeway Traffic Flow: A stochasti Concept of Capacity, Transportation and Traffic Theory, edited by H. S. Mahmassani, Elsevier Ltd., Oxford, 125–144, 2005

[10] W. Brilon, H. Zurlinden, Überlastungswahrscheinlichkeiten und Verkehrs-leistung als Bemessungskriterium for Straßenverkehrsanlagen (Breakdown probability and traffic efficiency as design criteria for freeways). Forschung Straßenbau und Straßenverkehrstechnik, No. 870, Bonn, 2003

[11] I. N. Bronshtein, et al., *Handbook of mathematics*, Springer, Berlin, 2004

[12] V. Capasso, D. Bakstein, *An introduction to continuous – time stochastic processes. Theory, models, and applications to finance, biology, and medicine*, Birkhäuser, Berlin, 2004

[13] M. H. Choi, R. F. Fox, Evolution of escape processes with a time-varying load, Phys. Rev. E **66**, 031103, 2002

Bibliography

[14] D. Chowdhury, L. Santen, and A. Schadschneider, Statistical physics of vehicular traffic and some related systems, Phys. Rep., **329**, 199–329, 2000

[15] K. L. Chung, R. J. Williams, *Introduction to stochastic integration*, Birkhäuser, Boston, 1990

[16] W. T. Coffey, Yu. P. Kalmykov, J. T. Waldron, *The Langevin equation with applications in physics, chemistry and electrical engineering*, Word Scientific Publishing, 1996

[17] C. F. Daganzo, M. J. Cassidy, R. L. Bertini, Possible explanations of phase transitions in highway traffic, Transp. Res., **33 A**, 365–379, 1999

[18] A. Einstein, Über die von der molekularkinetischen Theorie der Wärme geförderte Bewegung in ruhenden Flüssigkeiten suspendierten Teilchen, Annalen der Physik, **17**, 549–560, 1905

[19] T. M. R. Ellis, I. R. Philips, Th. M. Lahey, *Fortran 90 programming*, Addison–Wesley, 1994

[20] W. Feller, *An Introduction to probability theory and its applications*, Mir, Moscow, vol. 1, 1967

[21] S. Flügge, *Practical quantum mechanics*, Springer, Berlin, 1999

[22] R. F. Fox, M. H. Choi, Rectified brownian motion and kinesin motion along microtubules, Phys. Ref. E **63**, 051901, 2001

[23] T. D. Frank, *Nonlinear Fokker–Planck equations*, Springer, Berlin, 2005

[24] C. W. Gardiner, *Handbook of stochastic methods for physics, chemistry and the natural sciences*, Springer, Berlin, 2004

[25] D. C. Gazis, Mathematical theory of automobile traffic: improved understanding and control of traffic flow has become a fast-growing area of scientific research, Science, **157**, 273–281, 1967

[26] B. D. Greenshields, A study of highway capacity, in: *Proceedings of the Highway Research Board*, Washington, D. C., **14**, 448, 1935

[27] P. G. Gipps, Transp. Res., **15 B**, 105, 1981

[28] H. Haken, *Advanced Synergetics: Instability hierarchies of self-organizing systems and devices*, Springer Verlag, New York, 1983

[29] D. Helbing, Traffic and related self–driven many–particle system, Rev. Mod. Phys., **73**, 1067–1141, 2001

[30] D. Helbing, *Verkehrsdynamik*, Springer, Berlin, 1997

[31] D. Helbing, B. Tilch, Phys. Rev. E **58**, 133, 1998

[32] W. Helly, in: Proceedings of the Symposium on Theory of Traffic Flow, Research Laboratories, General Motors, Elsevier, New York, 207, 1959

[33] R. Herman, K. Gardels, Vehicular Traffic Flow, Sci. Am. **209** (6), 35, 1963

[34] J. Honerkamp, *Stochastische dynamische Systeme. Konzepte, numerische Methoden, Datenanalysen*, Wiley-VCH, Weinheim, 1990

[35] J. Honerkamp, *Statistical physics. An advanced approach with applications*, Springer, Berlin, 1998

[36] W. Horsthemke, R. Lefever, *Noise-induced phase transitions*, Springer, Berlin, 1984

[37] D. Jost, K. Nagel, Probabilistic traffic flow breakdown in stochastic car following models, Transportation Research Record, 1852, 152–158, 2003

[38] N. G. Kampen, *Stochastic processes in physics and chemistry*, Elsevier Science Publishers, 1992

[39] E. L. Kaplan, P. Meier, Nonparametric estimation from incomplete observations. Journal of the American Statistical Association, **53**, 457–481, 1958

[40] B. S. Kerner, Phase transitons in traffic flow, in: *Traffic and Granular Flow'99*, edited by D. Helbing, H. J. Herrmann, M. Schreckenberg and D. E. Wolf, Springer, Berlin, 253–283, 2000

[41] B. S. Kerner, Theory of congested traffic flow: self-organization without bottlenecks, in: *Transportation and Traffic Theory*, edited by A Ceder, Pergamon, Amsterdam, 147–171, 1999

[42] B. S. Kerner, Congested traffic flow. Observations and theory, Transp. Res. Rec. **1678**, 160–167, 1999

[43] B. S. Kerner, *The physics of traffic flow*, Springer, Berlin, 2004

[44] B. S. Kerner, S. L. Klenov, J. Phys. A, **35**, L31, 2005

[45] B. S. Kerner and H. Rehborn, Phys. Rev. E **53**, R1297, 1996

[46] B. S. Kerner and H. Rehborn, Phys. Rev. E **53**, R4275, 1996

[47] B. S. Kerner and H. Rehborn, Phys. Rev. Lett. **79**, 4030, 1997

Bibliography

[48] P. E. Kloeden, E. Platen, *Numerical solution of stochastic differential equations*, Springer, Berlin, 1992

[49] M. Krbalek, D. Helbing, Determination of interaction potentials in freeway traffic from steady-state statistics, Physica A **333**, 370, 2004

[50] S. Krauß, P. Wagner, C. Cawron, Phys. Rev. E **54**, 3707, 1996

[51] S. Krauß, P. Wagner, C. Cawron, Phys. Rev. E **55**, 5597, 1997

[52] R. Kühne, R. Mahnke, Controlling traffic breakdowns, International Symposium of Transportation and Traffic Theory, edited by H. S. Mahmassani, Elsevier Ltd., Oxford, 229–244, 2005

[53] R. Kühne, R. Mahnke, I. Lubashevsky, J. Kaupužs, Probabilistic description of traffic breakdowns, Phys. Rev. E **65**, 066125, 2002

[54] P. Lertworawanich, L. Elefteriadou, A methodology for estimating capacity at ramp weaves based on gap acceptance and linear optimization, Transp., **37 B**, 5, 459–483, 2003

[55] V. Linetsky, On the transition densities for reflected diffusions, *Adv. Appl. Prob.* **37**, 435–460, 2005

[56] V. Linetsky, The spectral representation of Bessel processes with constant drift: Applications in queueing and finance, *J. Appl. Prob.* **41**, 327–344, 2004

[57] M. E. Lárraga, J. A.del Rio, A. Mehta, Two effective temperatures in traffic flow models: analogies with granular flow, Physica A, **307**, 527–547, 2002

[58] M. Lorenz, L. Elfteriadou, A Probabilistic approach to defining freeway capacity and breakdown. In: Brilon, W. (ed.) 4th Int. Symp. on Highway Capacity, June 27 - July 1, Hawaii, Transp. Res. E Circular EDCO/8, 2000

[59] I. Lubashevsky, M. Hajimahmoodzadeh, A. Katsnelson, P. Wagner, Eur. Phys. J. B **36**, 115, 2003

[60] I. Lubashevsky, R. Mahnke, P. Wagner, S. Kalenkov, Long–lived states in synchronized traffic flow: empirical promt and dynamical trap model, Phys. Rev. E, **66**, 016117, 2002

[61] I. Lubashevsky, P. Wagner, R. Mahnke, Rational–driver approximatin in car–following model, Phys. Rev. E, **68**, 056109, 2003

[62] I. Lubashevsky, P. Wagner, R. Mahnke, Bounded rational driver models, Eur. Phys. J. B **32**, 243–247, 2003

[63] S. K. Ma, *Modern theory of critical phenomena*, Benjamin, Reading, 1976

[64] R. Mahnke, J. Kaupužs, Stochastic theory of freeway traffic, Phys. Rev. E **59**, 117–125, 1999

[65] R. Mahnke, J. Kaupužs, V. Frishfelds, Nucleation in physical and nonphysical systems, Atmospheric Research, **65**, 261–284, 2003

[66] R. Mahnke, J. Kaupužs, I. Lubashevsky, Probabilistic description of traffic flow, Phys. Rep., **408**, Nos. 1–2, 2005

[67] R. Mahnke, N. Pieret, Stochastic master–equation approach to aggregation in freeway traffic, Phys. Rev. E **56**, 2666–2671, 1997

[68] H. Malchow, L. Schimansky–Geier, *Noise and diffusion in bistable nonequilibrium systems*, Teubner–Texte zur Physik, Band 5, Berlin, 1986

[69] A. Mehta, *Granular matter. An interdisciplinary approach*, Springer, New York, 1994

[70] E. W. Montroll, *Fluctuation phenomena*, Amsterdam, 1987

[71] D. N. P. Muthly, M. Xie, R. Jiang, Weibull Models, Wiley, New Jersey, 2004

[72] K. Nagel, M. Schreckenberg, J. Phys. I, **2**, 2221, 1992

[73] E. Nelson, *Dynamical theories of brownian motion*, Princenton University Press, Princeton, 1967

[74] G. F. Newell, Oper. Res., **9**, 209, 1961

[75] B. Øksendal, A. Sulem, *Applied stochastic control of jump diffusion*, Springer, Berlin, 2005

[76] S. M. de Oliveira, P. M. C. de Oliveira, D. Stauffer, *Evolution, money, war, and computers*, Teubner-Texte zur Physik, Vol. 34, Teubner, Stuttgart, 1999

[77] P. Papon. J. Leblond, P. H. E. Meijer, *The physics of phase transitions*, Springer, Berlin, 2002

[78] L. A. Pipes, J. Appl. Phys., **24**, 274, 1953

[79] W. H. Press, et al., *Numerical recipes in Fortran. The art of scientific computing*, 2nd ed., Cambridge University Press, New York, 1992

[80] I. Prigogine, R. Hermann, *Kinetic theory of vehicular traffic*, Elsevier, Amsterdam, 1971

[81] H. Risken, *The Fokker-Planck equation. Methods of solution and applications*, Springer, Berlin, 1996

Bibliography

[82] S. Redner, *A guide to first–passage processes*, Cambridge University Press, New York, 2001

[83] M. Regler, Verkehrsablauf und Kapazität auf Autobahnen, Dissertation, Universität Bochum, 2004

[84] R. Remer, Theorie und Simulation von Zeitreihen mit Anwendungen auf die Aktienkursdynamik, Dissertation, Universität Rostock, 2005

[85] M. Resnick, *Turtles, termites, and traffic jams: explorations in massively parallel microworlds*, The MIT Press, Massachusetts, 1997

[86] S. I. Resnick, *A probability path*, Birkhäuser, Boston, 1999 (1st ed.), 2001

[87] A. Reuschel, Österr. Ingen.–Archiv **4**, 193, 1950

[88] A. A. Samarskii, P. N. Vabishchevich, *Computation heat transfer*, John Wiley & Sons, Chichester, 1995

[89] A. A. Samarskii, *Theorie der Differenzenverfahren*, Akademische Verlagsgesellschaft, Leipzig, 1984

[90] J. Schmelzer, G. Röpke, R. Mahnke, *Aggregation phenomena in complex systems*, Wiley–VCH, Weinheim, 1999

[91] F. Schweitzer, *Brownian agents and active particles. Collective dynamics in the natural and social sciences*, Springer, Berlin, 2003

[92] A. P. S. Selvadurai, *Partial differential equations in mechanics*, Springer, Berlin, 2000

[93] J. P. Sethna, *Statistical mechanics: entropy, order parameters and complexity*, Oxford University Press, New York, 2006

[94] R. Seydel, *Tools for computational finance*, Springer, Berlin, 2004

[95] B. Schmittmann, R. K. P. Zia, Phys. Rep., **301**, 45, 1998

[96] J. Treiterer, Ohio State Technical Report No. PB 246 094, 1975

[97] G. E. Uhlenbeck, L. S. Ornstein, On the theory of the brownian motion, Phys. Rev. **36**, 823, 1930

[98] J. Vollmer, Chaos, spatial extension, transport, and non-equilibrium thermodynamics, Phys.Rep., **372**, 148 – 155, 2002

[99] G. Weisbuch, *Complex systems dynamics*, Addison Wesley Longman, Boston, 1991

[100] S. Wolfram, *Theory and applications of cellular automata*, World Scientific, Singapore, 1986

[101] G. M. Zaslavsky, Dynamical traps, Physica D, **168–169**, 292–304, 2002

[102] D. Zwillinger, *Handbook of differential equations*, Academic Press, New York, 1992

[103] A. Zettl, *Sturm-Liouville Theory*, Providence, American Mathematical Society, 2005

[104] H. Zurlinden, Überlastungswahrscheinlichkeiten und Verkehrsleistung als Bemessungskriterium für Straßenverkehrsanlagen, FE-Nr.: 03.327/1999/KGB der Bundesanstalt für Straßenwesen, Januar 2003

List of Publications

1. J. Kaupužs, H. Weber, J. Tolmacheva, R. Mahnke:
   Applications to Traffic Breakdown on Highways,
   In: Progress in Industrial Mathematics at ECMI 2002 (Eds.: A. Buikis, R. Ciegis, A. D. Fitt), Springer–Verlag, Berlin, pp. 133–138, 2004

2. R. Mahnke, J. Kaupužs, I. Lubashevsky, J. Tolmacheva:
   Stochastic Approach to Highway Traffic,
   In: Noise in Complex Systems and Stochastic Dynamics II (Eds.: Z. Gingl, J. M. Sancho, L. Schimansky–Geier, J. Kertesz), Proceedings of SPIE, **5471**, pp. 298–310, 2004

2005

3. R. Mahnke, J. Kaupužs, J. Tolmacheva:
   Stochastic Description of Traffic Breakdown: Langevin Approach,
   In: Traffic and Granular Flow '03 (Eds.: S. P. Hoogendoorn, S. Luding, P. H. L. Bovy, M. Schreckenberg, D. E. Wolf), Springer–Verlag, Berlin, pp. 205–210, 2005

2006

4. J. Hinkel:
   How to Calculate Traffic Breakdown Probability?
   In: Traffic and Granular Flow '05 (Eds.: A. Schadschneider, T. Pöschel, R. Kühne, M. Schreckenberg, D. E. Wolf), Springer–Verlag, Berlin, pp. 531–536, 2006

<div align="center">

2007

</div>

5. J. Hinkel, R. Mahnke:
   Outflow Probability for Drift–Diffusion Dynamics,
   International Journal of Theoretical Physics, **46**, Nos. 6, pp. 1542 – 1561,
   2007

6. R. Kühne, R. Mahnke, J. Hinkel:
   Understanding Traffic Breakdown: A Stochastic Approach,
   In: International Symposium of Transportation and Traffic Theory, (Eds:
   M. Bell, B. Heydecker and R. Allsop), Elsevier Ltd., Oxford, pp. 777–789,
   2007

7. R. Mahnke, J. Kaupužs, J. Hinkel, H. Weber:
   Application of Thernodynamics to Driven Systems,
   European Physical Journal B, accepted for publication,
   `http://arxiv.org/pdf/cond-mat/0606509`, 2007

Acknowledgements

Erklärung

Ich versichere hiermit an Eides statt, dass ich die vorliegende Arbeit selbstständig angefertigt und ohne fremde Hilfe verfasst habe, keine außer den von mir angegebenen Hilfsmitteln und Quellen dazu verwendet habe und die den benutzten Werken inhaltlich und wörtlich entnommenen Stellen als solche kenntlich gemacht habe.

Rostock, 28.06.2007

Wissenschaftlicher Lebenslauf

Persönliche Angaben

- **Name**: Julia Hinkel geb. Tolmacheva

- **Staatsbürgerschaft**: ukrainisch

- **Geburtsdatum**: 06.08.1979

- **Geburtsort**: Charkiv, Ukraine

- **Familienstand**: verheiratet

Anschrift

- **Postanschrift**: Husumer Straße 2, 18109 Rostock

- **Telefon**: 03 81/ 2 52 65 49

- **e-mail**: julia.hinkel@uni-rostock.de

Ausbildung

- **1986 − 1996**: Charkiv, Lyceum Nr. 45 (bis 1994), Gymnasium Nr. 117. Abschluss: Mittelschulbildung mit Auszeichnung (Schwerpunkte: Mathematik, Englisch und Chemie)

- **1996 − 2001**: Studium an der Nationalen Universität Charkiv, Fakultät für Mechanik und Mathematik, Angewandte Mathematik, Mathematische Physik und Nummerische Mathematik. Abschluss: Magisterdiplom

Tätigkeiten

- **Oktober 2001 − Februar 2004**: Nationale Akademie der Wissenschaften, Institut für Einkristalle, Abteilung für Theoretische Physik, Doktorandin, (Schwerpunkt: Percolationtheorie)

- **Oktober 2003 − Dezember 2005**: Universität Rostock, Institut für Physik, Promotionsstudentin, gefördert durch das Akademische Auslandsamt, (Schwerpunkt: Stochastische Prozesse in der Physik mit Anwendung auf nichtlineare Systeme)

- **Januar 2005 − September 2006**: Universität Rostock, Institut für Physik, Promotionsstudentin im Rahmen des Graduiertenkollegs Vielteilchenphysik, (Schwerpunkt: Getriebene Vielteilchensysteme: Anwendungen auf Verkehrsphysik)

- **Oktober 2006 − Juni 2007**: Universität Rostock, Institut für Physik, wissenschaftliche Mitarbeiterin, (Schwerpunkt: Getriebene Vielteilchensysteme: Anwendungen auf Verkehrsphysik)